EVALUATION OF SEVERAL MULTIAXIAL HIGH CYCLE FATIGUE ENDURANCE CRITERIA

A THESIS SUBMITTED TO
THE GRADUATE SCHOOL OF NATURAL AND APPLIED SCIENCES
OF
MIDDLE EAST TECHNICAL UNIVERSITY

BY

ZAFER ENGİN

IN PARTIAL FULFILLMENT OF THE REQUIREMENTS
FOR
THE DEGREE OF MASTER OF SCIENCE
IN
AEROSPACE ENGINEERING

SEPTEMBER 2018

Approval of the thesis:

EVALUATION OF SEVERAL MULTIAXIAL HIGH CYCLE FATIGUE ENDURANCE CRITERIA

submitted by **ZAFER ENGİN** in partial fulfillment of the requirements for the degree of **Master of Science in Aerospace Engineering Department, Middle East Technical University** by,

Prof. Dr. Halil Kalıpçılar
Dean, Graduate School of **Natural and Applied Sciences** _____

Prof. Dr. Ozan Tekinalp
Head of Department, **Aerospace Engineering** _____

Assoc. Prof. Dr. Demirkan Çöker
Supervisor, **Aerospace Engineering Dept., METU** _____

Examining Committee Members:

Prof. Dr. Altan Kayran
Aerospace Engineering Dept., METU _____

Assoc. Prof. Dr. Demirkan Çöker
Aerospace Engineering Dept., METU _____

Prof. Dr. Erdem Acar
Mechanical Engineering Dept., TOBB University _____

Assoc. Prof. Dr. Ercan Gürses
Aerospace Engineering Dept., METU _____

Assoc. Prof. Dr. Tuncay Yalçınkaya
Aerospace Engineering Dept., METU _____

Date: 07.09.2018

I hereby declare that all information in this document has been obtained and presented in accordance with academic rules and ethical conduct. I also declare that, as required by these rules and conduct, I have fully cited and referenced all material and results that are not original to this work.

Name, Last name : Zafer Engin

Signature :

ABSTRACT

EVALUATION OF SEVERAL MULTIAXIAL HIGH CYCLE FATIGUE ENDURANCE CRITERIA

Engin, Zafer
MSc, Department of Aerospace Engineering
Supervisor: Assoc. Prof. Dr. Demirkan Çöker

September 2018, 175 Pages

Multiaxial high cycle fatigue is an important failure mode for industrial applications as it is experienced by many engineering parts such as rotor blades and crankshafts. Determining the critical locations and especially the fatigue lives of such components have great importance. Therefore, a methodology is needed which would replace expensive and time-consuming test campaigns as it is not possible and feasible to simulate all the loading scenarios that component would experience during the service life. The purpose of this thesis is to evaluate the state-of-the-art multiaxial endurance criteria available in the literature, with respect to their capability of handling multiaxial load interactions, phase difference, mean stress, and calculation speed. The criteria transform the multiaxial stress state to a damage parameter which is compared with endurance limit to determine whether the structure endures the loading or not. In this thesis, criteria from the literature belonging to equivalent stress, invariant based and critical plane are considered. Extensive experimental data is obtained from literature to compare the estimations of the criteria and a MATLAB code is written for calculations. Life estimations are obtained for each experimental data and statistical analysis is performed for obtaining the general behavior of the criteria. Comparing each type of criteria we conclude that the equivalent stress methods give highly scattered estimations while invariant based methods yield

more reliable results; however, best estimations are obtained by critical plane methods. For practical applications GAM (invariant based) or Papuga PCR (critical plane) may be implemented, former being fast and latter being more precise.

Keywords: Multiaxial fatigue, equivalent stress, critical plane, non-proportional loading, damage parameter

ÖZ

FARKLI ÇOK EKSENLİ YÜKSEK ÇEVRİMLİ YORULMA KRİTERLERİNİN DEĞERLENDİRİLMESİ

Engin, Zafer
Yüksek Lisans, Havacılık ve Uzay Mühendisliği Bölümü
Tez Yöneticisi: Doç. Dr. Demirkan Çöker

Eylül 2018, 175 Sayfa

Çok eksenli yüksek çevrimli yorulma, rotor palleri ve krank milleri gibi çoğu mühendislik parçasınca deneyimlendiği için sanayi uygulamaları açısından önemli bir kırılma modudur. Bu çeşit parçaların, yorulma kritik bölgelerinin ve özellikle yorulma ömürlerinin belirlenmesi büyük önem arz etmektedir. Bu sebeple ve parçanın servis ömrü boyunca deneyimleyebileceği tüm yükleme koşullarının simüle edilmesi olası ve yapılabilir olmadığı için pahalı ve zaman alıcı test kampanyalarının yerini alacak bir metodolojiye ihtiyaç duyulmaktadır. Bu tezin amacı, literatürde mevcut olan en gelişmiş çok eksenli dayanım kriterlerinin; çok eksenli yük etkileşimleri, faz farkı ve ortalama gerilim etkilerini ele alma becerileri ve hızları bakımından değerlendirilmesidir. Bu kriterler, çok eksenli gerilim durumunu, yapının yüklemeye dayanıp dayanamadığını belirlemek için yorulma dayanımıyla karşılaştırılan bir hasar parametresine dönüştürür. Bu tezde, literatürden alınan; eşdeğer gerilim, değişmez gerilim ve kritik düzlem kriter çeşitlerine ait metodlar incelenmiştir. Metodların ömür tahminlerini karşılaştırmak amacıyla literatürden kapsamlı bir deney datası alınmış ve hesaplamalar için bir MATLAB kodu yazılmıştır. Her deney datası için ömür tahminleri yapılmış ve metodların genel davranışını belirlemek için istatistiksel analizler yapılmıştır. Her tipte kriteri karşılaştırmamız sonucunda eşdeğer gerilim metotlarının hayli dağınık ömür tahminleri verdiği, bu esnada

değişmez gerilim esaslı metotların daha güvenilir tahminlere ulaştığı; fakat, en iyi öngörülerin kritik düzlem metotlarıyla elde edildiği sonucuna vardık. Pratik uygulamalar için, GAM (değişmez gerilim esaslı) metodu hızlı olduğu ve ya Papuga PCR (kritik düzlem) metodu GAM'a göre daha hassas olduğu için kullanılabilir.

Anahtar Kelimeler: Çok eksenli yorulma, eşdeğer gerilim, kritik düzlem, orantılı olmayan yüklemeler, hasar parametresi

To my fiancé Tuğçe Aktaş

ACKNOWLEDGMENTS

I would like to express sincere appreciation to my supervisor Assoc. Prof. Dr. Demirkan Çöker, whose encouragement, endless guidance, understanding and support from the initial to the final level enabled me to develop an understanding of the subject. This thesis would not have been possible without his kind support. I would also like to thank Aerospace Engineering Department instructors. I learned a lot from them.

I am truly indebted and thankful to our team leader, Serkan Özbay, and my colleagues Murat Şahin, Pelin Ergül and Remziye Demirci in Turkish Aerospace. They always supported and guided me throughout this study.

Additional thanks are given to my best friends, Burak Kayabaşı, Mehmet Kaygusuz, Mehmet Şahbaz and Mertcan Kurt for their encouragement throughout the thesis work and their friendship. I wish also good luck to them with all my heart.

Also, I would like to express my gratitude to my mother Enise Engin and my father Vasfiddin Engin. They provided endless support not only for this thesis but throughout my life. I would like to thank them for everything.

Finally, my deepest appreciation goes to my beloved fiancé Tuğçe Aktaş for her love and patience during my studies.

TABLE OF CONTENTS

LIST OF TABLES

LIST OF FIGURES

LIST OF SYMBOLS

α	Orientation of RH
α_{MRH}	Orientation of MRH
a_k	Sides of RH, k=1,2
a,b,c	Material constants of multiaxial endurance criteria
D_1, D_2, D_3, D_4, D_5	Alternating values of transformed deviatoric stresses
$f(\tau)$	Function of shear stress
$g(\sigma)$	Function of normal stress
I_1, I_2, I_3	Stress invariants
J_1, J_2, J_3	Deviatoric stress invariants
$\sqrt{J_2}$	Square root of second deviatoric stress invariant
$\sqrt{J_{2,a}}$	Alternating value of the square root of second deviatoric stress invariant
l_i, m_i, n_i	Direction cosines for oriented axes X'-Y'-Z'; i=1,2,3
n	Eigenvectors
n_{op}	Number of total evaluations in MCC algorithms
n_x, n_y, n_z	Directional cosines
$\mathbf{n_{x'}}$, $\mathbf{n_{y'}}$, $\mathbf{n_{z'}}$	Direction cosine vectors for oriented axes X'-Y'-Z'
P	Period
r	Fully reversed endurance limit ratio (σ_{-1}/τ_{-1})
r_0	Ratio of axial/bending pulsating endurance limit to fully reversed endurance limit (σ_{-1}/σ_0)
R	Stress ratio ($\sigma_{min}/\sigma_{max}$)
s	Deviatoric stress tensor
$\|\mathbf{s}\|_a$	Alternating value of deviatoric stress tensor
s_x, s_y, s_z	Deviatoric stresses in X-Y-Z coordinate system
S	Deviatoric stress vector in 5D Ilyushin transformed space
S_1, S_2, S_3, S_4, S_5	Deviatoric stress components in 5D Ilyushin transformed space

$\mathbf{t}$	Stress vector (traction) acting on a surface
$\mathbf{I}$	Second order identity tensor
$\boldsymbol{\sigma}$	Stress tensor
σ	Normal stress
σ_0	Pulsating axial/bending endurance limit
σ_a	Alternating stress
$\sigma_{a,al}$	Allowable alternating stress on mean stress curve
$\sigma_{a,R}$	Alternating endurance limit at different R ratios
$\sigma_{f'}$	True fracture strength
σ_h	Hydrostatic stress
$\sigma_{h,m}$	Mean hydrostatic stress
$\sigma_{h,max}$	Maximum hydrostatic stress
σ_m	Mean stress
σ_{min}	Minimum stress
σ_{max}	Maximum stress
$\sigma_{n,max}$	Maximum of the normal stress on material plane
σ_{oct}	Octahedral normal stress
σ_u	Ultimate strength
σ_y	Yield strength
σ_{-1}	Fully reversed axial/bending endurance limit
$(\sigma_{-1})_c$	Mean corrected alternating stress at R=-1
σ_{AMP}	Absolute maximum principle stress
$\sigma_{eq,\,AMP}$	Absolute maximum principle equivalent stress
σ_p	Eigenvalue of the stress tensor
σ_x, σ_y, σ_z	Normal stresses in X-Y-Z coordinate system
$\sigma_{x'}$, σ_n	Normal stress on a material plane
$\sigma_{x',a}$, $\sigma_{n,a}$	Alternating normal stress on a material plane
$\sigma_{x',m}$, $\sigma_{n,m}$	Mean normal stress on a material plane

$\sigma_{x,a}$, $\sigma_{y,a}$, $\sigma_{z,a}$	Alternating normal stresses in X-Y-Z coordinate system
σ_1, σ_2, σ_3	Principle stresses
σ_{SP12}, σ_{SP23}, σ_{SP13}	Normal stresses at principle shear stresses
σ_{ij}	Stress tensor
σ_{VM}	Von Mises stress
$\sigma_{eq,VM}$	Von Mises equivalent stress
τ	Shear stress
τ_{-1}	Fully reversed torsion endurance limit
τ_a	Alternating shear stress
τ_m	Mean shear stress
τ^*	Arbitrary shear vector
τ_{max}	Maximum shear stress
τ_{meso}	Mesoscopic shear stress
τ_{oct}	Octahedral shear stress
$\tau_{oct,y}$	Octahedral shear stress at yielding
τ_R, T	Resultant shear stress on a material plane
$\tau_{R,a}$, T_a	Alternating resultant shear stress on a material plane
$\tau_{R,m}$, T_m	Mean resultant shear stress on a material plane
τ_{xy}, τ_{yz}, τ_{xz}	Shear stresses in X-Y-Z coordinate system
$\tau_{x'y'}$, $\tau_{x'z'}$	Shear stresses on a material plane
$\tau_{xy,a}$, $\tau_{yz,a}$, $\tau_{xz,a}$	Alternating shear stresses in X-Y-Z coordinate system
τ_{12}, τ_{23}, τ_{13}	Principle shear stresses
$\tau_{xy,y}$	Shear yield strength
δ	Phase difference
θ, φ	Euler angles
κ	Expansion coefficient of MCC in incremental algorithm
Ψ	Shear stress path
Ψ_1	Non-proportional stress history

Ψ_2	Proportional stress history

LIST OF ABBREVIATIONS

ALL	All test data
AMP	Absolute maximum principal
Ax_MS	Loadings with axial/bending mean stresses
C_MS	Loadings with both axial/bending and torsion mean stresses
CP	Critical plane
CPD	Critical plane deviation
CROSS	Crossland Criterion
DP	Damage parameter
DV	Dang Van Criterion
FIE	Fatigue index error
FIN	Findley Criterion
GAM	Criterion proposed by Gonçalves, Araujo and Mamiya
GN	Goodman
GR	Gerber
IP	In-phase loadings with/without mean stresses
IP_Ax_MS	In-phase loadings with axial mean stresses
IP_nMS	In-phase loadings without mean stresses
IP_MS	In-phase loadings with mean stresses
LC	Longest chord
LP	Longest projection
MCC	Minimum circumscribed circle
MCH	Minimum circumscribed hypersphere
MCE	Minimum Circumscribed Ellipsoid
MDP	Maximum damage parameter
mFIE	Mean fatigue index error
MMPDS	Metallic Materials Properties Development and

	Standardization
MS	Loadings with mean stresses
MSA	Maximum shear stress amplitude
MSE	Mean stress effect
MRH	Maximum rectangular hull
nMS	Loadings without mean stresses
OP	Out-of-phase loadings with/without mean stresses
OP_Ax_MS	Out-of-phase loadings with axial mean stresses
OP_nMS	Out-of-phase loadings without mean stresses
OP_MS	Out-of-phase loadings with mean stresses
PCR	Papuga PCR Criterion
PE	Phase effect
RB	Robert Criterion
RH	Rectangular Hull
SG	Soderberg
SNS	Sines Criterion
SVM	Signed von Mises
SWM	Mean stress correction method of Smith, Watson and Topper
To_MS	Loadings with torsion mean stresses
2D	Two dimensional
3D	Three dimensional
5D	Five dimensional

CHAPTER 1

INTRODUCTION

Many engineering parts such as rotor blades, crankshafts, pressure vessels, railroad wheels and bolted joints experience cyclic loading which is a combination of tension, bending and torsion loads for millions of cycles (high cycle) leading to biaxial or triaxial stress states. Fatigue failure under such stress states is called multiaxial fatigue. Multiaxial fatigue involves at least two loading channels (multiaxial loading) that differentiates the phenomenon from uniaxial fatigue and complicates the problem. These complications are related to the interaction of loading channels which brings along additional mechanisms such as phase and frequency effects that influence the fatigue life. These effects cause principal axes to rotate during the loading and magnitude of principal stresses alter non-proportionally. Multiaxial fatigue may also occur for uniaxial loading cases if the component is geometrically complex like in the case of the threaded zones of fasteners. Unfortunately, multiaxial loading and geometric complexities are unavoidable in industrial applications. Therefore, conservative factor of safeties are utilized for critical parts and expensive and time-consuming test campaigns are carried out. However, testing all the load scenarios is not feasible. Therefore, a methodology is needed for determining the critical locations exposed to fatigue damage and estimating the fatigue lives of engineering components.

1.1. Brief History

For several decades, different methods are proposed and developed in order to estimate fatigue life of components under multiaxial loadings. However, none of those methods are universally accepted and applicable to all material types or

loading scenarios. Therefore, a good knowledge of methods is required for accurate life estimations.

Multiaxial fatigue problem was first investigated by Lanza [1] when he performed combined rotating bending/torsion experiments. Later, several researchers such as Mason [2], Haigh [3], Nishihara and Kawamoto [4] and Gough and Pollard [5, 6] correlated multiaxial test results with empirical relations. Among all these researchers, Gough and Pollard [5, 6] performed the most extensive set of experiments and proposed empirical formulations in the form of ellipse quadrant and arc in order to guide the mechanical design of rotating shafts which are subjected to combined cyclic bending and torsion loading. Later, extensions of static failure criteria were developed (von Mises, Max Principal etc. [7]) which reduce multiaxial cyclic stress state to an equivalent cyclic stress history. Then, whether the structure endures the loading or not is determined by comparing the alternating value of the equivalent stress (after mean stress correction) with endurance limits. Although equivalent stress methods provide estimations that are in good agreement with test data for proportional loading, experimental studies show that they fail to account the directivity of non-proportional loading and effects of shear and tensile stresses on fatigue life [8-14]. As an improvement to equivalent stress methods, Sines [15] come up with a different idea that multiaxial fatigue does not only depend on the octahedral stress (von Mises) but also it depends on hydrostatic stress. Therefore, a damage parameter that is a linear combination of alternating octahedral stress and mean hydrostatic stress, which are both invariants of stress tensor, is proposed. So called invariant methods are further investigated by Crossland. Crossland [16] suggested using the maximum value of the hydrostatic stress which turns out to be more successful [17, 18, and 19]. The idea of critical plane approach, which gained great popularity among multiaxial researchers, was first generated by Stansfield [20]. This new series of criteria are based on experimental observations of crack initiation and it is assumed that the main reason of multiaxial fatigue is shear stresses while normal stresses are responsible for crack opening. Findley [21], McDiarmid [22, 23] and Dang Van et al. [24] are

some of the first critical plane methods. Damage parameters of invariant and critical plane methods are similar in nature; however, in critical plane methods stresses on all material planes are investigated instead of examining a single plane (for example the octahedral plane). Again like in equivalent stress methods, endurance of the structure is determined by comparing the damage parameter with endurance limits for invariant based and critical plane criteria.

1.2. Research Objectives

The objectives of this thesis are as follows:

- Implement the criteria into a multiaxial life prediction code.
- Evaluate and compare the multiaxial endurance criteria in terms of performance and speed.
- Validate the criteria with experimental test results from literature.

1.3. Outline of the Thesis

Thesis begins with a literature review in Chapter 2 to gain depth into multiaxial fatigue phenomenon. First, some common stress quantities are briefly clarified since these stress quantities are utilized in multiaxial endurance criteria. Then, complex loading is explained as it is one of the main reasons of multiaxial fatigue and one needs to have a good knowledge about loading types and combinations. Chapter 2 continues with definitions of alternating and mean values of shear and normal stresses for non-proportional loading and with mean stress correction curves which are used for inclusion of mean stress effects in endurance criteria. Then, the main ideas and formulations of investigated criteria are introduced. For this research only the criteria appropriate to high cycle fatigue are chosen as it is more common in industry.

Most of the multiaxial endurance criteria include torsion endurance limits for calibrating weighting constants of shear and normal stresses. However, torsion endurance limit may not be always available; therefore, formulations of weighting constants for axial/bending endurance limits with different R ratios

(R=-1 and R=0) are derived for selected invariant and critical plane criteria (Crossland, GAM, Findley and Dang Van) and these are presented in Chapter 3.

In Chapter 4, general procedure of multiaxial fatigue endurance analysis and the methodology for evaluating/comparing the criteria are explained. Moreover, experimental data set which is obtained from literature and used for this evaluation is presented. This data set contains harmonic (loading as a function of sine or cosine) bending and torsion tests with phase difference and it is proper for the evaluation of phase and mean stress effects. Data set also contains uniaxial test results to investigate the performance of the criteria for simple tests. For this thesis ductile and brittle materials are analyzed. Cast irons are excluded from the data set since there are very few experimental results for these materials and the use of cast irons is very limited in industry. Finally, pseudocodes for equivalent stress, invariant based and critical plane criteria are presented for clarification of the procedures in these algorithms.

Estimations of each multiaxial endurance criteria are presented in Chapter 5. Calculations are carried out for each experimental data and predictive capabilities of the criteria are shown with histograms (after a statistical analysis) which is the usual representation adopted in literature. These histograms show the general behavior of the criteria; however, they are insufficient for investigating the partial effects namely phase and mean stress effects or their combinations; therefore, tables presenting the statistical results (mean, range and standard deviation) of these partial effects are also included. Furthermore, comparisons of each criterion within each type of criteria and with other types of criteria are performed in order to find out which type of criteria and which criterion performs better.

In Chapter 6, a summary of the thesis is presented with concluding remarks and also suggestions for future work are involved.

CHAPTER 2

LITERATURE REVIEW

In this chapter, type of multiaxial loading, multiaxial endurance criteria and common stress quantities used in these criteria are explained.

2.1. Common Stress Quantities

In this section stress quantities commonly encountered in multiaxial fatigue criteria are introduced for a better understanding of the criteria. Most of the definitions and formulations described here are taken from Socie and Marquis [7] and Budynas and Nisbett [25].

2.1.1. Stresses

Stress is the distribution of load (force or moment) acting on a surface. Stress is unique at a point on the surface and has two components as normal and shear stresses. These stress quantities are represented by Greek symbols; σ is used for normal stress and τ is used for shear stress. Double subscription is preferred for indicating the direction of the stress and also the normal of the surface.

The state of stress at a point can be described by six stress components acting on three orthonormal planes of an infinite-small cube. These stress components are $\sigma_{xx}, \sigma_{yy}, \sigma_{zz}, \tau_{xy}, \tau_{yz}$ and τ_{xz} described in Figure 2.1. Since normal stresses act perpendicular to the surface, usually they are shown with only one subscript (σ_x, σ_y and σ_z). If normal stress is in the same direction with its subscript than it has a positive value and called tensile stress while for the opposite case it is called compressive stress. For shear stresses, first subscript indicates the direction of the surface normal and second subscript indicates the direction with respect to

coordinate axis to which the shear stress is parallel. For equilibrium, cross-shear stresses are equal ($\tau_{xy} = \tau_{yx}, \tau_{yz} = \tau_{zy,} \tau_{zx} = \tau_{xz}$).

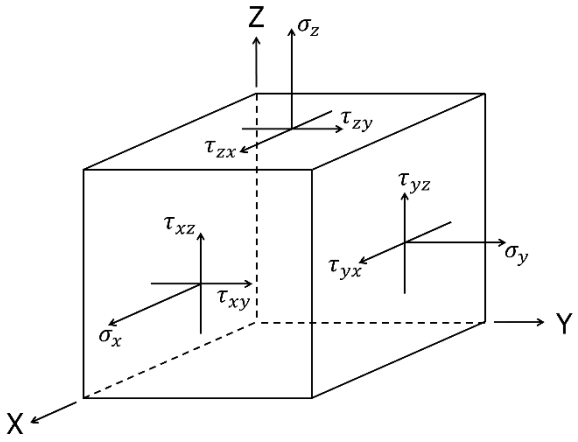

Figure 2.1: Stress state at a point

2.1.2. Principal Stresses

At a point on a component, there are infinitely many planes passing through thus, infinitely many stress states exist. For evaluation of fatigue strength, it is often of interest to investigate the maximum values of normal and shear stresses. This task may be achieved by transformation of stress state with respect to two Euler angles θ and φ. For a particular orientation, shear stresses on three orthonormal planes of the stress cube become zero while normal stresses take their maximum values. These are called principal stresses and related orientations give the principal axes. Principal stresses are denoted by σ_1, σ_2 and σ_3. Maximization of shear stresses is also possible. Principal shear stresses (τ_{12}, τ_{23} and τ_{13}) may be obtained by 45^o rotation around one of the principal axes. However, for this case normal stresses will not be zero, their value will be the average of principal stresses other than the the principal stress for which the rotation is made along it's direction.

Finding principal stresses is actually an eigenvalue problem. Since shear stresses become zero, stress matrix will be diagonal; therefore, principal stresses will be eigenvalues and their corresponding directions will be eigenvectors (directional cosines).

$$\boldsymbol{\sigma n} = \sigma_p \boldsymbol{n} \tag{2.1}$$

By rewriting

$$\left(\boldsymbol{\sigma} - \sigma_p \boldsymbol{I}\right)\boldsymbol{n} = 0 \tag{2.2}$$

where $\boldsymbol{\sigma}$ is the stress tensor, **n** is the eigenvectors, σ_p is the eigenvalue and **I** is the identity matrix. In order to avoid the trivial solution determinant of $\left(\boldsymbol{\sigma} - \sigma_p \boldsymbol{I}\right)$ should be zero. In other words,

$$\begin{vmatrix} \sigma_x - \sigma_p & \tau_{xy} & \tau_{xz} \\ \tau_{xy} & \sigma_y - \sigma_p & \tau_{yz} \\ \tau_{xz} & \tau_{yz} & \sigma_z - \sigma_p \end{vmatrix} = 0 \tag{2.3}$$

which leads to a cubic equation,

$$\begin{aligned} &\sigma_p^3 - \left(\sigma_x + \sigma_y + \sigma_z\right)\sigma_p^2 \\ &-\left(\tau_{xy}^2 + \tau_{yz}^2 + \tau_{xz}^2 - \sigma_x\sigma_y - \sigma_x\sigma_z - \sigma_y\sigma_z\right)\sigma_p \\ &-\left(\sigma_x\sigma_y\sigma_z + 2\tau_{xy}\tau_{yz}\tau_{zx} - \sigma_x\tau_{yz}^2 - \sigma_y\tau_{xz}^2 - \sigma_z\tau_{xy}^2\right) = 0 \end{aligned} \tag{2.4}$$

Solution of this equation gives three principal stresses. It is important to mention that principal stresses occur for one particular orientation regardless of the coordinate system chosen for representing the stress state. As a result, the coefficients of this cubic equation are constant.

$$I_1 = \sigma_x + \sigma_y + \sigma_z \tag{2.5}$$

$$I_2 = \tau_{xy}^2 + \tau_{yz}^2 + \tau_{xz}^2 - \sigma_x\sigma_y - \sigma_x\sigma_z - \sigma_y\sigma_z \tag{2.6}$$

$$I_3 = \sigma_x\sigma_y\sigma_z + 2\tau_{xy}\tau_{yz}\tau_{zx} - \sigma_x\tau_{yz}^2 - \sigma_y\tau_{xz}^2 - \sigma_z\tau_{xy}^2 \tag{2.7}$$

I_1, I_2 and I_3 are called stress invariants and these constants have importance in fatigue life estimations. Especially, first two invariants or their deviatoric

counterparts, which are explained in following sections, are used as a measure of mean normal stress and alternating shear stress respectively.

Roots of (2.4) can be found from the following formula [86],

$$\sigma_i = \omega cos(\beta_i) + \frac{I_1}{3} \tag{2.8}$$

where i=1,2,3. ω and β can be found from,

$$\omega = \frac{2}{3}\sqrt{I_1^2 - 3I_2} \tag{2.9}$$

$$\beta_i = \frac{\cos\left(\frac{2I_1^3 - 9I_1I_2 + 27I_3}{2(I_1^2 - 3I_2)^{\frac{3}{2}}}\right)^{-1} + 2\pi k}{3} \tag{2.10}$$

where $k = 0, \pm 1, \pm 2, ...$

After principal stresses are found, their directions may be obtained from (2.3) by writing the related principal stress value to σ_p and solving the three equations with three unknown eigenvectors. Since these three equations give infinitely many solutions, another condition is necessary which comes through the orthogonality. This relation is as follows:

$$n_x^2 + n_y^2 + n_z^2 = 1 \tag{2.11}$$

where n_x, n_y and n_z are directional cosines of the related principal stress. For a better understanding, principal stresses and directional cosines of the first principal stress are presented in Figure 2.2.

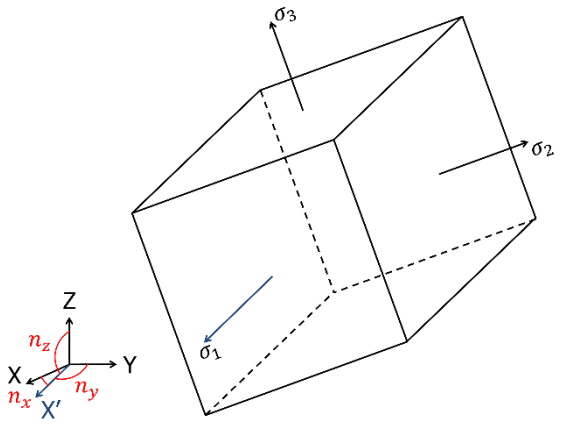

Figure 2.2: Principal stresses and directional cosines of the first principal stress

Knowing the principal stresses and for $\sigma_1 \geq \sigma_2 \geq \sigma_3$, principal shear stresses can be obtained by following equations,

$$\tau_{12} = \frac{\sigma_1 - \sigma_2}{2} \tag{2.12}$$

$$\tau_{23} = \frac{\sigma_2 - \sigma_3}{2} \tag{2.13}$$

$$\tau_{13} = \frac{\sigma_1 - \sigma_3}{2} \tag{2.14}$$

From (2.12) to (2.14), it may be concluded that $\tau_{max} = \tau_{13}$. Normal stresses on maximum shear stress planes can be found as follows:

$$\sigma_{SP12} = \frac{\sigma_1 + \sigma_2}{2} \tag{2.15}$$

$$\sigma_{SP23} = \frac{\sigma_2 + \sigma_3}{2} \tag{2.16}$$

$$\sigma_{SP13} = \frac{\sigma_1 + \sigma_3}{2} \tag{2.17}$$

Principal stresses can easily be visualized with Mohr's circle and they are presented in Figure 2.3.

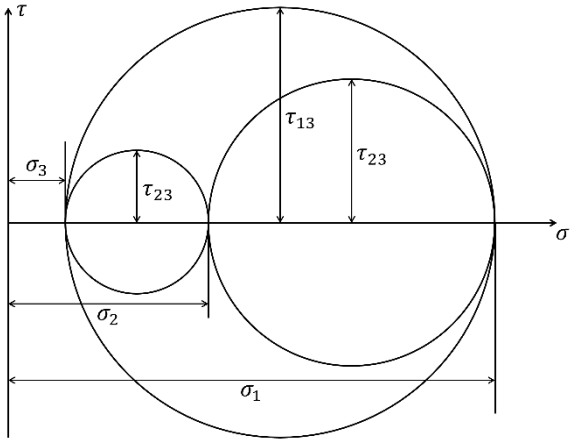

Figure 2.3: A three dimensional stress state representation with Mohr's circle

Another area of interest with respect to fatigue life evaluation is the stress state at free surfaces. Except for contact areas, regions with high residual stresses and inhomogenous regions of the material (e.g. defects), surfaces of the component will likely to be the most critical zones. Stress state at free surface in the absence of pressure loading is a special case since some of the stress components become zero; $\sigma_z = \tau_{xz} = \tau_{yz} = 0$. This stress state is called plane stress and a representation is shown in Figure 2.4.

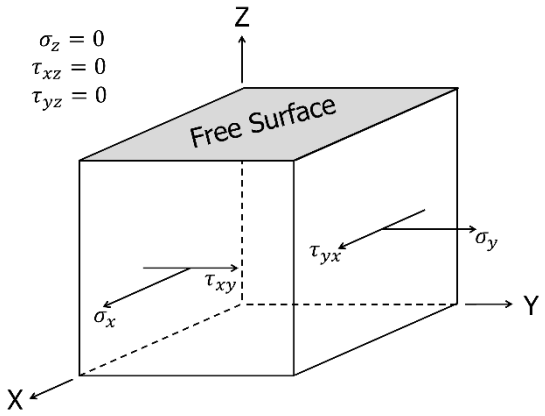

Figure 2.4: Plane stress state

Principal stresses for plane stress state are as follows:

$$\sigma_1, \sigma_2 = \frac{\sigma_x + \sigma_y}{2} \pm \sqrt{\left(\frac{\sigma_x - \sigma_y}{2}\right)^2 + \tau_{xy}^2} \tag{2.18}$$

$$\tau_1, \tau_2 = \pm \sqrt{\left(\frac{\sigma_x - \sigma_y}{2}\right)^2 + \tau_{xy}^2} \tag{2.19}$$

2.1.3. Stresses Acting on Octahedral Plane

Most widely used static failure criterion, octahedral shear stress theory (sometimes called as distortion energy theory) is based on stresses acting on octahedral plane. This criterion assumes that failure is related to angular distortion of the stressed element and predicts no failure under equally loaded principal stresses. Based on these assumptions, shear stress on octahedral plane comes out to be a good indicator of yielding as theory agrees well with ductile materials. Some adaptations of this theory are made to multiaxial fatigue in order to estimate fatigue life. These adaptations are namely; Signed von Mises, Sines and Crossland, which are explained in Section 2.3.1. and Section 2.3.4. respectively, that are one of the primary multiaxial endurance criteria.

Octahedral plane is an oblique plane that intersects the principal stress axes at equal distances. Direction cosines with respect to principal axes are equal and they have a value of $1/\sqrt{3}$. What makes this plane special is that the normal stress acting on this plane is the average of the principal stresses. There are eight planes that have the same stress state and these planes form an octahedron. Thus, it is called octahedral plane. The stress state on an octahedral plane is shown in Figure 2.5.

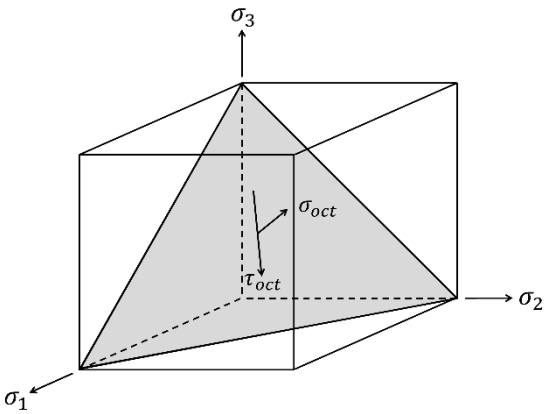

Figure 2.5: Stress state on an octahedron plane

2.1.3.1. Octahedral Shear and Effective Stresses

The resultant shear stress on octahedral plane is called the octahedral shear stress and through coordinate transformations it can be computed in terms of principal stresses,

$$\tau_{oct} = \frac{1}{3}\sqrt{(\sigma_1 - \sigma_2)^2 + (\sigma_2 - \sigma_3)^2 + (\sigma_1 - \sigma_3)^2} \tag{2.20}$$

or in terms of stress components octahedral shear stress can be shown as,

$$\tau_{oct} = \frac{1}{3}\sqrt{\left(\sigma_x - \sigma_y\right)^2 + \left(\sigma_y - \sigma_z\right)^2 + (\sigma_x - \sigma_z)^2 + 6(\tau_{xy}^2 + \tau_{yz}^2 + \tau_{xz}^2)} \tag{2.21}$$

According to octahedral shear stress theory, yield occurs when octahedral shear stress for any stress state exceeds the octahedral shear stress observed during simple tension test. For a simple tension test, specimen yields when $\sigma_1 = \sigma_y$ and $\sigma_2 = \sigma_3 = 0$. From (2.20) octahedral shear stress at yielding is,

$$\tau_{oct,y} = \frac{\sqrt{2}}{3}\sigma_y \tag{2.22}$$

For the general case, yield is predicted if (2.20) is greater than (2.22). This leads to,

$$\frac{1}{\sqrt{2}}\sqrt{(\sigma_1-\sigma_2)^2+(\sigma_2-\sigma_3)^2+(\sigma_1-\sigma_3)^2} \geq \sigma_y \tag{2.23}$$

Stress at left hand side is called octahedral effective stress or von Mises stress. Effective stress can be written in terms of stress components as,

$$\sigma_{VM} = \frac{1}{\sqrt{2}}\sqrt{\left(\sigma_x-\sigma_y\right)^2+\left(\sigma_y-\sigma_z\right)^2+(\sigma_x-\sigma_z)^2+6(\tau_{xy}^2+\tau_{yz}^2+\tau_{xz}^2)} \tag{2.24}$$

Effective stress transforms the multiaxial stress state to a uniaxial stress state which can be used for estimating static yielding. Furthermore, octahedral shear stress theory suggests and approximation for shear yield strength. For a pure shear test, from (2.23) we may conclude that,

$$\sqrt{3}\tau_{xy,y} = \sigma_y \quad or \quad \tau_{xy,y} = \frac{\sigma_y}{\sqrt{3}} = 0.577\sigma_y \tag{2.25}$$

where $\tau_{xy,y}$ is the shear yield strength.

2.1.3.2. Octahedral Normal Stress (Hydrostatic Stress)

Normal stress acting on octahedral plane is called hydrostatic stress. It can be calculated as

$$\sigma_h = \frac{1}{3}(\sigma_1+\sigma_2+\sigma_3) \tag{2.26}$$

Hydrostatic pressure is the average of principal stresses and it is used in some multiaxial endurance criteria such as Sines, Crossland and Dang Van as a measure of normal mean stress inclusion (Sections 2.3.4. and 2.3.7.).

2.1.4. Deviatoric Stresses

Stress is usually separated into hydrostatic and deviatoric stress for components that are subjected to plastic deformation. This is due to the fact that hydrostatic component of stress does not influence plastic flow while deviatoric part influences plastic yielding. In order to obtain deviatoric stresses, hydrostatic stress is subtracted from stress state. As hydrostatic stress is a stress invariant, subtraction operation will not affect the directions of principal stresses. In addition, shear stress components remain unchanged. Deviatoric stresses are defined as follows,

$$\begin{bmatrix} s_x & \tau_{xy} & \tau_{xz} \\ \tau_{xy} & s_y & \tau_{yz} \\ \tau_{xz} & \tau_{yz} & s_z \end{bmatrix} = \begin{bmatrix} \sigma_x & \tau_{xy} & \tau_{xz} \\ \tau_{xy} & \sigma_y & \tau_{yz} \\ \tau_{xz} & \tau_{yz} & \sigma_z \end{bmatrix} - \frac{1}{3}\begin{bmatrix} I_1 & 0 & 0 \\ 0 & I_1 & 0 \\ 0 & 0 & I_1 \end{bmatrix} \tag{2.27}$$

$$s_x = \sigma_x - \frac{1}{3}I_1 = \frac{2}{3}\sigma_x - \frac{1}{3}\sigma_y - \frac{1}{3}\sigma_z \tag{2.28}$$

$$s_y = \sigma_y - \frac{1}{3}I_1 = \frac{2}{3}\sigma_y - \frac{1}{3}\sigma_z - \frac{1}{3}\sigma_x \tag{2.29}$$

$$s_z = \sigma_z - \frac{1}{3}I_1 = \frac{2}{3}\sigma_z - \frac{1}{3}\sigma_x - \frac{1}{3}\sigma_y \tag{2.30}$$

Invariants for deviatoric stresses; J_1, J_2 and J_3 can be written in terms of I_1, I_2 and I_3 as follows,

$$J_1 = 0 \tag{2.31}$$

$$J_2 = \frac{I_1^2 + 3I_2}{3} \tag{2.32}$$

$$J_3 = \frac{2I_1^3 + 9I_1I_2 + 27I_3}{27} \tag{2.33}$$

Second invariant of deviatoric stress can also be written in terms of octahedral shear stress,

$$J_2 = \frac{3}{2}\tau_{oct}^2 \tag{2.34}$$

2.1.5. Cyclic Stresses

Engineering components usually encounter cyclic loading which is the main cause of fatigue failure (uniaxial or multiaxial). In order to evalute the devastating effects of cyclic stresses, several definitions were made that are used in multiaxial endurance criteria and these are explained in this section.

A cyclic stress is composed of two stress quantites which are mean or static (σ_m) and alternating stress (σ_a). The difference of maximum (σ_{max}) and minimum (σ_{min}) values of the cyclic stress is called range (σ_r) which can be expressed as follows:

$$\sigma_r = \sigma_{max} - \sigma_{min} \tag{2.35}$$

Alternating stress is the one-half of the range and it always has a positive value:

$$\sigma_a = \left|\frac{\sigma_{max} - \sigma_{min}}{2}\right| \tag{2.36}$$

while mean value is the algebraic average of maximum and minimum stresses in the cycle:

$$\sigma_m = \frac{\sigma_{max} + \sigma_{min}}{2} \tag{2.37}$$

For a constant amplitude loading one cycle includes two reversals (see Figure 2.6) and the period (P) is the time needed for one complete cycle of the loading to pass in a given point. Frequency (f) of the cyclic loading is related to period and it can be shown as:

$$f = \frac{1}{P} \tag{2.38}$$

Another definition is the stress ratio (R) which is used for expressing the loading condition and it is the ratio of minimum and maximum stress:

$$R = \frac{\sigma_{min}}{\sigma_{max}} \tag{2.39}$$

Fully reversed loading (R=-1) and pulsating loading (R=0) are two common loading conditions used in testing and for obtaining fatigue properties (i.e. endurance limits). For the former loading condition, loading does not have a mean component and maximum tensile and compressive loads are equal while for the latter loading condition minimum stress is zero leading always to a tensile loading.

All definitions clarified in this section and different loading cases according to R ratios are presented in Figure 2.6.

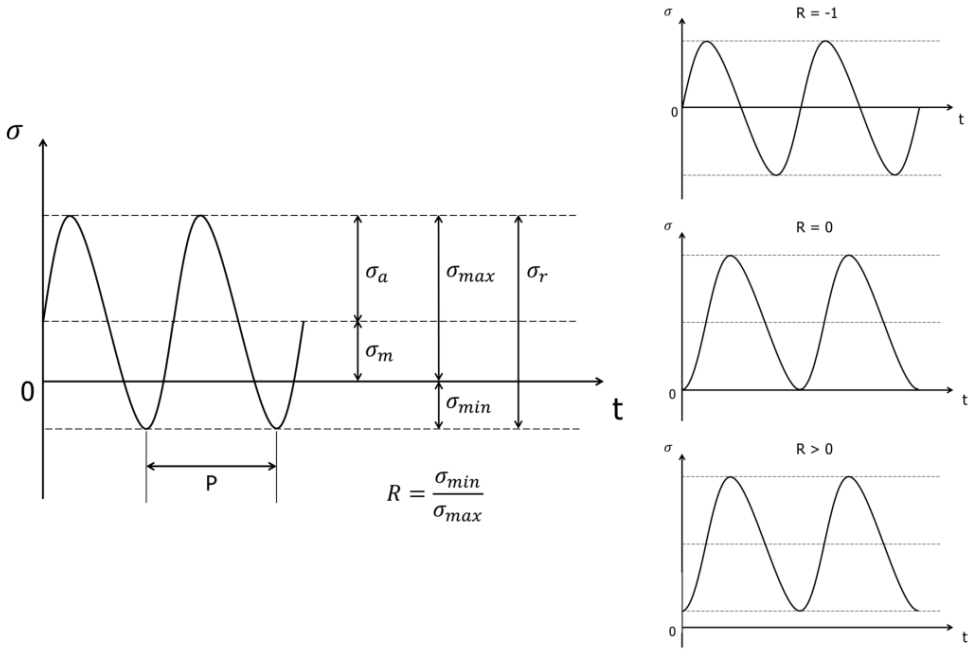

Figure 2.6: Definition of stress quantities for cyclic stresses and example loadings for R=-1 (fully reversed loading), R=0 (pulsating loading) and R>0

2.2. Multiaxial Loading

Stress state will be multiaxial if a combination of axial, bending or torsion load acts on a component. These load combinations are very common in engineering components. For instance, crankshafts experience bending-torsion loading while a biaxial stress state occurs in pressure vessels.

Combined load histories can be classified as proportional and non-proportional. Any loading that causes a change in principal stress directions and/or principal stress ratio in time is called non-proportional loading whereas principal directions and stress ratio remains constant for proportional loading. Loading may be non-proportional due to several reasons such as type of loading (bending, torsion, axial), phase difference, frequency difference between loading channels and mean loads. For periodic loadings such as sinusoidal or triangular, some definitions should be clarified. These definitions are related to phase and frequency difference. A loading whose load channels act simultaneously is defined as in-phase loading. However, if a phase shift between loading channels exist this loading is called out-of-phase loading. In-phase and out-of-phase loadings are illustrated in Figure 2.7. For the in-phase loading both bending and torsion loads reach to their maximum or minimum values at the same time (see Figure 2.7a); however, for out-of-phase loading, loadings reach their maximum (or minimum) values at different times (see Figure 2.7b) i.e. there is a phase shift. Another definition relates to frequency of loadings. If both channels have the same frequency, this loading is called synchronous and asynchronous if there is frequency difference. Synchronous and asynchronous loadings are illustrated in Figure 2.7. For the synchronous loading, both load channels have the same wave length (see Figure Figure 2.7c); however, for asynchronous loading one of the loading channels have a lower or higher wave length i.e. a higher or lower frequency (see Figure Figure 2.7d) which creates a frequency difference. For multiaxial testing, constant amplitude synchronous sinusoidal loadings are preferred for investigating the effects of phase difference and mean loads.

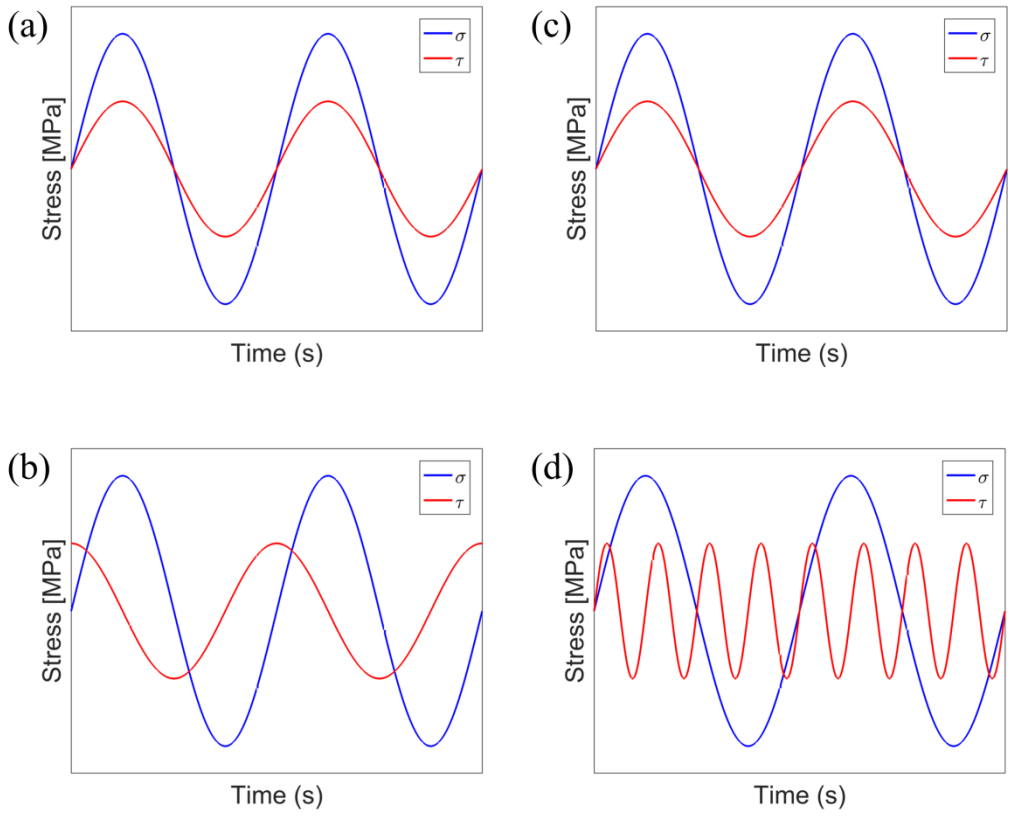

Figure 2.7 Periodic loadings; a) In-phase loading, b) Out-of-phase loading, c) Synchronous loading, d) Asynchronous loading

For a clear identification of the loading history; effect of phase, frequency and mean loads are investigated. We conclude that any in-phase loading without mean stresses leads to a proportional loading history (see Figure 2.8 and Figure 2.12). However, addition of mean load to any load channel or a load channel having only mean load for axial/bending-torsion loading, results in non-proportional loading (see Figure 2.10). Furthermore, for axial/bending-torsion loading, phase and/or frequency difference induce non-proportional loading (see Figure 2.9 and Figure 2.11). On the other hand, these effects are not seen in biaxial tension. Loading is always proportional for biaxial tension even for out-of-phase or asynchronous loadings with/without mean stresses (see Figure 2.13 to Figure 2.15). These findings are agreeable with the arguments made by Socie and Marquis [7]. Example loadings are shown through Figure 2.8 and Figure 2.15.

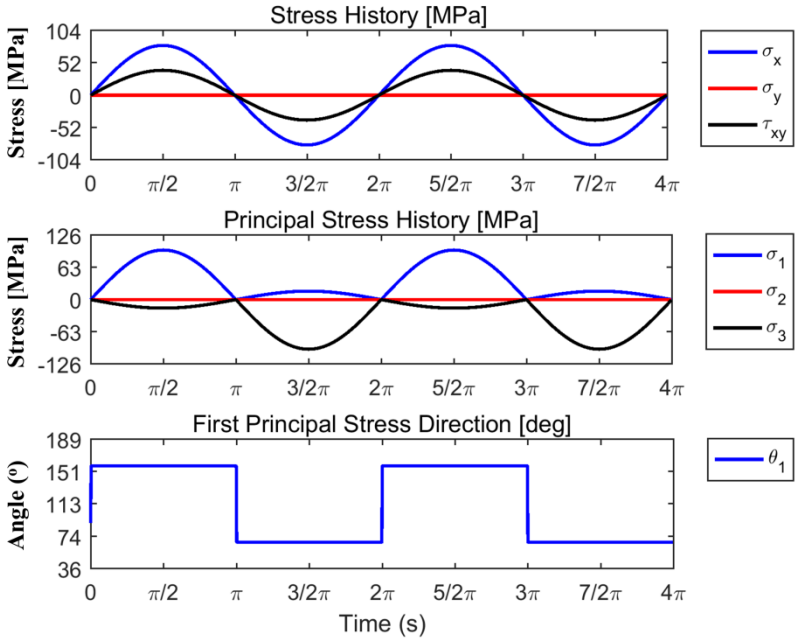

Figure 2.8: Bending/Torsion Proportional Loading

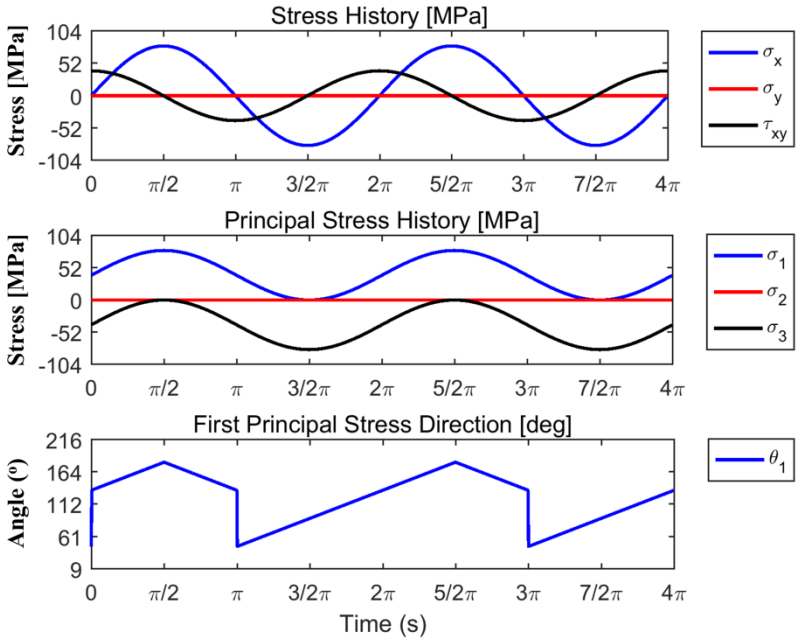

Figure 2.9 Bending/Torsion Loading with 90^{o} Phase Effect

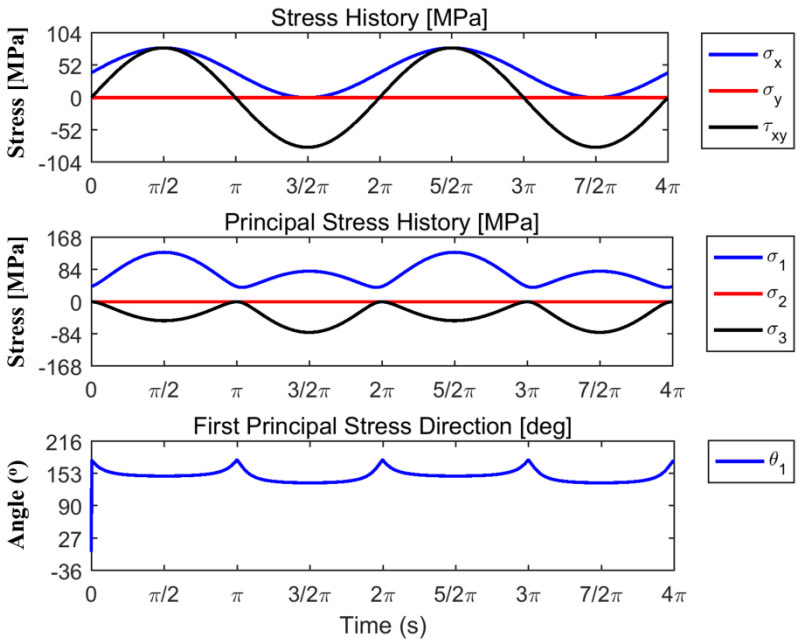

Figure 2.10 Bending/Torsion Loading with Mean Stress Effect

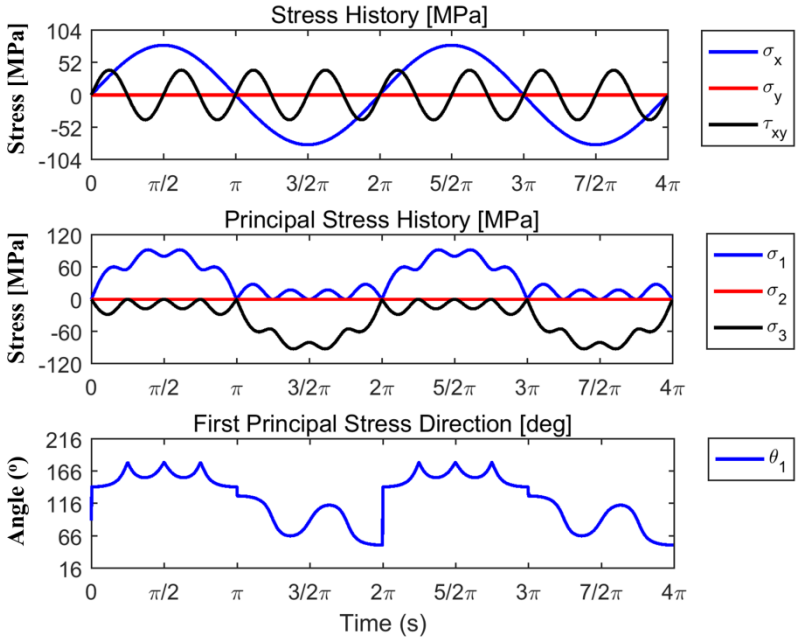

Figure 2.11 Bending/Torsion Loading with Frequency Difference

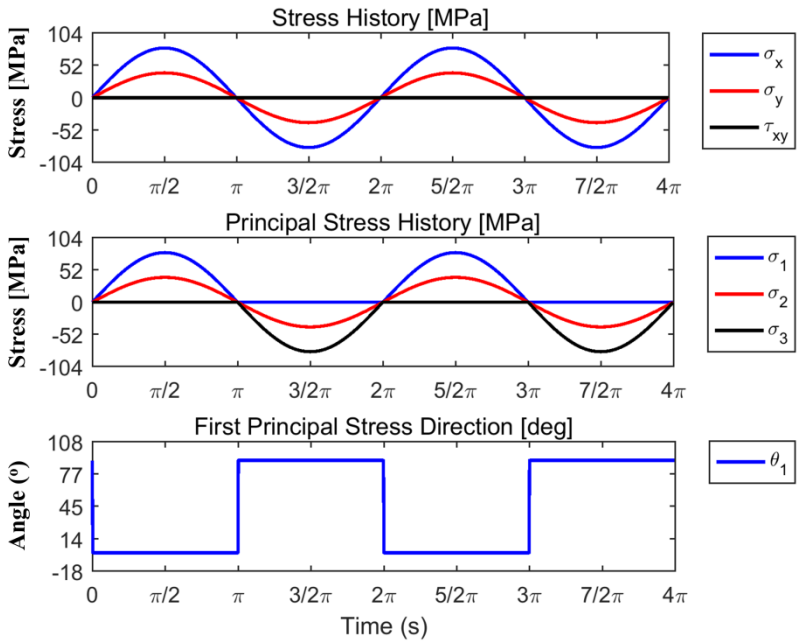

Figure 2.12: Biaxial Proportional Loading

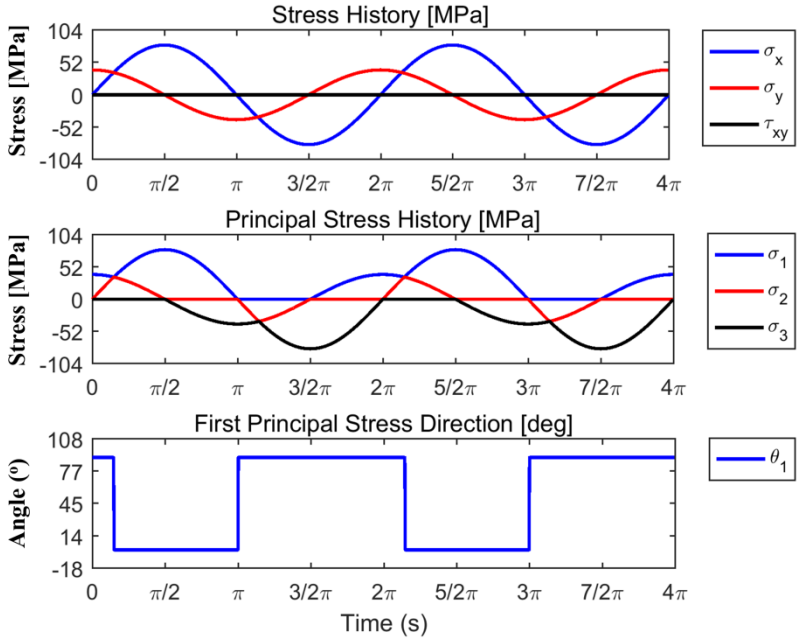

Figure 2.13 Biaxial Loading with 90^{o} Phase Effect

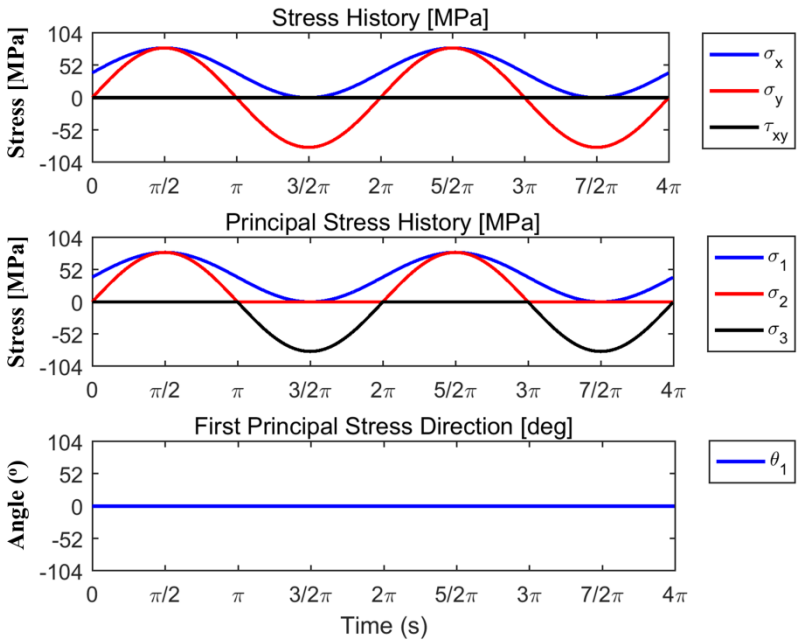

Figure 2.14 Biaxial Loading with Mean Stress Effect

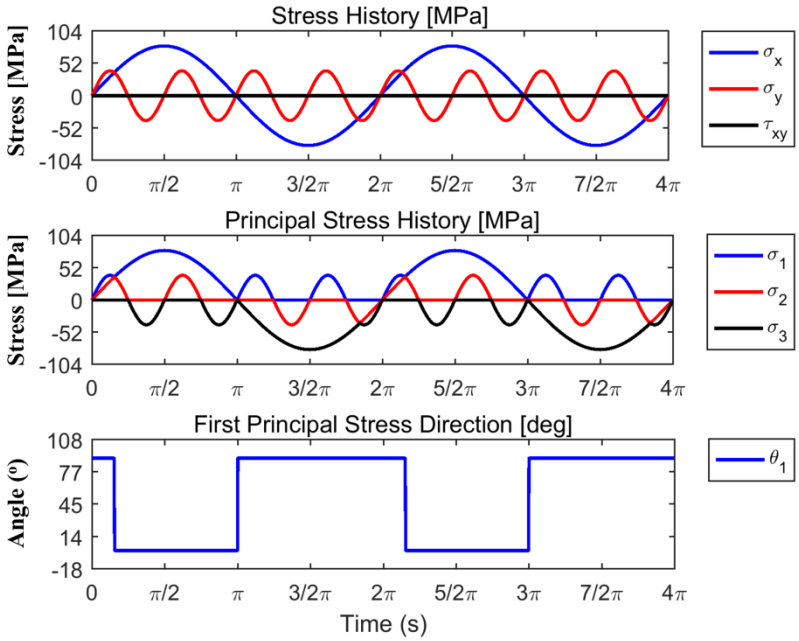

Figure 2.15 Biaxial Loading with Frequency Difference

2.3. Multiaxial Endurance Criteria

All methods presented in this thesis are in the form:

$$af(\tau) + bg(\sigma) \leq \sigma_{-1} \tag{2.40}$$

where a and b are material constants that may be obtained from uniaxial fatigue test results (endurance limits), $f(\tau)$ and $g(\sigma)$ are functions of shear and normal stresses respectively (alternating and/or mean) and σ_{-1} is the fully reversed axial/bending endurance limit. Left hand side of (2.40) is the damage parameter which is the stress state assumed to cause failure. Material constants are usually calibrated with axial (or bending) and torsion fully reversed endurance limits (σ_{-1} and τ_{-1}) which will be called bending-torsion calibration (or classical calibration) henceforth.

2.3.1. Equivalent Stress Criteria

After Gough and Pollard [5, 6] proposed empirical relations for correlating multiaxial bending/torsion tests, researchers attempted to come up with multiaxial endurance criteria that does not depend purely on experimental test results but criteria that are based on physical mechanisms of the multiaxial fatigue process. This endeavor is mainly to avoid the multiaxial testing campaigns which are time-consuming and expensive. Furthermore, it is not possible to simulate all different loading scenarios by these campaigns. As a result, extensions of static failure criteria (maximum normal stress, octahedral shear stress theory vs.) adapted to multiaxial fatigue were developed. These criteria transform the multiaxial stress history into a uniaxial stress history so that the alternating part (after mean stress correction) may be compared with endurance limits to predict the high cycle fatigue life of the component. Two of these criteria are investigated in this study namely Absolute Maximum Principal Stress and Signed von Mises Stress which are explained below in detail.

2.3.1.1. Absolute Maximum Principal Stress Criterion (AMP)

Absolute Maximum Principal Stress method is an adapted version of the static failure criterion; maximum normal stress theory, to multiaxial fatigue problem. Multiaxial stress state is transformed into an equivalent uniaxial stress history from principal stresses and a signing procedure, in which the sign of equivalent stress at a time is the sign of absolute maximum principal stress, is applied. This signing procedure is required for including the compressive stresses and for simulating the load spectrum more properly. Formulation is as follows:

$$\sigma_{eq,AMP}(t) = sign\big(\sigma_{AMP}(t)\big) * \sigma_{AMP}(t) \tag{2.41}$$

where

$$\sigma_{AMP}(t) = \max([abs(\sigma_1(t)), abs(\sigma_2(t)), abs(\sigma_3(t))]) \tag{2.42}$$

(2.41) can though to be the $g(\sigma)$ in (2.40) where $a = 0$ and $b = 1$.

2.3.1.2. Signed von Mises Stress Criterion (SVM)

The idea of Signed von Mises Stress criterion is similar to Absolute Maximum Principal Stress criterion. However, this time principal stresses are replaced with von Mises stress at a time. Like in Absolute Maximum Principal Stress method a signing procedure is needed. Since von Mises stress is always positive, compressive stresses can only be included with this signing operation. Furthermore, for some loading conditions von Mises history does not reflect reality. For example, if signing will not be applied, von Mises history comes out to be a constant stress value without any oscillation for bending/torsion loading with 90^o phase shift which is not true as this loading case is the most damaging situation stated by several researchers [26-30]. Different signings are proposed in literature. Bishop and Sherrat [31] claims sign should be the sign of absolute maximum principal stress and Papuga et al. [13] suggests that signing should be applied according to the sign of the first invariant. In this study we implemented the suggestion of Bishop and Sherrat's to be consistent with the Absolute

Maximum Principal method. Signed von Mises stress at a time can be formulated in terms of principal stresses as follows:

$$\sigma_{eq,SVM}(t) = sign(\sigma_{AMP}(t))\sqrt{(\sigma_1(t)-\sigma_2(t))^2+(\sigma_2(t)-\sigma_3(t))^2+(\sigma_3(t)-\sigma_1(t))^2} \quad (2.43)$$

(2.43) can though to be the $f(\tau)$ in (2.40) where $a = 1$ and $b = 0$.

For both methods, after equivalent stress history is obtained, alternating and mean stresses may be calculated as follows:

$$\sigma_{eq,a} = abs\left(\frac{\max(\sigma_{eq}(t)) - \min(\sigma_{eq}(t))}{2}\right)$$
$$\sigma_{eq,m} = \frac{\max(\sigma_{eq}(t)) + \min(\sigma_{eq}(t))}{2} \quad (2.44)$$

If loading includes tensile mean stresses, a mean stress correction is necessary to obtain the fully reversed equivalent stress history. For compressive mean stresses, the favorable effect shown by Sines [32] is ignored by taking the mean value as zero. Several mean stress corrections that can be applied are explained in Section 2.3.2. . In this study, all mean stress corrections explained in Section 2.3.2. are applied in order to compare their performances. When fully reversed equivalent history is obtained alternating stress is compared with the axial/bending endurance limit at R=-1 for determining if the component endures the loading or not.

Although equivalent stress methods are relatively easy to compute and fast, according to researchers [8-14] they are not appropriate for estimating fatigue lifes of components under non-proportional loadings. Signing operation is one of the reasons for this situation. This operation is used for equivalent stress methods in order to include compressive stresses into stress history and to avoid some special cases where alternating stress comes out to be very small which is not realistic. An example to this situation is shown in Figure 2.16 for Signed von Mises Stress criterion. As shown in Figure 2.16a without signing procedure,

criterion leads to a stress history without alternating stresses (only mean stress); however, alternating stresses are the most damaging stresses for fatigue life and this loading is one of the severest loading as for being a non-proportional loading. When signing is applied, a more realistic stress history is obtained (see Figure 2.16b); on the other hand, it may be observed that the alternating stress is same as the alternating stress of the normal stress which shows that the criteria still ignores the normal and shear stress interactions. Moreover, signing procedure brings along some other drawbacks. One drawback is that equivalent stress methods underestimate the fatigue damage (being non-conservative) for non-proportional loadings and they end up with estimations declaring proportional loadings are more critical. A good example to this behavior is shown in Figure 2.17. As seen from Figure 2.17a, for proportional loading case a higher value of alternating stress is obtained while for non-proportional loading, alternating stress is much lower (see Figure 2.17b). Another drawback is that signing procedure leads to sudden jumps in the stress history which does not reflect real load spectrums and results in highly conservative estimations for some loading scenarios. For instance, this situation arises when absolute values of principal stresses are very close like shown in Figure 2.18. Although the alternating values of principal stresses is very low as being 5 MPa for this loading case in Figure 2.18, the alternating value of the stress history is 20 times higher than that of principal stresses which is not logical leading to highly conservative estimates. Therefore, we may conclude that signing operation is a must for equivalent stress criteria but it is not much effective for including the directivity and complexity of the non-proportional loadings. In addition, since these methods include only one shear/normal stress component ($f(\tau)$ or $g(\sigma)$) in the damage parameter, criteria may lead to inaccurate estimations for simple loading cases like fully reversed torsion or bending. Conidering all the drawbacks above, two different types of endurance criteria are developed (as improvements on equivalent stress methods) through the years which are invariant based and critical plane methods and these methods are explained in the following sections.

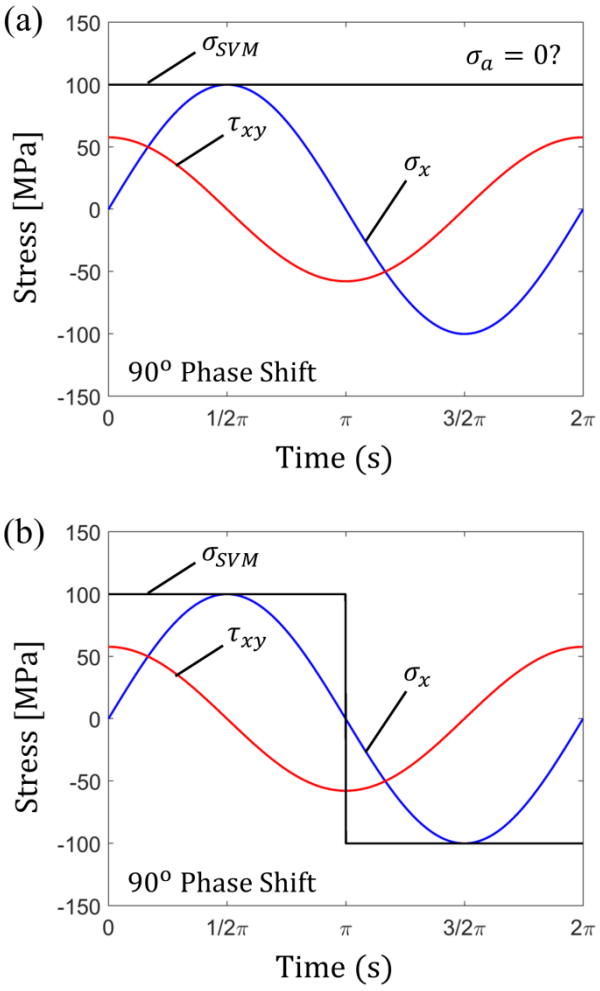

Figure 2.16 a) von Mises History, b) Signed von Mises History for multiaxial stresses consist of bending stress of 100 MPa and torsion stress of $100/\sqrt{3}$ MPa

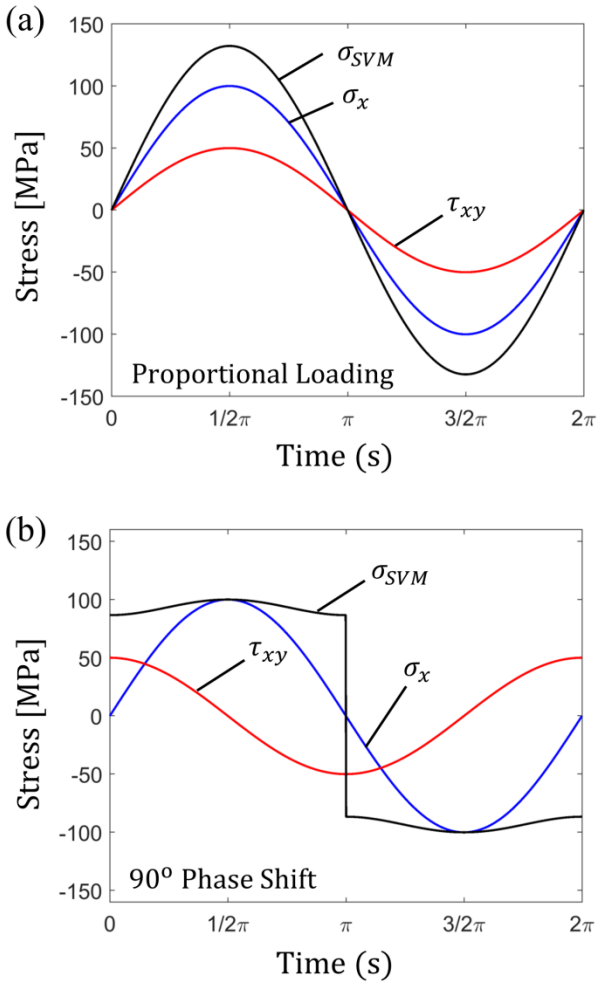

Figure 2.17 Signed von Mises history for a) Proportional loading, b) Non-proportional loading

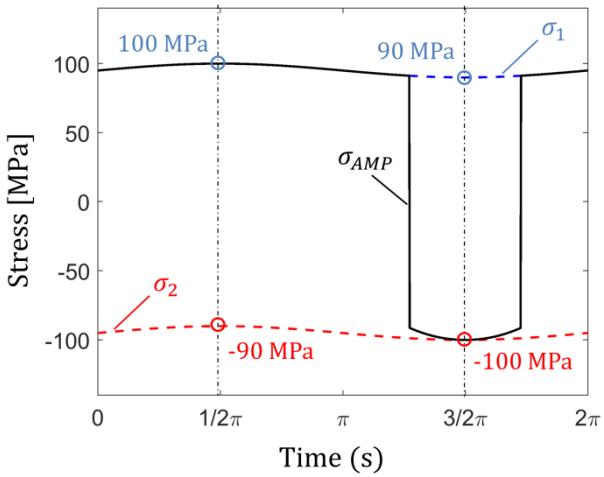

Figure 2.18 Absolute Maximum Principal Stress history of a loading for which absolute value of principal stresses are close

2.3.2. Mean Stress Correction Curves

Detrimental effects of tensile mean stresses on fatigue life and how to design components under cyclic loading with mean stresses have long been studied since Wöhler developed the S/N curves. For this purpose several methods are proposed, most famous methods are being Soderberg [33], Goodman [34] and Gerber [35]. These methods are based on experiments conducted with different R ratios and they use allowable alternating and mean stress values for determining the safe zone where no failure is expected to occur. Failure is expected, for any method, if the stress state passes the mean stress curve. Allowable alternating stress is usually taken as the endurance limit at 10^7 cycles obtained from a fully reversed loading while allowable mean stress differs for each method.

Approaches proposed by Soderberg and Goodman are linear formulations of alternating and mean stresses and they only deviate in allowable mean stress values. Soderberg takes yield strength (σ_y) as the allowable mean stress while ultimate strength (σ_u) is taken in Goodman. Gerber suggests a parabolic formulation for which again the allowable mean stress is the ultimate strength. It is clear that Soderberg is conservative as the formulation takes yield strength as the mean stress limitation. However the accuracy of Goodman and Gerber curves are questionable. There is a common belief that most of the experimental data lie

between Goodman and Gerber curves. Dowling [36, 37 and 38] analyzed an extensive set of steel, aluminum and titanium alloys and he concluded that Goodman is highly conservative while Gerber is non-conservative. Moreover, Dowling studied two other approaches being Morrow and Smith, Watson and Topper (SWT) and found out that both methods give more accurate correlations for all alloys investigated. Morrow formulation is the improvement of Goodman with the replacement of the ultimate strength with true fracture strength (σ_f). On the other hand, true fracture strength may not always be available for the materials considered. As a result, this formulation is not used in this study. SWT method is a non-linear formulation of alternating and maximum stress and does not include an allowable mean stress which might be appealing. However, due to this property of the method, accuracy of the SWT approach for high mean stresses is uncertain (which is not examined in literature). Mean stress curves of Soderberg, Goodman, Gerber and SWT shown in Figure 2.19 for 34Cr4 whose material properties are presented in Table 4.1.

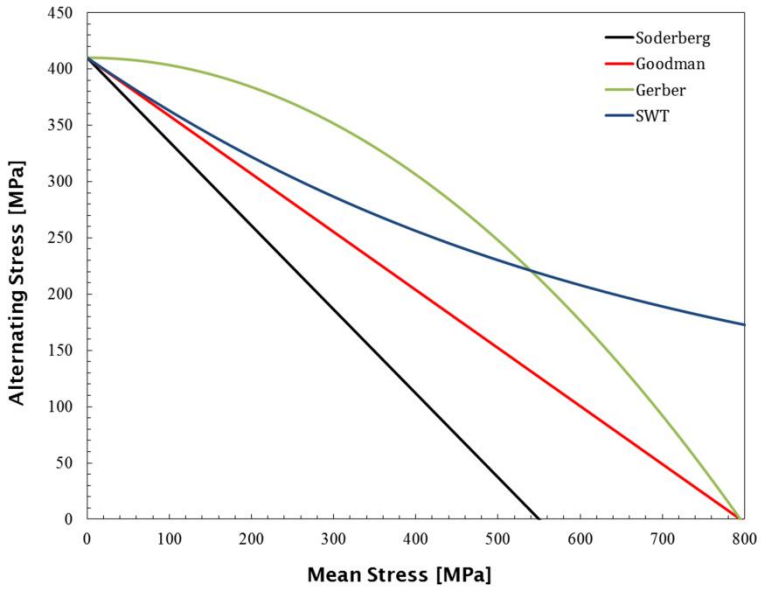

Figure 2.19: Mean Stress Curves for Al 7050 T7452

Mean stress methods may be used for various purposes. One aim is to transform the stress state, which includes mean stresses, to a fully reversed (R=-1) stress state, that is free of mean stresses. This function is mainly used for mean stress

correction of equivalent stress methods' stress history (see Section 2.3.1.). After mean stress correction, alternating stress can be compared with fully reversed axial/bending endurance limit and the performance of the method may be evaluated. Another aim is to obtain endurance limits at different R ratios. This function is useful for critical plane approaches (see Section 2.3.7.) if the formulation includes an endurance limit in different R ratio than R=-1 and if the necessary endurance limit is not available.

Formulations of mean stress curves used in this study are given in Table 2.1 with their functionalities. Furthermore, mean stress corrections for a random stress state and endurance limits calculated for R=0 for 34Cr4 are shown in Figure 2.20 as an example.

Table 2.1: Mean stress curves and functionalities

Mean Stress Curves				
Formulas	Soderberg	Goodman	Gerber	SWT
Curve	$\frac{\sigma_a}{\sigma_{-1}} + \frac{\sigma_m}{\sigma_y} = 1$	$\frac{\sigma_a}{\sigma_{-1}} + \frac{\sigma_m}{\sigma_u} = 1$	$\frac{\sigma_a}{\sigma_{-1}} + \left(\frac{\sigma_m}{\sigma_u}\right)^2 = 1$	$\sqrt{\frac{\sigma_a}{\sigma_{-1}}\frac{(\sigma_m + \sigma_a)}{\sigma_{-1}}} = 1$
Alternating Stress on Curve, $\sigma_{a,f}$	$\left(1 - \frac{\sigma_m}{\sigma_y}\right)\sigma_{-1}$	$\left(1 - \frac{\sigma_m}{\sigma_u}\right)\sigma_{-1}$	$\left(1 - \left(\frac{\sigma_m}{\sigma_u}\right)^2\right)\sigma_{-1}$	$\frac{\sqrt{\sigma_m^2 + 4\sigma_{-1}^2} - \sigma_m}{2}$
Mean Stress Correction, $(\sigma_{-1})_c$	$\frac{\sigma_y \sigma_a}{\sigma_y - \sigma_m}$	$\frac{\sigma_u \sigma_a}{\sigma_u - \sigma_m}$	$\frac{\sigma_u^2 \sigma_a}{\sigma_u^2 - \sigma_m^2}$	$\sqrt{\sigma_a(\sigma_a + \sigma_m)}$
Allowable at Different R Ratios, $\sigma_{a,R}$	$\frac{\sigma_y \sigma_{-1}(1-R)}{(1-R)\sigma_y + (1+R)\sigma_{-1}}$	$\frac{\sigma_u \sigma_{-1}(1-R)}{(1-R)\sigma_u + (1+R)\sigma_{-1}}$	$\frac{\sigma_u^2(1-R)}{(1+R)^2}\left[\sqrt{\left(\frac{1-R}{2\sigma_{-1}}\right)^2 + \left(\frac{1+R}{\sigma_u}\right)^2} - \left(\frac{1-R}{2\sigma_{-1}}\right)\right]$	$\sqrt{\frac{1-R}{2}}\sigma_{-1}$

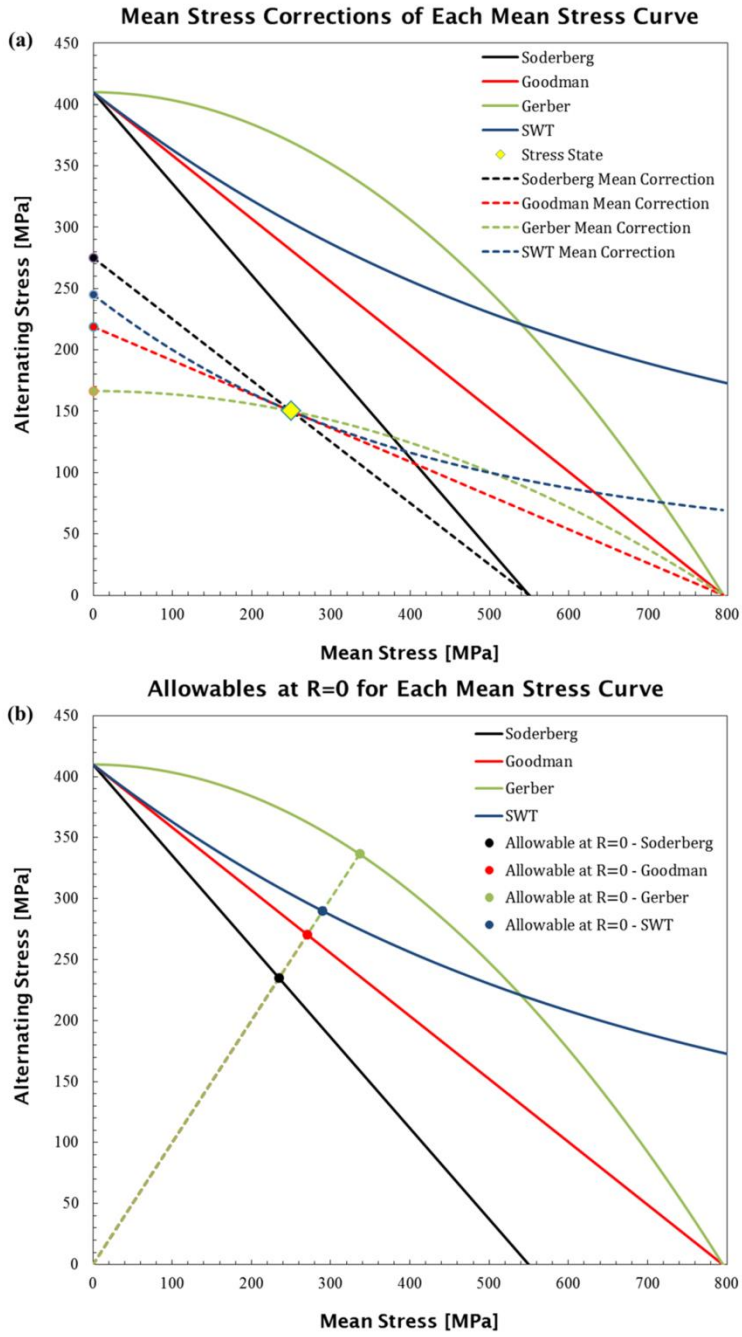

Figure 2.20: a) Mean stress correction for a random stress state, and b) Endurance limit at R=0 for 34Cr4

2.3.3. Invariant Methods Background

Invariant methods are based on invariants or history of the stress tensor/deviatoric stress tensor. The earlier approaches of these methods (Sines [15] and Crossland [16]) can be thought to be the improved versions of static failure criteria based on

stresses on octahedral plane. These methods assume the cause of crack initiation is the alternating value of the octahedral shear stress, which is related to the second invariant of the deviatoric stress tensor, and the cause of crack opening is the hydrostatic stress, which is the first invariant of the stress tensor. Newer versions of these methods (Mamiya and Araujo [39] and GAM [40]) claim alternating value of the deviatoric stress tensor itself should be used as a measure of shear stress. Hydrostatic stress is still used for including the mean stress effects in Mamiya and Araujo method; however, GAM method uses the maximum value of the first principal stress history for the mean normal stress term.

Since octahedral stress is related to square root of second invariant of deviatoric stress tensor ($\sqrt{J_2}$), calculation of this stress measure is necessary for invariant methods. Analytical formulation of $\sqrt{J_2}$ and its alternating value is well defined for proportional loading as stated by Reis et al. [9] and Balthazar and Malcher [41] and can be shown as:

$$\sqrt{J_2} = \sqrt{\frac{3}{2}}\tau_{oct} = \frac{1}{\sqrt{6}}\sqrt{\left(\sigma_x - \sigma_y\right)^2 + \left(\sigma_y - \sigma_z\right)^2 + (\sigma_x - \sigma_z)^2 + 6(\tau_{xy}^2 + \tau_{yz}^2 + \tau_{xz}^2)} \tag{2.45}$$

$$\sqrt{J_{2,\mathrm{a}}} = \frac{1}{\sqrt{6}} \times \sqrt{\left(\sigma_{x,a} - \sigma_{y,a}\right)^2 + \left(\sigma_{y,a} - \sigma_{z,a}\right)^2 + \left(\sigma_{x,a} - \sigma_{z,a}\right)^2 + 6(\tau_{xy,a}^2 + \tau_{yz,a}^2 + \tau_{xz,a}^2)} \tag{2.46}$$

On the other hand, for non-proportional loading these equations are not valid as stress components may have phase shift or frequency difference creating a complex stress path in space. Several methodologies are proposed up to now to determine the correct definition of alternating value of the second deviatoric stress invariant. First attempt to involve the non-proportionality is made by Fucks (as reported by Bernasconi [42]) by using the longest chord method which is

criticized by Papadopoulos et al. [18] as the method leads to non-unique solution for some cases. Papadopoulos suggested another method called Minimum Circumscribed Hypersphere (MCH) which surrounds the second deviatoric stress invariant history with a hyper-sphere (which becomes a circle for plane stress/strain problems). Another definition was made by Freitas et al. [43] which is called Minimum Circumscribed Ellipsoid (MCE) that surrounds the path with an ellipsoid (which becomes an ellipse for plane stress/strain problems).

In literature, experimental data which is used to evaluate the performance of different multiaxial endurance criteria, are based on smooth specimens loaded with synchronous bending/axial and torsion loading with phase shift. This loading creates special stress states which are plane stress and plane strain. For these special cases, Papadopoulos et al. [18] formulated the alternating value of second invariant for MCH approach. Formulation involves the use of deviatoric stresses and Ilyushin space transformation [44] which is shown below.

Stress state for synchronous sinusoidal bending/axial and torsion with phase shift is as follows:

$$\boldsymbol{\sigma} = \begin{bmatrix} \sigma_a \sin(2\pi t/P) + \sigma_m & \tau_a \sin(2\pi t/P - \delta) + \tau_m & 0 \\ \tau_a \sin(2\pi t/P - \delta) + \tau_m & 0 & 0 \\ 0 & 0 & 0 \end{bmatrix} \tag{2.47}$$

where P and δ are period and phase difference respectively. Second deviatoric invariant (J_2) can also be derived from deviatoric stresses as follows:

$$\boldsymbol{s} = \boldsymbol{\sigma} - \frac{1}{3} I_1 \boldsymbol{I} \tag{2.48}$$

$$\sqrt{J_2} = \sqrt{\frac{1}{2}\boldsymbol{s} : \boldsymbol{s}} \tag{2.49}$$

Ilyushin transformation is used in order to facilitate the calculations by transforming the deviatoric stress tensor to a vector in 5 dimensional spaces (5D). Rules for this transformation are as follows:

$$S_1 = \sqrt{\frac{3}{2}}s_x; \quad S_2 = \frac{1}{\sqrt{2}}(s_y - s_z)$$
$$S_3 = \sqrt{2}s_{xy}; \quad S_4 = \sqrt{2}s_{xz}; \quad S_5 = \sqrt{2}s_{yz} \tag{2.50}$$

$$\boldsymbol{S} = [S_1\ S_2\ S_3\ S_4\ S_5] \tag{2.51}$$

As a result

$$\sqrt{J_2} = \sqrt{\frac{1}{2}\boldsymbol{s} : \boldsymbol{s}} = \sqrt{\frac{1}{2}\boldsymbol{S} \cdot \boldsymbol{S}} \tag{2.52}$$

For harmonic bending/axial and torsion loading (loading as a function of sine or cosine), components of this vector are as follows [45]:

$$S_1 = \sqrt{\frac{2}{3}}(\sigma_a \sin(2\pi t/P) + \sigma_m); \quad S_2 = 0;$$
$$S_3 = \sqrt{2}(\tau_a \sin(2\pi t/P - \delta) + \tau_m); \quad S_4 = S_5 = 0 \tag{2.53}$$

This stress state creates an ellipse in $S_1 - S_3$ plane which gives the history of deviatoric second invariant. According to Papadopoulos et al. [18], value of the major semi-axis gives the range of the second deviatoric invariant (MCC approach).

$$\sqrt{J_{2,a}} = \frac{1}{\sqrt{2}}\sqrt{\frac{\sigma_a^2}{3} + \tau_a^2 + \sqrt{\left(\frac{\sigma_a^2}{3} + \tau_a^2\right)^2 - \frac{4}{3}\sigma_a^2\tau_a^2\sin^2(\delta)}} \tag{2.54}$$

For calculation of the alternating value of deviatoric stress path similar proposals were made like in $\sqrt{J_{2,a}}$. Magnitude of the deviatoric stress tensor can be found from;

$$\|\boldsymbol{s}\| = \sqrt{\boldsymbol{s} : \boldsymbol{s}} \tag{2.55}$$

Deperrois [46] proposed the longest chord approach in order to calculate the alternating value of deviatoric stress path. A different methodology is suggested for elliptical stress paths by Mamiya and Araujo [39] which surrounds the stress path with a minimum ellipsoid. This approach is used for calculation of shear stress term in GAM method explained in Section 2.3.4.2. as the loadings in literature create elliptical paths (synchronous harmonic bending-torsion loading with phase shift). For this methodology, alternating value of the stress tensor can be found as follows:

$$D_i = \frac{1}{2}\left(\max_i s_i(t) - \min_i s_i(t)\right); \quad \text{i} = 1,..,5 \tag{2.56}$$

$$\|\boldsymbol{s}\|_a = \sqrt{\sum_{i=1}^{5} D_i^2} \tag{2.57}$$

For general loading, maximum rectangular hull method based on Jacobi rotations in ten two-dimensional spaces (1-2, 1-3, 1-4, 1-5, 2-3, 2-4, 2-5, 3-4, 3-5 and 4-5) is presented by Mamiya et al. [47] which is the most recent solution for the alternating value of deviatoric stress tensor.

2.3.4. Invariant Based Criteria

In this section, historical background and formulations of some widely utilized invariant criteria are clarified.

2.3.4.1. Sines (SNS) and Crossland (CROSS) Criteria

Sines [15, 32] is one of the oldest and well known multiaxial endurance criteria and it is the linear formulation of alternating value of the second invariant of deviatoric stress tensor and the mean value of the first invariant of stress tensor for inclusion of normal mean stresses. Sines came up with this formulation after studying Gough, Pollard [5, 6] and Smith's [48, 49] experimental data that include in total 27 metals and several failure criteria such as Maximum Shear Stress and Octahedral Shear Stress theories. Sines choose to use octahedral shear stresses as the alternating part of the damage parameter since octahedral stresses

can be directly calculated from the stress tensor without any transformations even for 3D stress state (lengthy principal stress calculations are required in the case of Maximum Shear Stress theory). The choice of using hydrostatic stress as the normal mean stress component of the damage parameter and combining this stress value with alternating octahedral shear stress by a linear formulation is based on the experimental data Sines studied. Sines categorized this data set into four groups which are:

- Loading of cyclic axial with mean tension/compression
- Loading of cyclic torsion with mean torsion
- Loading of cyclic bending with mean torsion
- Loading of cyclic torsion with mean bending

He concluded that [7]:

- Mean tension has an adverse effect on axial fatigue strength and the relation is linear unless maximum axial stress does not exceed the axial yield strength
- Mean torsion has no effect on torsional fatigue strength unless maximum shear stress does not exceed the shear yield strength.
- Mean torsion has no effect on bending fatigue strength unless the torsional yield strength is not exceeded by at least 50%.
- Mean bending stress has an adverse effect on torsional fatigue life and the relation is linear.

Based on these conclusions Sines did not use any mean shear stress component in the damage parameter and he claimed that hydrostatic stresses influence the fatigue life with a linear relation. The idea of ineffectiveness of mean torsion influenced many other researchers such as Findley [21], Dang Van [24] and Liu and Mahadevan [50] as these methods also only include the effect of mean

normal stresses. However, this assumption is shown to be incorrect according to Kluger et al. [26] based on test results of Krgo et al.[51], Kallmyer et al. [52] on Ti-6Al-4V and test results of Kluger and Lagoda [53, 54], Kluger [55] on 2017(A)-T4 aluminum alloy. Kluger et al. [26] also stated that mean torsion sensitivity is not observed for all metals (30NCD16 steel stated by Nieslony et al. [56]). Sines damage parameter is as follows:

$$a\sqrt{J_{2,a}} + b\sigma_{h,m} \leq \sigma_{-1} \tag{2.58}$$

Material parameters a and b may be obtained from fully reversed torsion and pulsating bending. For the case of calibration with fully reversed bending and torsion, method leads to a singular solution giving the ratio $\tau_{-1}/\sigma_{-1} = 1/\sqrt{3}$. However, according to Papadopoulos et al. [18] this behavior does not reflect the reality since this ratio is not the same for all metals. Material parameters are as follows:

$$a = r \tag{2.59}$$

$$b = (6\mathrm{r}_0 - \sqrt{3}.\mathrm{r}) \tag{2.60}$$

r and r_0 are stress ratios and they are defined as $r = \sigma_{-1}/\tau_{-1}$; $r_0 = \sigma_{-1}/\sigma_0$. Pulsating bending endurance limit (σ_0) is the maximum stress value (not the alternating stress) at failure point. As seen from the formulation, three endurance limits are required in order to calibrate the Sines criterion which may be a disadvantage compared to other multiaxial criteria (Sections 2.3.4.2. and 2.3.7.). Furthermore, use of mean hydrostatic stress is criticized by Claudio et al. [17] for the case of biaxial tension. For this special stress state, Sines approach calculates the normal mean stress as zero leading to worse estimations compared with Crossland method that uses the same formulation except the mean stress component which is the maximum value of hydrostatic stress.

Crossland [16] is a modification of the Sines criterion and it only differentiates with the mean stress inclusion. Crossland prefers to use maximum hydrostatic

stress as the normal mean stress contribution and it gives better estimations of fatigue lives according to several authors [17, 18 and 19]. General formulation of the criterion is as follows:

$$a\sqrt{J_{2,a}} + b\sigma_{h,max} \leq \sigma_{-1} \tag{2.61}$$

Crossland material constants (a, b) for bending-torsion calibration are given below:

$$a = r \tag{2.62}$$

$$b = 3 - \sqrt{3}r \tag{2.63}$$

2.3.4.2. Gonçalves, Araujo and Mamiya Criterion (GAM)

This method is newer compared to other multiaxial endurance criteria [40]. It is a modification of the method proposed by Mamiya and Araujo [39]. GAM method claims the geometric properties of the rectangular hull enclosing the deviatoric stress history (after transforming the deviatoric stress tensor into a vector in five-dimensional Ilyushin subspace), give the correct measure of alternating shear stress. Authors also criticize the use of hydrostatic stress as a measure of mean normal stress (arguing that it underestimates the effect of normal stress on fatigue life) in other multiaxial endurance criteria (Sines, Crossland, Mamiya and Araujo, Dang Van etc.) and suggest the use of maximum value of the first principal stress history. Although, this criterion does not utilize any invariant for calculation of shear or normal stresses, it is categorized as an invariant method as the method does not fit to any other criteria. General formulation of the method is as follows:

$$a\sqrt{\sum_{i=1}^{5} D_i^2} + b\sigma_{1,max} \leq \sigma_{-1} \tag{2.64}$$

In this formulation D_i are the alternating values of transformed deviatoric stresses:

$$D_i = \frac{1}{2}(\max_t S_i(t) - \min_t S_i(t)) \tag{2.65}$$

GAM material constants for bending-torsion calibration is shown below:

$$a = \frac{\mathrm{r} - 1}{\sqrt{2}(1 - \frac{1}{\sqrt{3}})} \tag{2.66}$$

$$b = \frac{\sqrt{3} - \mathrm{r}}{\sqrt{3} - 1} \tag{2.67}$$

2.3.5. Critical Plane Methods Background

Critical plane theories involve calculation of mean and alternating values of shear and normal stresses on every material plane to find the maximum value of a proposed damage parameter. This task could be achieved by successful coordinate transformations of the stress state. In this section formulations of shear and normal stresses on material planes are presented which are mostly taken from Socie and Marquis [7] and Papadopoulos et al. [18].

For the most general case, a stress vector (traction) acts on a surface that is the combination of stress components. Cauchy's stress theorem, which is based on force equilibrium, states that traction on a surface can be obtained by the dot product of stress state and normal of the surface as follows,

$$\boldsymbol{t} = \boldsymbol{\sigma} \cdot \boldsymbol{n}_{x'} \tag{2.68}$$

Any plane may be defined by two Euler angles θ and φ (Figure 2.21) and direction cosines for oriented axes (x', y' and z') are as follows and shown in Table 2.2,

$$\begin{aligned} \boldsymbol{n}_{x'} &= \begin{bmatrix} l_1 \\ m_1 \\ n_1 \end{bmatrix} = \begin{bmatrix} \sin(\varphi)\cos(\theta) \\ \sin(\varphi)\sin(\theta) \\ \cos(\varphi) \end{bmatrix}, \quad \boldsymbol{n}_{y'} = \begin{bmatrix} l_2 \\ m_2 \\ n_3 \end{bmatrix} = \begin{bmatrix} -\sin(\theta) \\ \cos(\theta) \\ 0 \end{bmatrix} \\ \boldsymbol{n}_{z'} &= \begin{bmatrix} l_3 \\ m_3 \\ n_3 \end{bmatrix} = \begin{bmatrix} -\cos(\varphi)\cos(\theta) \\ -\cos(\varphi)\sin(\theta) \\ \sin(\varphi) \end{bmatrix} \end{aligned} \tag{2.69}$$

Table 2.2: Direction cosines for oriented axes

	x	y	z
x'	l_1	m_1	n_1
y'	l_2	m_2	n_2
z'	l_3	m_3	n_3

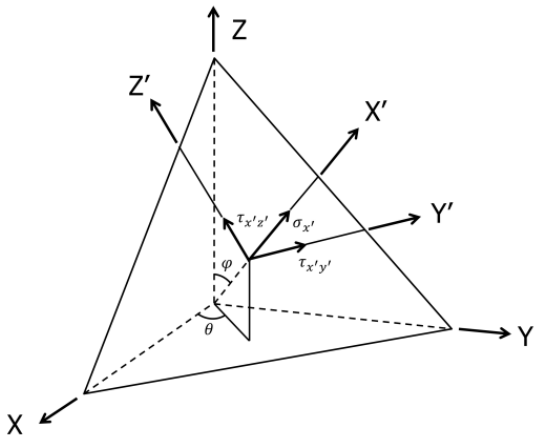

Figure 2.21: Stresses on a plane

Normal and shear stresses acting on the surface can be obtained by projections of traction on oriented axes. Normal stress acting on a plane is as follows,

$$\sigma_{x'} = \sigma_{\mathrm{n}} = \boldsymbol{n}_{\boldsymbol{x}'} \cdot \boldsymbol{t} = \boldsymbol{n}_{\boldsymbol{x}'} \cdot \boldsymbol{\sigma} \cdot \boldsymbol{n}_{\boldsymbol{x}'} \tag{2.70}$$

$$\begin{aligned} \sigma_{x'} = \sigma_{\mathrm{n}} &= \begin{bmatrix} l_1 & m_1 & n_1 \end{bmatrix} \begin{bmatrix} \sigma_x & \tau_{xy} & \tau_{xz} \\ \tau_{xy} & \sigma_y & \tau_{yz} \\ \tau_{xz} & \tau_{yz} & \sigma_z \end{bmatrix} \begin{bmatrix} l_1 \\ m_1 \\ n_1 \end{bmatrix} \\ &= \sigma_x l_1^2 + \sigma_y m_1^2 + \sigma_z n_1^2 + 2(\tau_{xy} l_1 m_1 + \tau_{xz} l_1 n_1 + \tau_{yz} m_1 n_1) \end{aligned} \tag{2.71}$$

Normal stress has a significant property from the point of multiaxial fatigue. Although magnitude of normal stress changes with time, it always acts along the same direction for any loading history. Therefore, mean and alternating values of normal stress can be obtained by [45],

$$\sigma_{x',m} = \sigma_{\mathrm{n,m}} = \frac{1}{2}(\max_{t\in T}(\boldsymbol{n_{x'}}\cdot\boldsymbol{\sigma(t)}\cdot\boldsymbol{n_{x'}}) + \min_{t\in T}(\boldsymbol{n_{x'}}\cdot\boldsymbol{\sigma(t)}\cdot\boldsymbol{n_{x'}})) \tag{2.72}$$

$$\sigma_{x',a} = \sigma_{\mathrm{n,a}} = \frac{1}{2}(\max_{t\in T}(\boldsymbol{n_{x'}}\cdot\boldsymbol{\sigma(t)}\cdot\boldsymbol{n_{x'}}) - \min_{t\in T}(\boldsymbol{n_{x'}}\cdot\boldsymbol{\sigma(t)}\cdot\boldsymbol{n_{x'}})) \tag{2.73}$$

where t is any time in time history (T).

Expressions for shear stresses on the material plane are given by,

$$\tau_{x'y'} = \boldsymbol{n_{y'}}\cdot\boldsymbol{t} = \boldsymbol{n_{y'}}\cdot\boldsymbol{\sigma}\cdot\boldsymbol{n_{x'}} \tag{2.74}$$

$$\tau_{x'y'} = \begin{bmatrix} l_2 & m_2 & n_2 \end{bmatrix}\begin{bmatrix} \sigma_x & \tau_{xy} & \tau_{xz} \\ \tau_{xy} & \sigma_y & \tau_{yz} \\ \tau_{xz} & \tau_{yz} & \sigma_z \end{bmatrix}\begin{bmatrix} l_1 \\ m_1 \\ n_1 \end{bmatrix} \tag{2.75}$$

$$\tau_{x'y'} = \sigma_x l_1 l_2 + \sigma_y m_1 m_2 + \sigma_z n_1 n_2 + \tau_{xy}(l_1 m_2 + l_2 m_1) + \tau_{yz}(m_1 n_2 + m_2 n_1) + \tau_{zx}(l_1 n_2 + l_2 n_1) \tag{2.76}$$

$$\tau_{x'z'} = \boldsymbol{n_{z'}}\cdot\boldsymbol{t} = \boldsymbol{n_{z'}}\cdot\boldsymbol{\sigma}\cdot\boldsymbol{n_{x'}} \tag{2.77}$$

$$\tau_{x'z'} = \begin{bmatrix} l_3 & m_3 & n_3 \end{bmatrix}\begin{bmatrix} \sigma_x & \tau_{xy} & \tau_{xz} \\ \tau_{xy} & \sigma_y & \tau_{yz} \\ \tau_{xz} & \tau_{yz} & \sigma_z \end{bmatrix}\begin{bmatrix} l_1 \\ m_1 \\ n_1 \end{bmatrix} \tag{2.78}$$

$$\tau_{x'z'} = \sigma_x l_1 l_3 + \sigma_y m_1 m_3 + \sigma_z n_1 n_3 + \tau_{xy}(l_1 m_3 + l_3 m_1) + \tau_{yz}(m_1 n_3 + m_3 n_1) + \tau_{zx}(l_1 n_3 + l_3 n_1) \tag{2.79}$$

It is more convenient to use the resultant shear stress vector for multiaxial fatigue calculations which includes the combined effects of shear stress components. Magnitude of this vector is as follows,

$$\tau_R = \sqrt{(\tau_{x'y'})^2 + (\tau_{x'z'})^2} \tag{2.80}$$

As already mentioned before, special cases plane stress and plane strain plays an important role in multiaxial fatigue in order to determine the prediction capabilities of different methods. Therefore, analytical derivations were made for stress measures on material planes by Papadopoulos et al. [18]. History of the normal stress can be obtained using the stress state given in (2.47) in (2.70):

$$\sigma_{x'}(t) = \sigma_{\mathrm{n}}(t) = \sin^2(\varphi)\{\left[\sigma_a \sin\left(\frac{2\pi t}{P}\right) + \sigma_m\right]\cos^2(\theta) + \left[\tau_a \sin\left(\frac{2\pi t}{P} - \delta\right) + \tau_m\right]\sin(2\theta)\} \quad (2.81)$$

Mean value of the normal stress is the part which is independent of time.

$$\sigma_{x',m} = \sigma_{\mathrm{n,m}} = \sin^2(\varphi)\,(\sigma_m \cos^2(\theta) + \tau_m \sin(2\theta)) \quad (2.82)$$

Since any harmonic stress component can be presented as the sum of it's mean and alternating values, alternating value of the normal stress is the value obtained by subtraction of (2.82) from the maximum value of (2.81).

$$\sigma_{x',a} = \sigma_{\mathrm{n,a}} = \sin^2(\varphi) \times \sqrt{\sigma_a^2 \cos^4(\theta) + 4\tau_a^2 \sin^2(\theta)\cos^2(\theta) + 2\sigma_a\tau_a \sin(2\theta)\cos^2(\theta)\cos(\delta)} \quad (2.83)$$

History of the shear stresses acting on a material plane can be obtained by using the stress state given by (2.47) in (2.74) and (2.77):

$$\tau_{x'y'}(t) = \frac{1}{2}\left[\sigma_a \sin\left(\frac{2\pi t}{P}\right) + \sigma_m\right]\sin(2\varphi)\cos^2(\theta) + \frac{1}{2}\left[\tau_a \sin\left(\frac{2\pi t}{P} - \delta\right) + \tau_m\right]\sin(2\varphi)\sin(2\theta) \quad (2.84)$$

$$\tau_{x'z'}(t) = \frac{1}{2}\left[\sigma_a \sin\left(\frac{2\pi t}{P}\right) + \sigma_m\right]\sin(\varphi)\sin(2\theta) - \left[\tau_a \sin\left(\frac{2\pi t}{P} - \delta\right) + \tau_m\right]\sin(\varphi)\cos(2\theta) \quad (2.85)$$

From lengthy manipulations, (2.84) and (2.85) lead to:

$$\tau_{x'y'}(t) = -p\sin\left(\frac{2\pi t}{P}\right) - q\cos\left(\frac{2\pi t}{P}\right) + \left[\frac{\sigma_m}{2}\cos^2(\theta) + \frac{\tau_m}{2}\sin(2\theta)\right]\sin(2\varphi) \quad (2.86)$$

$$\tau_{x'z'}(t) = -f\sin\left(\frac{2\pi t}{P}\right) - g\cos\left(\frac{2\pi t}{P}\right) + \left[\frac{\sigma_m}{2}\sin(2\theta) - \tau_m\cos(2\theta)\right]\sin(\varphi) \tag{2.87}$$

where auxiliary functions f, g, p and q are:

$$\begin{aligned} f &= \sin(\varphi)(-\frac{\sigma_a}{2}\sin(2\theta) + \tau_a\cos(2\theta)\cos(\delta)) \\ g &= -\tau_a\sin(\varphi)\cos(2\theta)\sin(\delta) \\ p &= -\frac{1}{2}\sin(2\varphi)(\sigma_a\cos^2(\theta) + \tau_a\sin(2\theta)\cos(\delta)) \\ q &= \tfrac{1}{2}\tau_a\sin(2\varphi)\sin(2\theta)\sin(\delta) \end{aligned} \tag{2.88}$$

Resultant shear stress on the material plane creates an ellipse for harmonic axial/bending torsion loading. Mean of this shear stress can be obtained from (2.86) and (2.87):

$$\tau_{R,m} = T_m = \sqrt{\left[\left(\frac{\sigma_m}{2}\cos^2(\theta) + \frac{\tau_m}{2}\sin(2\theta)\right)\sin(2\varphi)\right]^2 + \left[(\frac{\sigma_m}{2}\sin(2\theta) - \tau_m\cos(2\theta))\sin(\varphi)\right]^2} \tag{2.89}$$

Major semi axes of the ellipse created by two shear stresses are as follows:

$$e_{maj}, e_{min} = \sqrt{\frac{f^2 + g^2 + p^2 + q^2}{2} \pm \sqrt{\left(\frac{f^2 + g^2 + p^2 + q^2}{2}\right)^2 - (fq - gp)^2}} \tag{2.90}$$

for which e_{maj} is the major semi axis and e_{min} is the minor semi axis of the ellipse. According to Papadopoulos et al. [18] alternating value of the resultant shear stress corresponds to the half-length of the major semi axis (MCC approach). Thus,

$$\tau_{R,a} = T_a = \sqrt{\frac{f^2 + g^2 + p^2 + q^2}{2} + \sqrt{\left(\frac{f^2 + g^2 + p^2 + q^2}{2}\right)^2 - (fq - gp)^2}} \quad (2.91)$$

These equations are used for formulation of critical plane methods and for their calibrations at different loading conditions.

2.3.5.1. Alternating value of resultant shear stress

Calculation of mean and alternating values of resultant shear stress is straightforward for proportional loading as both shear stresses vary proportionally in magnitude without any change in their direction. However, same is not true for non-proportional loading as both the direction and magnitude changes. Therefore, sophisticated methods are required which is discussed in this section.

There are several methods for determining the alternating and mean values of the resultant shear stress. Those methods are Longest Chord (LC), Longest Projection (LP), Minimum Circumscribed Circle (MCC) and the most recent method, Maximum Rectangular Hull (MRH).

2.3.5.1.1. Longest Chord (LC)

One of the very first methods is the longest chord method. In longest chord, any two points in the shear stress path Ψ (Figure 2.22) are joined with a straight line and the line with the maximum length is called the longest chord. Method defines the alternating shear stress as the half length of the longest chord while mean value is the magnitude of the vector drawn to the midpoint of the longest chord. Although computation is really simple and fast, solution is not unique where there may exist more than one chord with the same length. A common example (see Figure 2.22b) to this situation is the shear stress path of an isosceles triangle in which alternating shear stress is well defined; however, due to existence of two different mean shear stress vectors an ambiguous situation arises about the mean value of the shear stress [27, 57].

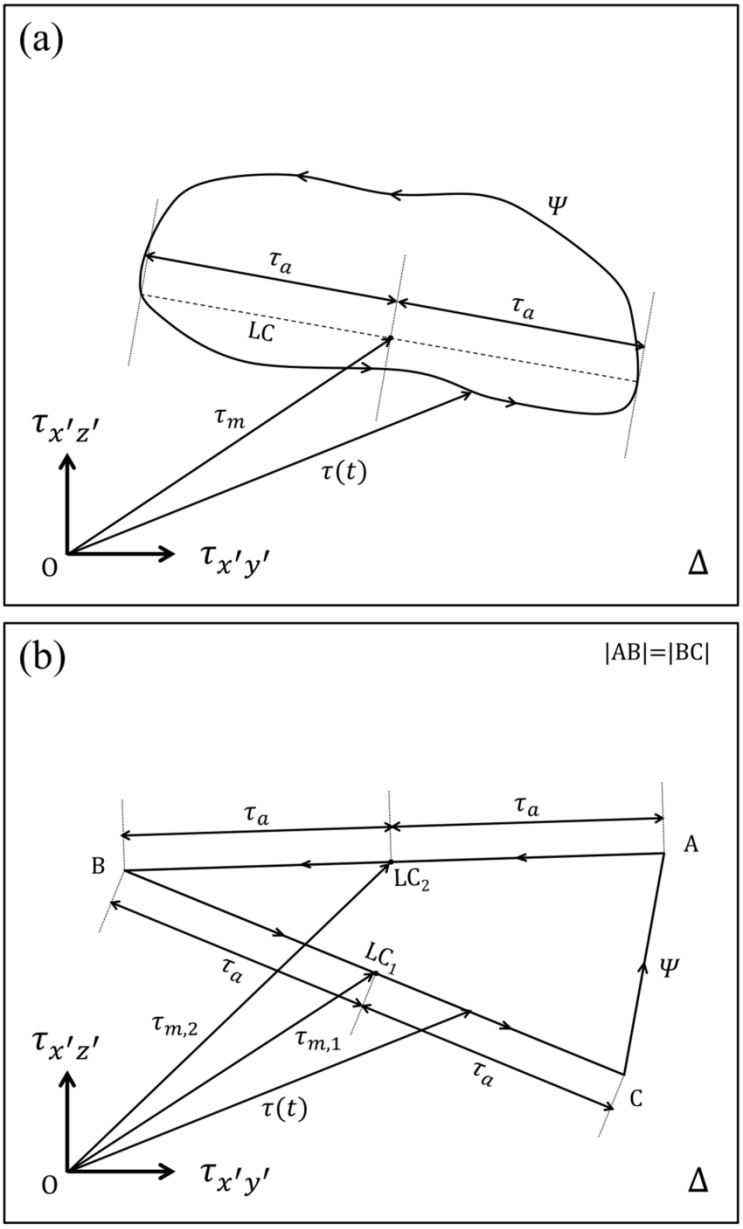

Figure 2.22: a) Longest chord definition, b) Drawback of Longest chord

2.3.5.1.2. Longest Projection (LP)

In longest projection method, main purpose is to maximize the projection of stress path Ψ on a straight line passing through the origin. After longest (maximum) projection is found, alternating shear stress is the half length of the projection whereas mean value is the distance between the origin and the midpoint of the projection. Like in the longest chord method, this approach

suffers from the same problem which questions solutions' uniqueness for mean shear stress [57]. To illustrate, for some cases method calculates mean shear stress as zero (see Figure 2.23b) even the shear stress path Ψ has non-zero mean value [27].

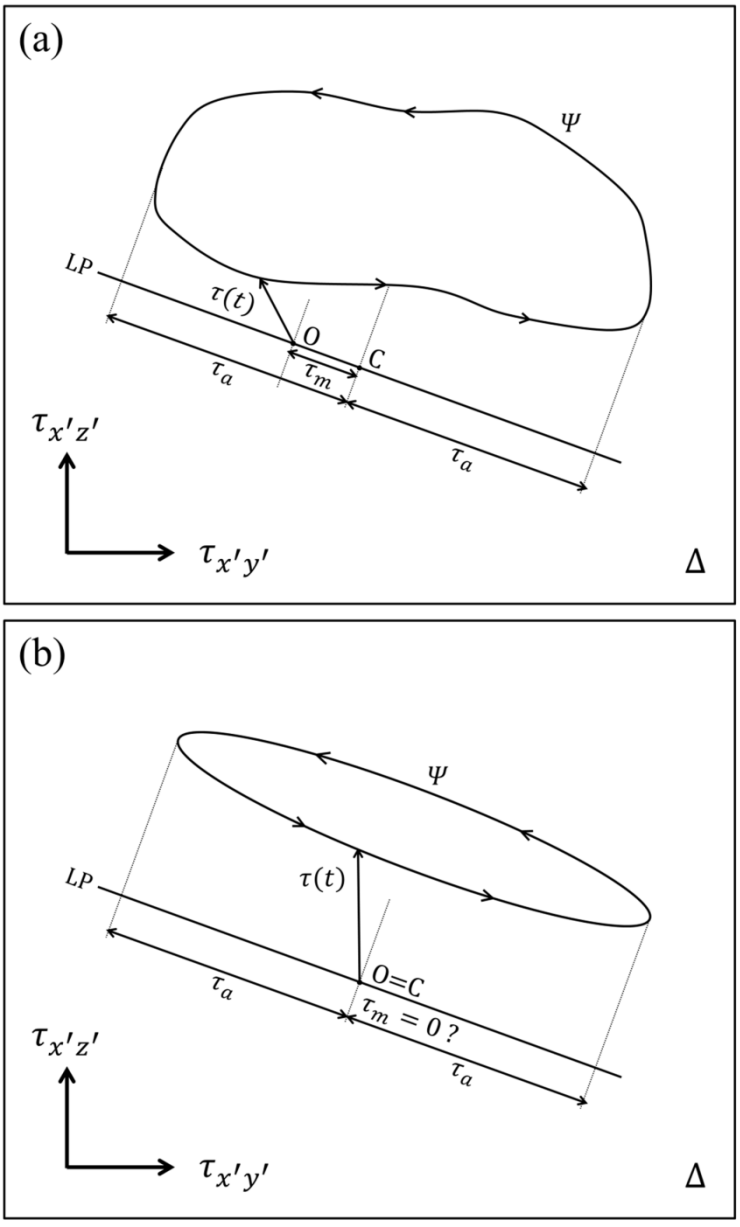

Figure 2.23: a) Longest projection definition, b) Drawback of Longest projection

2.3.5.1.3. Minimum Circumscribed Circle (MCC)

In order to cope with the drawbacks stated above, enclosure methods such as MCC and MRH were developed. Minimum Circumscribe Circle (MCC) method was first proposed by Dan Vang et al. [58] and later improved by Papadopoulos et al. [18]. The idea of the MCC is basically environing the shear stress path Ψ with a circle, thus the radius of the circle gives the alternating value of the shear stress and mean value is the magnitude of the vector joining the center of the MCC and the origin.

The problem of computing the MCC is not an easy task as complex algorithms are required. In literature there have been several proposals for finding the MCC. Algorithms are mainly based on geometrical computations that use two or more data points for constructing the minimum circle and these algorithms are explained in detail below.

2.3.5.1.3.1. Incremental Algorithm

When Dang Van et al. [58] came out with the idea of finding MCC of the shear stress path for obtaining mean and alternating values of the resultant shear stress, they also proposed an incremental algorithm for an approximate solution of the problem. This algorithm was inspired from the physical mechanisms of isotropic and kinematic hardening which are usually employed in theory of plasticity.

Incremental algorithm initializes by forming a circle with an infinite small (close to zero) radius and an initial center, which is usually chosen as the centroid of the shear stress path (centroid of the data points). This circle can be expanded and shifted towards data points on the shear stress path. The expansion of the circle is analogous to the isotropic hardening in which the elastic domain increases and shift of the circle is analogous to kinematic hardening in which the elastic domain moves in the stress space. Algorithm searches all data points one by one and if any shear stress is outside the range of the circle, circle expands with an expansion coefficient of κ and it is shifted towards the shear stress point so that this data point now lies inside the circumscribing circle. However, one may

notice that when a data point is surrounded, another point may be left out from the circle as it not only expands but also shifts leading to an iterative process for engulfing all the data points. When the distance of shear stresses is less than or equal to the radius of the circumscribing circle, algorithm stops and the MCC is found. According to Bernasconi and Papadopoulos [57], this algorithm runs in linear time with shear stress points, which can be shown with O(n) time. On the other hand, this approach has some drawbacks as stated by Weber et al. [59] and these drawbacks are as follows:

- Excluding some special cases, solution is always approximate. Furthermore the accuracy and the speed of the algorithm strongly depend on the value of κ. For lower values of κ, accuracy will be high but speed drops down and the opposite is true for higher values of κ.

- Final result should not depend on the sequence of the data points examined. However, for incremental algorithm different sequences for which the shear stress points are searched leads to different final results of MCC.

- Algorithm may not converge to a solution if radius growth is not equal or greater than the displacement of the circle center.

2.3.5.1.3.2. Points-Combination Algorithm

Considering the drawbacks of the incremental algorithm, which may lead to inaccurate solutions or long calculation times due to convergence issues, Ballard et al. [60] and later Papadopoulos [61] proposed another algorithm. In this algorithm, two set of circles are formed. First set includes all the possible circles constructed by pairs of points (i.e. chords) and the second set includes circles constructed by triple set of points (i.e. triangles). Then, for each circle in the first set, all data points (shear stresses) are checked whether they are enclosed by the circle or not. After control of the first circle set is completed, the second set is controlled and finally circle with minimum diameter, which circumscribes all the data points, is selected from both sets. Ballard et al. suggests that the algorithm

shall stop the controlling operation when a circle in the first set fulfills the necessary condition (surrounding all data points); on the other hand, according to Papadopoulos search should continue until control of the second set is completed. This algorithm does not have the drawbacks of the incremental algorithm and the solution is exact; however, computational cost may be too high for large data sets. Points combination algorithm requires the evaluation of distances of each data to the center of each circle which demands the following amount of computations according to Bernasconi and Papadopoulos [57]:

$$n_{op} = (n-2).\frac{n!}{2(n-2)!} + (n-3).\frac{n!}{3(n-3)!} \\ = \frac{1}{2}n(n-1)(n-2) + \frac{1}{6}n(n-1)(n-2)(n-3) \quad (2.92)$$

n_{op} in (2.92) is the number of total evaluations while n is the total data points. From (2.92), one may interpret that the algorithm runs in $O(n^4)$ time. This high amount of computation is due to the search of all possible circles which may not be necessary for finding the MCC. Therefore, Bernasconi and Papadopoulos [57] suggested a modification based on the improvements recommended by Weber et al. [59] for critical plane search algorithm. As a result of this modification, amount of calculations would be as follows:

$$n_{op} = 3[n(n-1) - 3] \quad (2.93)$$

which is a second order polynomial and the new run time is $O(n^2)$.

2.3.5.1.3.3. Optimization Algorithm (fminmax)

Although points-combination algorithm gives exact solution, the calculation time may become large depending on the number of data points. Therefore a different approach is presented by Bernasconi et al. [42, 57] stating that the MCC is actually a min-max optimization problem and it can be solved by a minmax algorithm available in commercial mathematical softwares. These minmax algorithms give exact solution with faster computation time than points

combination algorithm; however, they are not as fast as the incremental algorithm as shown by Bernasconi and Papadopoulos. [57].

For any minmax algorithm, at first, mean stress vector is calculated and then alternating value of the shear stress may be obtained by an algebraic calculation. Mean shear stress vector may be obtained by minimizing an arbitrary shear vector τ* which maximizes the norm of the difference (τ-τ*) as follows,

$$\boldsymbol{T_m} = \min_{\tau^*}(\max_t \|\boldsymbol{\tau(t)} - \boldsymbol{\tau}^*\|) \tag{2.94}$$

After center of the MCC (mean shear stress vector) is obtained, radius which corresponds to the alternating value of shear stress is the maximum value of the norm of the difference (τ-τ*) which can be formulated as

$$T_a = \max_t \|\boldsymbol{\tau(t)} - \boldsymbol{T_m}\| \tag{2.95}$$

For this study fminmax algorithm of MATLAB Optimization Package, which performs a sequential quadratic programing routine, is utilized.

2.3.5.1.3.4. Randomized Algorithm

Another type of algorithm that is encountered in literature is the randomized algorithm proposed by Berg et al. [62]. This algorithm is similar to points-combination algorithm but this time points are chosen randomly and circles may be formed with two or three data points. Again all the data points are controlled whether they are encircled or not. However, with randomized algorithm MCC may be obtained without controlling all the possible circles that are constructed with two or three data points. Like in points-combination algorithm solution is exact. Main advantage of the randomized algorithm is that it has a run time of O(n) as claimed by Bernasconi and Papadopoulos [57]. Steps of the algorithm can be summarized as follows:

1. Data points are sorted randomly and stored in a vector. Then an initial circle is constructed from the first two points of this vector.

2. Data points other than the first two points are controlled whether they are encircled or not. If points lie inside the circle, the circle remains unchanged. However, when a point comes out to be outside the initial circle, then all the data points investigated are passed to a subroutine.

3. Under the first subroutine, the point which is outside the initial circle is chosen and called q1. Other data points are randomly sorted and stored in a vector. A new circle is constructed with the point q1 and the first point of this new vector. Again all data points in the vector are controlled whether they lie in the new circle or not. If a point comes out to be outside the circle, then all data points investigated are passed to another subroutine.

4. Under this second subroutine, the point which is outside the initial circle is chosen and called q2. Other data points are randomly sorted and stored in a vector. A new circle is constructed with the point q1 and the q2. Again all data points in the vector are controlled whether they lie in the new circle or not. If a point comes out to be outside the circle, this point is called p and a new circle is constructed with q1, q2 and p. After the second subroutine, there are two possibilities of circles; a circle constructed with q1 and q2 or a circle constructed with q1, q2 and p.

After step 4 is completed, procedure returns to step 3 with the circle found in step 4 being the initial circle of step 3. Then step 3 continues to control the data points and whenever necessary step 4 is called. After step 3 is completed, procedure returns back to step 2 with the initial circle as the one found in step 3. Then, remaining data points of the first randomly sorted data points are controlled. Again step 3 is called whenever it is necessary. Algorithm stops when all the data points of the first randomly sorted data points are controlled and MCC is found.

For this study fminmax and randomized algorithm are employed as both algorithms yield exact solution and they are the fastest ones in literature.

Minimum circumscribed circle gives a unique solution unlike Longest Chord and Longest Projection and currently it is the most popular method [28]. However, the method has some drawbacks. One drawback is that MCC requires complicated optimization algorithms. Another drawback is MCC method may not distinguish between proportional and non-proportional loading i.e. method bounds some proportional and non-proportional stress histories with the same MCC [28, 63]. For MCC, two stress paths (Ψ_1, Ψ_2) are shown in Figure 2.24b. Ψ_1 is a non-proportional stress history while Ψ_2 is a proportional stress history. As can be seen from the figure same alternating shear stress is calculated for both histories which do not reflect the reality since experimental studies show non-proportional histories are more damaging than proportional ones [26-30].

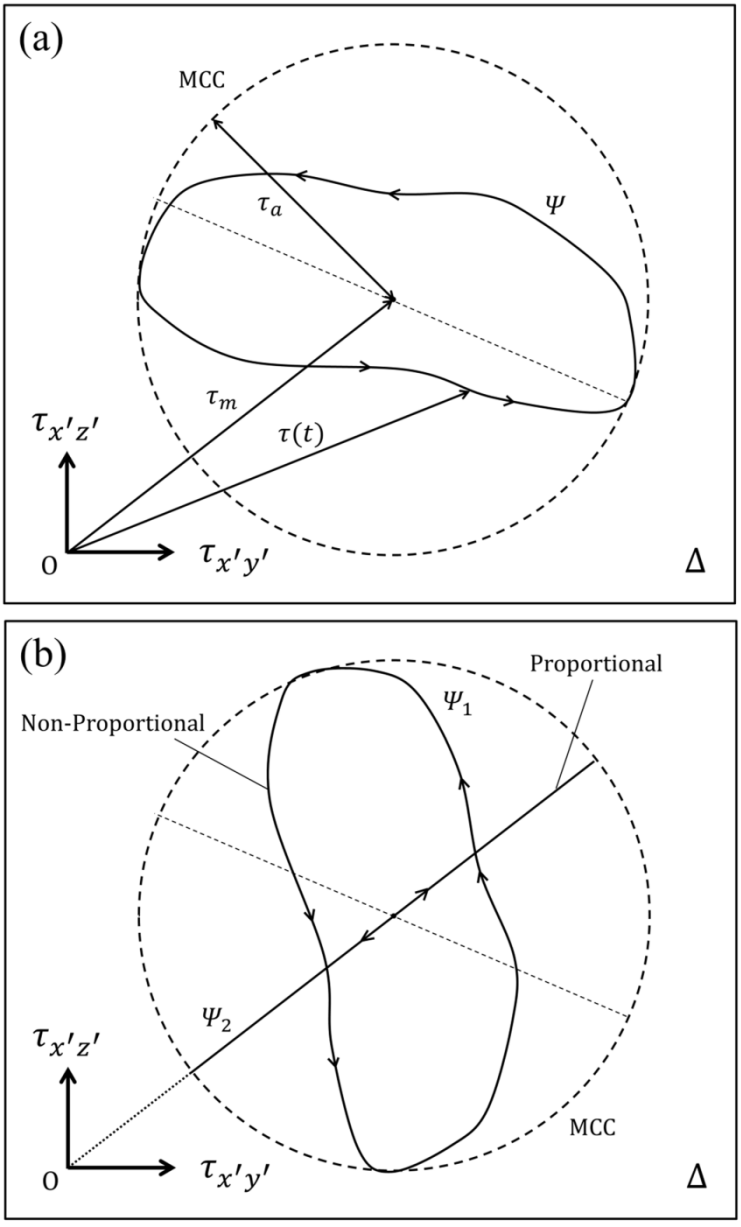

Figure 2.24: a) Minimum circumscribed circle definition, b) Drawback of Minimum circumscribed circle

2.3.5.1.4. Maximum Rectangular Hull (MRH)

Maximum Rectangular Hull (MRH), which is first introduced by Mamiya et al. [47] for invariant methods and later by Araujo et al. [28] for critical plane methods, does not have drawbacks stated above. Main idea of the MRH is to enclose the shear stress path Ψ with a rectangular hull (RH) and to find the maximum of RH by 2D rotation on material plane Δ (see Figure 2.25b). Half

sides of the rectangular hull for an orientation of α may be obtained from (Figure 2.25a):

$$a_k(\alpha) = \frac{1}{2}\left(\max_t\left(\tau_k(\alpha,t)\right) - \min_t\left(\tau_k(\alpha,t)\right)\right), \quad k = 1,2 \tag{2.96}$$

For each rectangular hull alternating value of the resultant shear stress is defined as:

$$T_a(\alpha) = \sqrt{a_1^2(\alpha) + a_2^2(\alpha)} \tag{2.97}$$

Maximum Rectangular Hull is defined as the hull where orientation α maximizes the alternating shear stress. Once the MRH is obtained, like in MCC distance from origin to the center of MRH gives the mean value of resultant shear stress. In this study, maximum rectangular hull search is carried out with 1^o increments from 0^o up to 90^o.

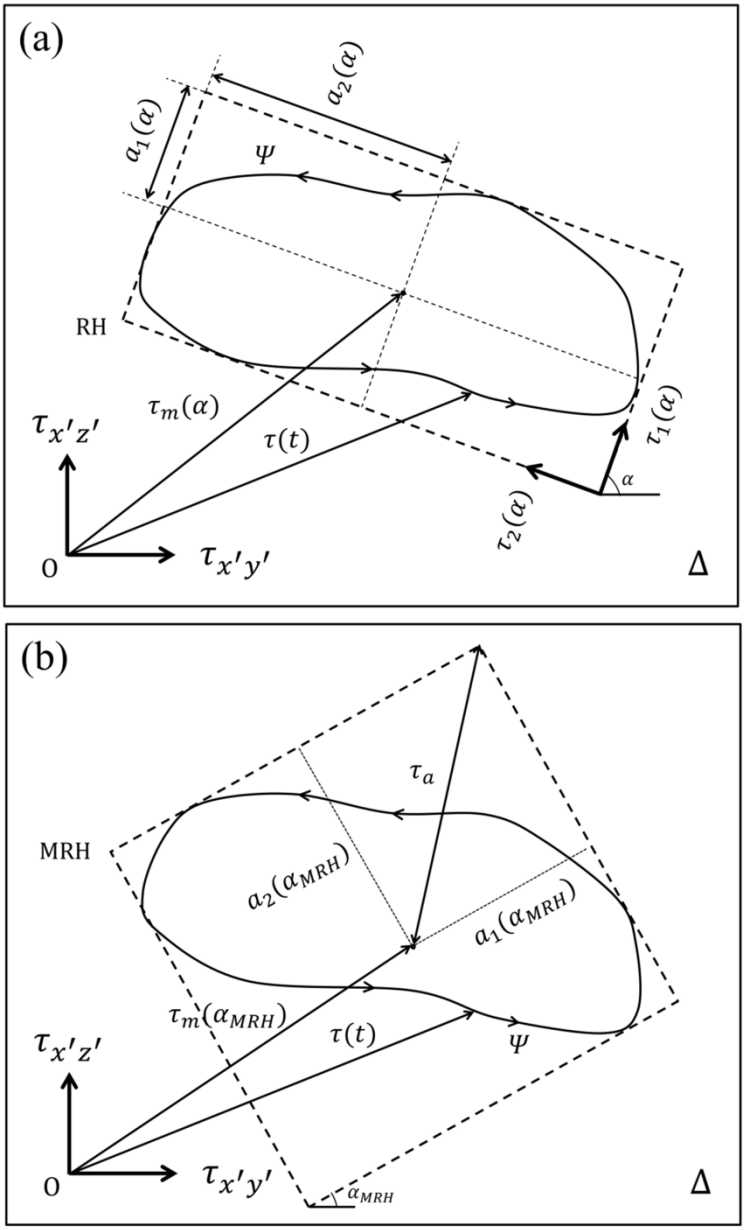

Figure 2.25: a) Rectangular hull, b) Maximum rectangular hull

2.3.6. Critical Plane Definitions

In literature, different approaches have been proposed for defining the critical plane. Proposals are mostly based on physical mechanisms of crack initiation and crack opening. There are three approaches according to Papuga [19] and Li et al. [11] which are Maximum Shear Stress Amplitude (MSA), Maximum Damage

Parameter (MDP) and Critical Plane Deviation (CPD). These approaches are explained in detail below:

2.3.6.1. Maximum Shear Stress Amplitude (MSA)

According to maximum shear stress amplitude approach, shear stresses are the decisive stress values that determine the critical plane. This assumption supposes normal stresses are only effective for crack opening not for crack initiation. Plane with the maximum shear stress amplitude (or alternating shear stress) is accepted to be the critical plane. However the original idea appears to create an ill-posed problem since there may be more than one plane that experiences the maximum shear stress amplitude. This problem was discussed by Araujo et al. [28] and an additional step is proposed in critical plane algorithm. Authors' proposal is to find the plane with the maximum normal stress and the shear stress amplitude within a tolerance of the maximum value of shear stress amplitude. Although this algorithm solves the uniqueness problem it clearly increases the calculation time. Matake [64] and Susmel [65] methods are some examples of this approach.

2.3.6.2. Maximum Damage Parameter (MDP)

Maximum damage parameter approach assumes the plane with maximum value of the damage parameter caused by shear and normal stress components leads to failure of the component. Unlike MSA, MDP approach assumes that normal stresses also have effect in crack initiation. This concept of critical plane is quite popular as many researches preferred this assumption. Findley [21], Dang Van [24] and Papuga PCR [66] methods are some examples that use this approach for finding the critical plane.

2.3.6.3. Critical Plane Deviation (CPD)

Critical plane deviation approach not only tries to obtain the critical plane but also the deviation of the critical plane from the fracture plane for which the crack is observed in macro level. According to this approach, first the fracture plane is attained by assuming it is the plane with maximum value of the alternating normal stress and then the deviation of the critical plane is searched by

maximization of the damage parameter. This deviation is not only depends on the stress state but also the type of material that is loaded. There are two methods which are Liu and Mahadevan [50] and Carpinteri and Spagnoli [67] that use this approach. Both methods give quite close estimations of the deviation angle for the test data presented by Macha [68].

2.3.7. Critical Plane Criteria

In this section, historical background and formulations of some widely utilized critical plane criteria are clarified. All the critical plane criteria examined here adopt the MDP assumption.

2.3.7.1. Findley Criterion (FIN)

Idea of calculating shear and normal stress on a material plane and formulating a damage parameter as a combination of these stress measures was first proposed by Stanfield [20]. However, Stanfield did not verify these proposals nor he made extensive studies based on experimental data. Damage parameter he proposed is the linear combination of alternating resultant shear stress and normal stress acting on a material plane. Same formulation was come out by Stullen and Cummings [69] with a critical plane concept, assuming the critical plane is the material plane in which the ratio of alternating resultant shear stress to normal stress is maximum. Findley [21] proposed a damage parameter with again similar formulation but with a different mean stress term (maximum value of the normal stress) and a different critical plane definition. Parabolic forms were also studied by Findley using Gough and Pollard's experimental data [5, 6]; however, linear formulation was found to be sufficient. Findley defines the critical plane as the material plane where damage parameter is maximized (MDP approach). This damage parameter usually presented as [7, 21, 70, 71, 72, 59, 63, 26];

$$T_a + k\sigma_{n,max} \leq f \tag{2.98}$$

where k and f are material constants, k being the weighting constant of the normal stress and f being the damage allowable. However, for better

understanding the effects of different shear and normal stress measures and for methods investigated to be consistent in formulations, demonstration used by Papuga [45] is obtained:

$$a.T_a + b.\sigma_{n,max} \leq \sigma_{-1} \tag{2.99}$$

Findley material constants for the calibration bending-torsion are shown below:

$$a = 2\sqrt{r-1} \tag{2.100}$$

$$b = 2 - \mathrm{r} \tag{2.101}$$

2.3.7.2. Dang Van Criterion (DV)

Dang Van [24] is one of the widely used and implemented critical plane criteria. Method is based on stresses on mesoscopic scale (grain level). The idea of the method comes from the observations that fatigue crack nucleation is a local process which starts at grains that are plastically deformed and form slip bands. According to the criterion, fatigue failure does not occur when plastically deformed grains are stabilized by neighboring grains, which are elastically deformed, at the state of stable elastic shakedown. However, if the material reaches a plastic shakedown state, in which persistent slip bands are formed, fatigue failure will occur even though the material shows an elastic behavior on macroscopic scale.

Criterion is the linear combination of instantaneous mesoscopic shear stress and the hydrostatic normal stress (same value for mesoscopic and macroscopic scale). When the combination of these stress quantities exceeds the elastic stress state level, fatigue failure occurs. Mesoscopic shear stress is a deviatoric stress measure (calculated according to Tresca maximum shear stress theory) that includes the effects of isotropic and kinematic hardening of the material. Criterion can be formulated as follows:

$$\tau_{meso}(t) + k\sigma_h(t) \leq f \tag{2.102}$$

where k and f are material parameters, like in Findley k is the weighting of the normal stress (for Dang Van it is the hydrostatic stress) and f is the damage allowable. Although this is the original version proposed by Dang Van, a different form applicable to macroscopic scale is commonly used [70, 71, 26, 19, 14, 73] which is also adopted in this study. It is worth to mention that in macroscopic scale there are different approaches. Kluger and Lagoda [26] use instantaneous shear and hydrostatic stresses while Papuga [19] suggested the use of alternating value of shear stress and maximum value of hydrostatic stress as estimations are improved for non-proportional loadings. Formulation used here is as follows:

$$a.T_a + b.\sigma_{h,max} \leq \sigma_{-1} \tag{2.103}$$

Critical plane is assumed to be the plane with maximum of the damage parameter and the material constants for bending-torsion calibration are shown below:

$$a = \mathrm{r} \tag{2.104}$$

$$b = 3 - \frac{3}{2}r \tag{2.105}$$

2.3.7.3. Robert Criterion (RB)

Robert criterion [74, 75] is a modification of the Findley criterion. This method separates the effects of alternating and mean parts of the normal stress in order to improve estimation capability of Findley criterion for loadings with mean stresses. However, this separation comes with a price as the criterion requires another material parameter for calibration. Since only the mean normal stress part is modified, both Findley and Robert criteria give same estimations for loadings without mean stresses. According to Papuga [45, 19], a slight improvement is observed for loadings with mean stresses as the Robert criterion shifts the average value of estimations to zero while the scatter is increased and the range is very similar compared to Findley criterion. Furthermore, Papuga states that the linear combination of alternating and mean values of the normal stress has made the

criterion very sensitive to mean normal stress effect. Criterion can be formulated as follows:

$$a.T_a + b.\sigma_{n,a} + c.\sigma_{n,m} \leq \sigma_{-1} \tag{2.106}$$

Robert criterion does not fit to equation (2.40) completely since it is a three parameter method. As a result, criterion requires three endurance limits for calibration. Material parameters may be obtained from fully reversed axial/bending, fully reversed torsion and pulsating axial/bending and their values are given below:

$$a = 2.\sqrt{r-1} \tag{2.107}$$

$$b = 2 - r \tag{2.108}$$

$$c = \frac{2.\sigma_{-1}}{\sigma_0} - \frac{\sigma_0}{2.\sigma_{-1}}(r-1) - (2+r) \tag{2.109}$$

2.3.7.4. Papuga PCR Criterion (PCR)

Papuga carried out an extensive study for developing a multiaxial endurance criterion that is suitable for both phase and mean stress effect in his PhD thesis [45]. First, several combinations of alternating shear stress with alternating normal stress and hydrostatic stress are tested and Papuga concluded that use of alternating hydrostatic stress is not suitable for correlating the phase effect. Therefore, a formulation including alternating normal stress is chosen and the study continued for inclusion of mean stress effect. Also linear and non-linear formulations are investigated and it resulted in the choice of a non-linear damage parameter that is consisted of alternating shear and normal stress values as damage indicators. For including the mean stress effect, three different options are examined. These possible solutions are to utilize the maximum normal stress (σ_{max}), SWT mean stress correction ($\sqrt{\sigma_a.\sigma_{max}}$) or to separately employ alternating and mean values of normal stresses (σ_a and σ_m) which is inspired from the Robert criterion. After all these combinations are analyzed for the

experimental data set studied, the approach proposed by Robert is adopted but with an empirical constant weighting the mean normal stress component. Papuga also controlled the second derivatives of the final criterion in order to determine the limitations of the formulation i.e. the domain that guarantees the maximum extrema. Criterion can be shown as follows:

$$\sqrt{a.T_a^2 + b.(\sigma_{n,a} + \frac{\tau_{-1}}{\sigma_0}.\sigma_{n,m})} \leq \sigma_{-1} \tag{2.110}$$

Material parameters a and b take different values based on the type of material (ductile, brittle) and their formulations are given below:

$$r < \sqrt{\frac{4}{3}} \cong 1.155: \quad a = \frac{r^2}{2} + \frac{\sqrt{r^4 - r^2}}{2}, \quad b = \sigma_{-1} \tag{2.111}$$

$$r \geq \sqrt{\frac{4}{3}} \cong 1.155; \quad a = \left(\frac{4r^2}{4 + r^2}\right)^2, \quad b = \frac{8\sigma_{-1}r^2(4 - r^2)}{(4 + r^2)^2} \tag{2.112}$$

As seen from the formulations, criterion requires three endurance limits for the calibration which may be a disadvantage. Like other critical plane methods investigated in this study, this criterion does not include a mean shear stress term which is criticized by Papuga [14, 19] and stated that the inclusion of T_m may be an improvement for preventing the shift of results to the non-conservative side which occurs in loadings with mean torsion stresses.

2.3.8. Summary of Multiaxial Endurance Criteria

In section 2.3. three different types of multiaxial endurance criteria are explained which are equivalent stress, invariant based and critical plane. In this section a brief summary of the investigated criteria is made in terms of their formulation, shear stress term, inclusion of mean stress and required endurance limits which are presented in Table 2.3. As one may observe from the table, methods except equivalent stress criteria and Sines have an alternating stress part that is a combination of shear and normal stresses. The alternating stress part of the

criteria are used for handling the phase effect and the remaining part of the damage parameters, which is the mean stress part, is for handling the mean stress effects (normal mean stress, shear mean stress or both).

Table 2.3 Summary of Multiaxial Endurance Criteria

Criteria	Formulation	Parameters			Alternating Stress Inclusion	Mean Stress Inclusion	Required Endurance Limits
		a	b	c			
Absolute Maximum Stress	$sign(\sigma_{AMP}(t)).\lvert\sigma_{AMP}(t)\rvert$	0	1	-	$\sigma_{eq,AMP}$	Mean Correction	σ_{-1}or τ_{-1}
Signed von Mises	$sign(\sigma_{AMP}(t)).\lvert\sigma_{\mathrm{VM}}(t)\rvert$	1	0	-	$\sigma_{eq,SVM}$	Mean Correction	σ_{-1}or τ_{-1}
Sines	$a\sqrt{J_{2,a}} + b\sigma_{h,m}$	r	$(6\mathrm{r}_0 - \sqrt{3}.\mathrm{r})$	-	$\sqrt{J_{2,a}}$	$\sigma_{h,m}$	$\sigma_{-1}, \tau_{-1}, \sigma_0$
Crossland	$a\sqrt{J_{2,a}} + b\sigma_{h,max}$	r	$3 - \sqrt{3}r$	-	$\sqrt{J_{2,a}}$ and $\sigma_{h,a}$	$\sigma_{h,m}$	σ_{-1}, τ_{-1}
Gonçalves, Araujo and Mamiya	$a\sqrt{\sum_{i=1}^{5} D_i^2} + b\sigma_{1,max}$	$\frac{\mathrm{r}-1}{\sqrt{2}(1-\frac{1}{\sqrt{3}})}$	$\frac{\sqrt{3}-\mathrm{r}}{\sqrt{3}-1}$	-	$\sqrt{\sum_{i=1}^{5} D_i^2}$ and $\sigma_{1,a}$	$\sigma_{1,m}$	σ_{-1}, τ_{-1}
Findley	$a.T_a + b.\sigma_{n,max}$	$2\sqrt{r-1}$	$2-\mathrm{r}$	-	T_a and $\sigma_{n,a}$	$\sigma_{n,m}$	σ_{-1}, τ_{-1}
Dang Van	$a.T_a + b.\sigma_{h,max}$	r	$3-\frac{3}{2}r$	-	T_a and $\sigma_{h,a}$	$\sigma_{h,m}$	σ_{-1}, τ_{-1}

Robert	$a.T_a + b.\sigma_{n,a} + c.\sigma_{n,m}$	$2.\sqrt{r-1}$	$2-r$	$\frac{2.\sigma_{-1}}{\sigma_0}$ $-\frac{\sigma_0}{2.\sigma_{-1}}(r-1)$ $-(2+r)$	T_a and $\sigma_{n,a}$	$\sigma_{n,m}$	$\sigma_{-1}, \tau_{-1}, \sigma_0$
Papuga PCR; r<1.155	$\sqrt{a.T_a^2 + b.(\sigma_{n,a} + \frac{\tau_{-1}}{\sigma_0}.\sigma_{n,m})}$	$\frac{r^2}{2} + \frac{\sqrt{r^4 - r^2}}{2}$	σ_{-1}	-	T_a and $\sigma_{n,a}$	$\sigma_{n,m}$	$\sigma_{-1}, \tau_{-1}, \sigma_0$
Papuga PCR; r>1.155		$\left(\frac{4r^2}{4+r^2}\right)^2$	$\frac{8\sigma_{-1}r^2(4-r^2)}{(4+r^2)^2}$	-			

CHAPTER 3

AXIAL/BENDING CALIBRATIONS OF MULTIAXIAL ENDURANCE CRITERIA

Invariant and critical plane criteria have a common property that their formulations include weighting constants (material parameters) to adjust the effect of shear and normal stress terms on the damage parameter. These weighting constants are calibrated for two different uniaxial loading cases for two parameter methods. Calibration is usually made with fully reversed axial/bending and torsion endurance limits (bending-torsion calibration). However, torsion endurance limit may not always be available as many engineering handbooks such as MMPDS only include axial fatigue tests. In literature some authors studied different adjustments of material constants. Karolczuk et al. [70, 71] calibrate the material constant of Findley, Matake and Dang Van at different number of cycles unlike the classical calibration (bending-torsion calibration) and they obtain good conformity with calculated and experimental fatigue lives. Kallmeyer et al. [52, 76] calibrated the material constants from uniaxial test data (bending and torsion) of Ti-6Al-4V for different R ratios by a least-squares error minimization method. Karolczuk and Macha [72] made multiaxial proportional/non-proportional, constant and variable amplitude bending/torsion experiments on 18G3A steel smooth specimens. They linearly modified the material constant of Findley (without relating to endurance limits) and found the optimum value which gives the closest estimates to experimental tests. Papuga [45] made an extensive study and evaluated the effects of different stress measures and calibrations to develop a new method. His final criterion, Papuga

PCR, came out to be a three parameter critical plane method with adjusting endurance limits of fully reversed bending, fully reversed torsion and pulsating bending. However, none of these studies evaluate the performance of a calibration with only axial/bending endurance limits with different R ratios. Therefore, in this chapter, a calibration with fully reversed axial/bending and pulsating axial/bending endurance limits, which will be called axial/bending calibration throughout the thesis in following sections, is tested for four different endurance criteria which are Crossland, GAM, Findley and Dang Van. For the experimental data set obtained from literature, performances of these methods are investigated and acceptability of the axial/bending calibration is questioned in Section 5.4.

3.1. Derivation of Material Parameters for Crossland

Axial/bending calibration of Crossland is derived in this section by calculating the stress state at fully reversed and pulsating axial/bending.

3.1.1. Damage Parameter for Fully Reversed Axial/Bending Loading

For fully reversed axial/bending case loading is as follows:

$$\sigma_a = \sigma_{-1}; \qquad \sigma_m = \tau_a = \tau_m = 0 \tag{3.1}$$

For this loading, alternating value of second invariant can be obtained from (2.54) knowing that $\delta = 0$ as the loading is uniaxial:

$$\sqrt{J_{2,a}} = \frac{1}{\sqrt{2}}\sqrt{\frac{2}{3}\sigma_{-1}^2} = \frac{\sigma_{-1}}{\sqrt{3}} \tag{3.2}$$

and maximum value of hydrostatic stress is

$$\sigma_{h,max} = \frac{1}{3}(\sigma_1 + \sigma_2 + \sigma_3) = \frac{\sigma_{-1}}{3} \tag{3.3}$$

Thus, Crossland damage parameter for fully reversed axial/bending case can be calculated from (2.61):

$$a.\frac{\sigma_{-1}}{\sqrt{3}} + b.\frac{\sigma_{-1}}{3} = \sigma_{-1} \tag{3.4}$$

After simplification,

$$a.\frac{1}{\sqrt{3}} + b.\frac{1}{3} = 1 \tag{3.5}$$

3.1.2. Damage Parameter for Pulsating Axial/Bending Loading

For pulsating axial/bending case loading is as follows:

$$\begin{aligned} \sigma_a &= \sigma_m = \frac{\sigma_0}{2} \\ \tau_a &= \tau_m = 0 \end{aligned} \tag{3.6}$$

For this loading case $\sqrt{J_{2,a}}$ is as follows:

$$\sqrt{J_{2,a}} = \frac{1}{\sqrt{2}}\sqrt{\frac{2}{3}.\frac{\sigma_0^2}{4}} = \frac{\sigma_0}{2\sqrt{3}} \tag{3.7}$$

And maximum value of hydrostatic force is

$$\sigma_{h,max} = \frac{\sigma_0}{3} \tag{3.8}$$

Therefore, Crossland damage parameter for pulsating axial/bending case is as follows:

$$a.\frac{\sigma_0}{2\sqrt{3}} + b.\frac{\sigma_0}{3} = \sigma_{-1} \tag{3.9}$$

After simplification,

$$a.\frac{1}{2\sqrt{3}} + b.\frac{1}{3} = r_0 \tag{3.10}$$

Material parameters of Crossland for axial/bending calibration may be obtained from (3.5) and (3.10); by subtracting ((3.10) from (3.5) following expression may be obtained:

$$a.\frac{1}{2\sqrt{3}} = 1 - r_0 \tag{3.11}$$

As a result, a parameter can be written in terms of r_0:

$$a = 2\sqrt{3}(1 - r_0) \tag{3.12}$$

Since parameter a is computed, parameter b may be found from (3.5) or (3.10):

$$2\sqrt{3}(1 - r_0).\frac{1}{2\sqrt{3}} + b.\frac{1}{3} = r_0$$

$$b = 3(2r_0 - 1) \tag{3.13}$$

3.2. Derivation of Material Parameters for Gonçalves, Araujo and Mamiya (GAM)

Axial/bending calibration of GAM is derived in this section by calculating the stress state at fully reversed and pulsating axial/bending.

3.2.1. Damage Parameter for Fully Reversed Axial/Bending Loading

For loading conditions stated in (3.1), minimum and maximum values of transformed stress quantities on Ilyushin deviatoric space can be calculated from (2.53),

$$S_{1,min} = -\sqrt{\frac{2}{3}}\sigma_{-1}$$

$$S_{1,max} = \sqrt{\frac{2}{3}}\sigma_{-1}$$

From which alternating value can be obtained,

$$S_{1,a} = \sqrt{\frac{2}{3}}\sigma_{-1} \tag{3.14}$$

As loading is uniaxial tension/bending, other deviatoric stress quantities (S_3) turn out to be zero. Maximum value of principal stress may be obtained from plane stress/strain formulations,

$$\sigma_{1,max} = \max(\frac{\sigma_x(t) + \sigma_y(t)}{2} + \sqrt{\left(\frac{\sigma_x(t) - \sigma_y(t)}{2}\right)^2 + \tau_{xy}^2(t)}) \tag{3.15}$$

$$\sigma_{1,max} = \sigma_{-1} \tag{3.16}$$

Therefore, GAM damage parameter may be calculated from (2.64):

$$a.\sqrt{\frac{2}{3}}\sigma_{-1} + b.\sigma_{-1} = \sigma_{-1} \tag{3.17}$$

Simplification of (3.17) leads to,

$$a.\sqrt{\frac{2}{3}} + b = 1 \tag{3.18}$$

3.2.2. Damage Parameter for Pulsating Axial/Bending Loading

For loading conditions stated in (3.6), again S_3 would be again zero while S_1 is:

$$S_{1,min} = 0$$

$$S_{1,max} = \sqrt{\frac{2}{3}}\sigma_0$$

which leads to an alternating value of,

$$S_{1,a} = \frac{1}{2}\sqrt{\frac{2}{3}}\sigma_0 \tag{3.19}$$

Maximum value of principal stress can be obtained from (3.15),

$$\sigma_{1,max} = \sigma_0 \tag{3.20}$$

Thus, damage parameter of GAM may be calculated for pulsating axial/bending case,

$$a.\frac{1}{2}\sqrt{\frac{2}{3}}\sigma_0 + b.\sigma_0 = \sigma_{-1} \tag{3.21}$$

After simplification (3.21) becomes,

$$a.\frac{1}{2}\sqrt{\frac{2}{3}} + b = r_0 \tag{3.22}$$

Material parameters of GAM for axial/bending calibration may be obtained from (3.18) and (3.22); by subtracting (3.22) from (3.18) following expression may be obtained:

$$a.\frac{1}{2}\sqrt{\frac{2}{3}} = 1 - r_0 \tag{3.23}$$

Therefore, parameter a can be written in terms of r_0:

$$a = \sqrt{6}(1 - r_0) \tag{3.24}$$

Since parameter a is computed, parameter b may be found from (3.18) or (3.22):

$$\sqrt{6}(1 - r_0).\sqrt{\frac{2}{3}} + b = 1$$

$$b = (2r_0 - 1) \tag{3.25}$$

3.3. Derivation of Material Parameters for Findley

Material constants (a, b) for the axial/bending calibration of Findley is derived by transforming the k calibration results of Socie and Marquis [7] and the following relations are obtained for the material constants:

$$a = \frac{2}{\left(\frac{r_0^2 - \frac{1}{4}}{\sqrt{-r_0(4r_0^2 - 5r_0 + 1)}} + \sqrt{\frac{1 - \left(r_0^2 - \frac{1}{4}\right)^2}{r_0(4r_0^2 - 5r_0 + 1)}}\right)} \tag{3.26}$$

$$b = \frac{r_0^2 - \frac{1}{4}}{\sqrt{-r_0(4r_0^2 - 5r_0 + 1)}} \tag{3.27}$$

3.4. Derivation of Material Parameters for Dang Van

Axial/bending calibration of Dang Van is derived in this section by calculating the stress state at fully reversed and pulsating axial/bending.

3.4.1. Damage Parameter for Fully Reversed Axial/Bending Loading

Alternating shear stress that appear in (2.103) can be derived from (2.91) and for fully reversed axial/bending case formulation turns out to be,

$$T_{\mathrm{a}} = \frac{\sigma_{-1}}{2}\sqrt{\sin^2(\varphi).\sin^2(2\theta) + \sin^2(2\varphi)\cos^4(\theta)} \tag{3.28}$$

Hydrostatic force has already be obtained in (3.3) thus, Dang Van damage parameter takes the form,

$$a.\frac{\sigma_{-1}}{2}\sqrt{\sin^2(\varphi).\sin^2(2\theta) + \sin^2(2\varphi)\cos^4(\theta)} + b.\frac{\sigma_{-1}}{3} = \sigma_{-1} \tag{3.29}$$

Since the criterion defines the critical plane as the plane where damage parameter is maximized, derivatives of (3.29) with respect to θ and φ should be equal to zero,

$$\frac{\partial \sigma_{-1}}{\partial \theta_{cp}} = a.\frac{\sigma_{-1}}{4} \times \frac{4\sin(2\theta_{cp})\cos(2\theta_{cp})\sin^2(\varphi_{cp}) - 4\cos^3(\theta_{cp})\sin(\theta_{cp})\sin^2(2\varphi_{cp})}{\sqrt{\sin^2(\varphi_{cp}).\sin^2(2\theta_{cp}) + \sin^2(2\varphi_{cp})\cos^4(\theta_{cp})}} = 0$$
$$= \frac{4\sin(2\theta_{cp})\sin^2(\varphi_{cp})\,[2\cos^2(\theta_{cp}).(1-\cos^2(\varphi_{cp})) - 1]}{\sqrt{\sin^2(\varphi_{cp}).\sin^2(2\theta_{cp}) + \sin^2(2\varphi_{cp})\cos^4(\theta_{cp})}} = 0 \quad (3.30)$$

$$\frac{\partial \sigma_{-1}}{\partial \varphi_{cp}} = a.\frac{\sigma_{-1}}{4}.\frac{\sin(2\varphi_{cp})\sin^2(2\theta_{cp}) + 4\sin(2\varphi_{cp})\cos(2\varphi_{cp})\cos^4(\theta_{cp})}{\sqrt{\sin^2(\varphi_{cp}).\sin^2(2\theta_{cp}) + \sin^2(2\varphi_{cp})\cos^4(\theta_{cp})}} + 0 = 0$$
$$= \frac{\sin(2\varphi_{cp})\sin^2(2\theta_{cp})\,[1 + \frac{4\cos(2\varphi_{cp})}{\tan^2(\theta_{cp})}]}{\sqrt{\sin^2(\varphi_{cp}).\sin^2(2\theta_{cp}) + \sin^2(2\varphi_{cp})\cos^4(\theta_{cp})}} = 0 \quad (3.31)$$

The three equations (3.29)-(3.31) include a total of four unknown parameters that are a, b, θ_{cp} and φ_{cp}. However, from (3.30) and (3.31) Eulerian angles for the critical plane can be determined. Two possible combinations are found which give the same result. These are,

$$(\theta_{cp,1}, \varphi_{cp,1}) = (\frac{\pi}{4}, 0)$$
$$(\theta_{cp,2}, \varphi_{cp,2}) = (\frac{\pi}{2}, \frac{\pi}{4}) \quad (3.32)$$

Both of these angle combinations yield the critical plane and the damage parameter from (3.29) gives,

$$a.\frac{1}{2} + b.\frac{1}{3} = 1 \quad (3.33)$$

3.4.2. Damage Parameter for Pulsating Axial/Bending Loading

For the pulsating axial/bending loading case damage parameter presented in (2.103) takes the form,

$$a.\frac{\sigma_0}{4}\sqrt{\sin^2(\varphi)\sin^2(2\theta)+\sin^2(2\varphi)\cos^4(\varphi)}+b.\frac{\sigma_0}{3}=\sigma_{-1} \tag{3.34}$$

From (3.34), it is clear that this equation is very similar to (3.29) with the only difference being $\frac{\sigma_0}{4}$ term in shear stress term. Therefore, Eulerian angles at critical plane would be the same. As a result, damage parameter becomes,

$$a.\frac{1}{4}+b.\frac{1}{3}=r_0 \tag{3.35}$$

Material parameters of Dang Van for axial/bending calibration may be obtained from (3.33) and (3.35); by subtracting (3.35) from (3.33) following expression may be obtained:

$$a.\frac{1}{4}=1-r_0 \tag{3.36}$$

Therefore, parameter a can be written in terms of r_0:

$$a=4(1-r_0) \tag{3.37}$$

Since parameter a is computed, parameter b may be found from (3.33) or (3.35):

$$2(1-r_0)+b.\frac{1}{3}=1$$

$$b=3(2r_0-1) \tag{3.38}$$

3.5. Summary of Axial/Bending Calibrations of Multiaxial Endurance Criteria

In this chapter calibration of several invariant and critical plane criteria is made which is based on only axial/bending endurance limits with different R ratios

(R=-1 and R=0). In this section a brief summary of the derieved weigthing constants are presented in Table 3.1.

Table 3.1: Weighting constants of multiaxial endurance criteria for axial/bending calibration

Axial/Bending Calibration	Weigthing Constants	
Criteria	a	b
Crossland	$2\sqrt{3}(1-r_0)$	$3(2r_0-1)$
Gonçalves, Araujo and Mamiya	$\sqrt{6}(1-r_0)$	$(2r_0-1)$
Findley	$\frac{2}{\left(\frac{r_0^2-\frac{1}{4}}{\sqrt{-r_0(4r_0^2-5r_0+1)}}+\sqrt{\frac{1-\left(r_0^2-\frac{1}{4}\right)^2}{r_0(4r_0^2-5r_0+1)}}\right)}$	$\frac{r_0^2-\frac{1}{4}}{\sqrt{-r_0(4r_0^2-5r_0+1)}}$
Dang Van	$4(1-r_0)$	$b=3(2r_0-1)$

CHAPTER 4

METHODOLOGY AND EVALUATION OF CRITERIA

4.1. Type of Evaluation

All the criteria (equivalent stress, invariant based and critical plane) presented in this study are developed against high cycle multiaxial fatigue; therefore, the evaluation is concerned about whether the specimen withstands an infinite life or not. For this purpose, experimental data presented in Section 4.3. is used and fatigue index error (FIE) is introduced. FIE shows the derivation of the damage parameter, calculated either with an equivalent stress, an invariant or a critical plane criterion, from fully reversed axial/bending endurance limit. It can be shown as follows:

$$FIE(\%) = \frac{DP - \sigma_{-1}}{\sigma_{-1}} * 100 \tag{4.1}$$

A negative value of FIE means that the criterion predicts no failure; although it actually occurred in the experiment. Therefore, such estimation is evaluated as non-conservative while opposite is true for positive values of FIE.

Histograms are utilized in this study for presenting the overall behavior of the criteria. Papadopoulos et al. [18] is the first author that uses histograms for comparison of the criteria and later it is adopted by all other multiaxial researchers. Histograms are bar graphs that show the number of occurrences of a particular parameter. This parameter is the mean fatigue index error for this study as the overall predictive capabilities of the criteria is investigated. As explained above a negative value of the FIE is undesired which means the estimation is non-conservative; therefore, in histograms shift to left side means that the criterion becomes non-conservative. Opposite is true for the shift to right side in a

histogram meaning that the estimations become conservative. For an ideal criteria, fatigue index errors and the median of the graph should be as close as possible to zero and histogram should have a range of approximately 20% (or a lower value) giving a mean fatigue index tolerance of -10% to 10% [45]. A representation of a histogram is shown in Figure 4.1 for a better understanding of the graph type.

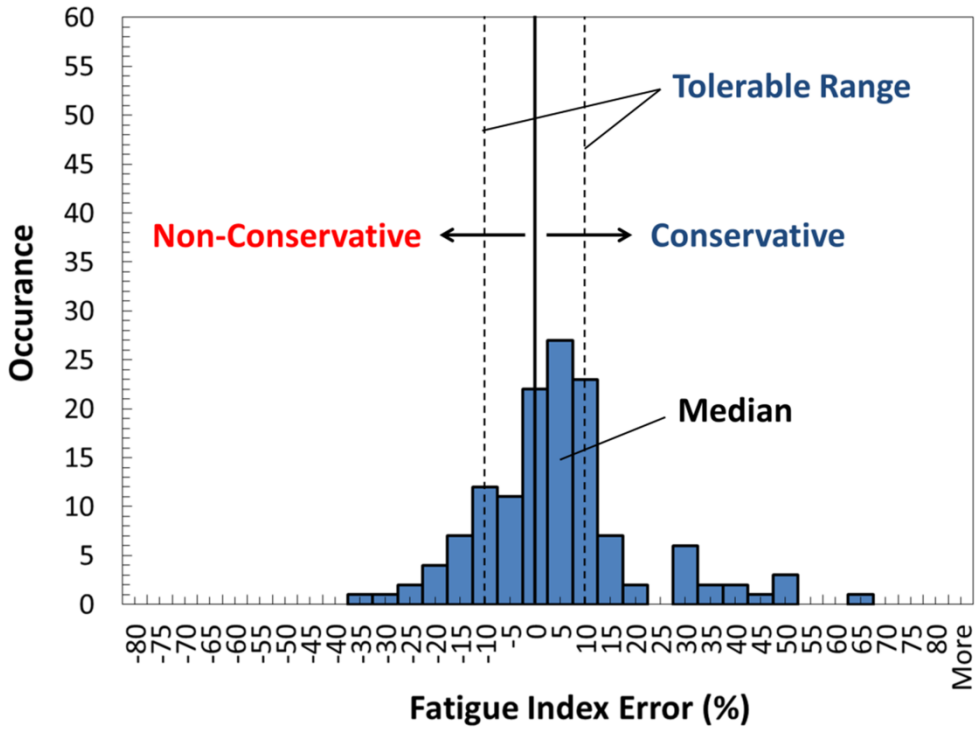

Figure 4.1: Example of a histogram showing conservative and non-conservative sides, median of the graph and the tolerable range

For large data sets, like in this study, this kind of a presentation may not sufficiently clarify the predictive capabilities of the criteria. Therefore, statistical analysis measures (applied on mean fatigue index errors) i.e. mean, range and standard deviations are calculated for all experimental data and for partial effects (ex. estimations of in-phase loadings without mean stresses). Definitions of statistical analysis measures are given below (x denotes a single analysis result):

$$x_m = \frac{\sum_{i=1}^{N} x_i}{N} \tag{4.2}$$

$$x_r = x_{max} - x_{min} \tag{4.3}$$

$$x_{st.dev} = \sqrt{\frac{\sum_{i=1}^{N} (x_i - x_m)^2}{N-1}} \tag{4.4}$$

4.2. Procedures of Multiaxial Fatigue Endurance Analysis

A general computation process, which is implemented in a MATLAB code for the multiaxial fatigue endurance calculations and evaluation of the criteria, is shown in Figure 4.2. Fatigue analysis is actually a post-process and for the multiaxial fatigue endurance anaylsis, stress state (normal and shear stresses with phase and frequency differences) is obtained from multiaxial tests which are conducted on smooth speciments and reported in literature. In addition, endurance limits (alternating stress usually taken at 10^7 cycles) for fully reversed bending and torsion are inputs of the analysis for calibration of the criteria and for life estimations. Process starts with the calculation of weighting constants that are presented in Section 2.3. to be used in related multiaxial endurance criteria. Then, stress tensor is formed for each data in time. From this stress tensor, stress histories on each material plane can be obtained by tensor rotations. For critical plane criteria, all material planes are searched and normal and shear stress on each plane are calculated while for invariant based criteria (except GAM) only octahedral plane is investigated from which octahedral shear and hydrostatic stresses are calculated. For GAM criterion deviatoric stresses are calculated and alternating deviatoric stress tensor is computed. Equivalent stress criteria also relies on stresses on a single plane like in invariant based criteria. Octahedral shear stress is calculated for Signed von Mises while for Absolute Maximum Principal, which is based on maximum principal stress plane, absolute maximum principal stress is required. Calculations end when the damage parameter of the selected criterion (indicator of fatigue failure) is computed. In order to evaluate the performances of the criteria, fatigue index error (FIE) is calculated (for each

test data) from damage parameter and endurance limits as explained in section 4.1. Then, for determining the general behavior of the criteria histograms are formed. However, since histograms do not give information about partial effects (phase and mean stress effects) statistical analysis is performed from which the mean, range and standard deviation of FIE is computed.

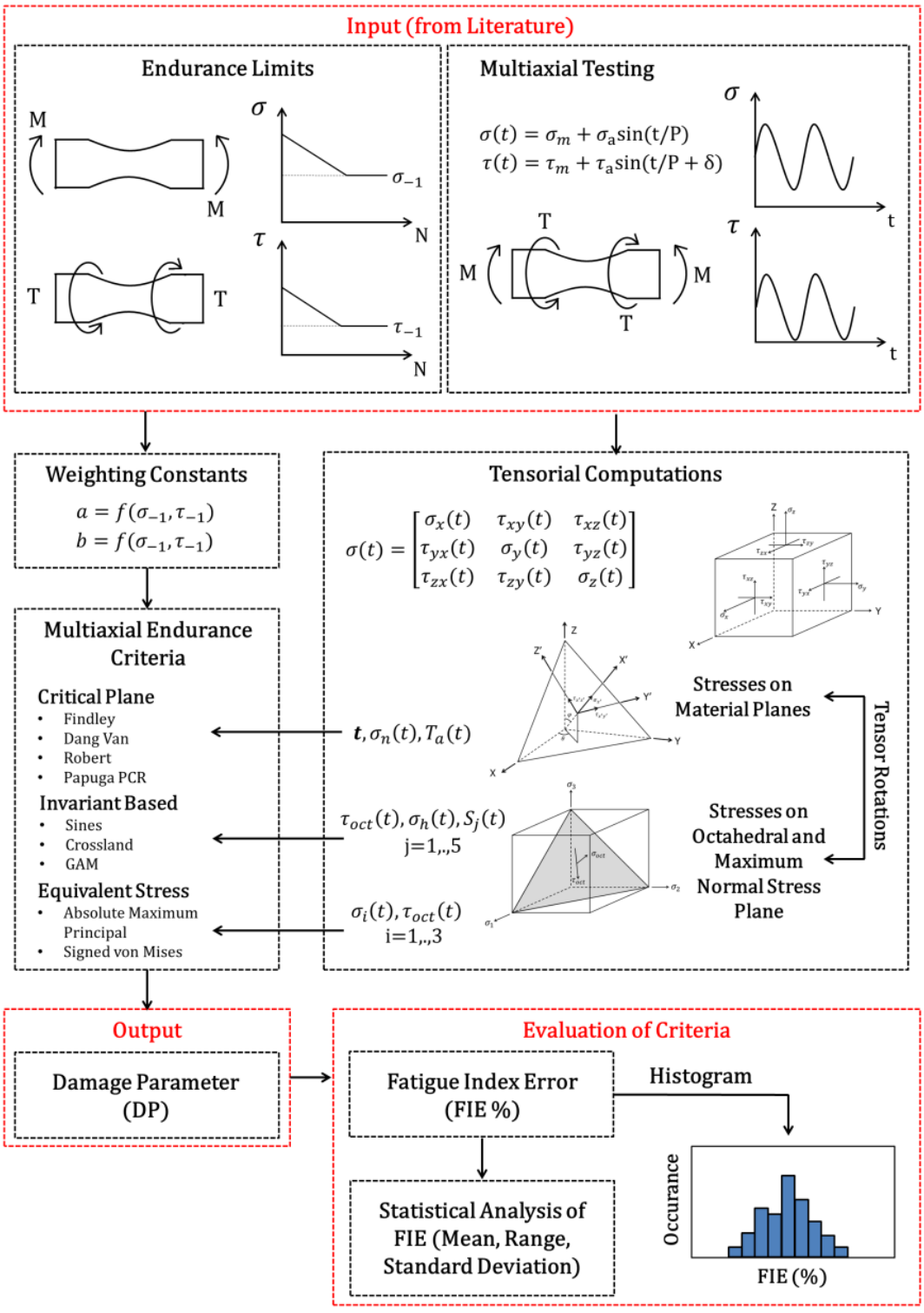

Figure 4.2: Computational flow chart of multiaxial fatigue endurance calculations and evaluation of criteria

4.3. Experimental Data Set

The experimental data is obtained from several resources and tested materials are shown with their respective references and material properties in Table 4.1. Data set includes proportional and non-proportional multiaxial high cycle fatigue tests that is appropriate in size for evaluation of phase and mean stress effects individually and also of their combined effects. Most of the tests are harmonic synchronous plane bending and torsion experiments conducted on smooth specimens. Experimental data set also include uniaxial tests such as plane bending, tension/compression and torsion in order to evaluate the capability of methods for these simple tests. However, data set does not include experiments performed with asynchronous loads; therefore, effect of frequency difference can not be investigated. The ratio of torsion and axial/bending endurance limits shown in Table 4.1 is used for classification of materials by Papadopoulos et al. [18] and Liu and Mahadevan [50]. According to these authors, materials with $\tau_{-1}/\sigma_{-1} < 1/\sqrt{3}$ are classified as ductile (mild) metals while materials with $1/\sqrt{3} < \tau_{-1}/\sigma_{-1} < 1$ are classified as hard (brittle) metals and materials with $\tau_{-1}/\sigma_{-1} > 1$ are classified as extremely brittle metals. In this study, special attention is given on ductile and brittle metals; therefore, grey cast iron (extremely brittle metal) test results of Nishihara and Kawamato [77] are not investigated.

Yield and ultimate strength values of materials which are tested with mean stresses are also given in Table 4.1, as these values are used in mean stress corrections of equivalent stress methods. However, fatigue limit in pulsating bending (σ_0) is not found in any of the experimental data except for the material S65A which is tested by Gough [6]. Therefore, Smith-Watson and Topper (SWT) formulation is used for obtaining the σ_0 as it is suggested by Dowling [37] instead of other mean stress corrections such as Goodman or Gerber, which are explained in Section 2.3.2. Through Table 4.1 to Table 4.16, abbreviation is used for plane bending (PB), torsion (To), rotating bending (RB), in-phase (IP) and for out-of-phase (OP).

Table 4.1: General Information about Experimental Data Set

Material	Reference	Number of Tests	τ_{-1}/σ_{-1}	σ_y [MPa]	σ_u [MPa]	σ_{-1} [MPa]	τ_{-1} [MPa]	σ_0 [MPa]	Type of Loading
Hard Steel	[77]	22	0.63	-	-	313.9	196.2	443.9	PB+To, PB, To
Mild Steel	[77]	10	0.58	-	-	235.4	137.3	332.9	PB+To, PB, To
42CrMo4	[78], [45]	9	0.65	920.7	1111.0	398.0	260.0	562.9	PB+To
34Cr4	[78], [84]	14	0.62	550.0	795.0	410.0	256.0	579.8	PB+To
30NCD16	[79], [85]	13	0.62	950.0	1200.0	660.0	410.0	933.4	PB+To
30NCD16	[80] , [85]	26	0.62	950.0	1200.0	690.0	428.0	975.8	PB+To, PB
30NCD16	[80] , [85]	2	0.65	950.0	1200.0	658.0	428.0	930.5	RB+To
30NCD16	[80] , [85]	3	0.76	950.0	1200.0	560.0	428.0	791.9	To
XC18	[81]	3	0.56	-	-	332.0	186.0	469.5	PB+To
FGS800_2	[82], [83]	3	0.75	-	-	294.0	220.0	415.8	PB+To
S65A	[6], [84]	29	0.63	947.0	1001.0	583.8	370.7	1065.7	PB+To

Experimental data is divided into two groups according to what kind of partial effects are evaluated (phase effect or mean stress effect). These groups are called nMS (tests without mean stresses) and MS (tests with mean stresses) groups. All individual tests are labelled with respect to their related groups (nMS or MS) and test loads are shown in Table 4.2 through Table 4.13 with phase differences (δ_{xy}) for each material. MS group is also divided into three groups which are Ax_MS (tests with only axial mean stress), To_MS (tests with only torsion mean stress) and C_MS (tests with both axial and torsion mean stress) that are clarified in tables.

Table 4.2: Test Loads for nMS Experimental Data Set – Hard Steel [77]

Label	Loading Type	Partial Effects	σ_{x_a} [MPa]	σ_{x_m} [MPa]	τ_{xy_a} [MPa]	τ_{xy_m} [MPa]	$\delta_{xy}(^o)$
nMS1	PB	IP	327.0	0.0	0.0	0.0	0.0
nMS2	PB+To	IP	308.0	0.0	63.9	0.0	0.0
nMS3	PB+To	IP	255.1	0.0	127.5	0.0	0.0
nMS4	PB+To	IP	141.9	0.0	171.3	0.0	0.0
nMS5	To	IP	0.0	0.0	201.1	0.0	0.0
nMS6	PB+To	OP	255.1	0.0	127.5	0.0	30.0
nMS7	PB+To	OP	142.0	0.0	171.2	0.0	30.0
nMS8	PB+To	OP	255.1	0.0	127.5	0.0	60.0
nMS9	PB+To	OP	147.2	0.0	177.6	0.0	60.0
nMS10	PB+To	OP	308.0	0.0	63.9	0.0	90.0
nMS11	PB+To	OP	264.9	0.0	132.4	0.0	90.0
nMS12	PB+To	OP	152.5	0.0	184.2	0.0	90.0
nMS13	PB+To	IP	138.1	0.0	167.1	0.0	0.0
nMS14	PB+To	OP	140.4	0.0	169.9	0.0	30.0
nMS15	PB+To	OP	145.7	0.0	176.3	0.0	60.0
nMS16	PB+To	OP	150.2	0.0	181.7	0.0	90.0
nMS17	PB+To	IP	245.3	0.0	122.7	0.0	0.0
nMS18	PB+To	OP	249.7	0.0	124.9	0.0	30.0
nMS19	PB+To	OP	252.4	0.0	126.2	0.0	60.0

nMS20	PB+To	OP	258.0	0.0	129.0	0.0	90.0
nMS21	PB+To	IP	299.1	0.0	62.8	0.0	0.0
nMS22	PB+To	OP	304.5	0.0	63.9	0.0	90.0

Table 4.3: Test Loads for nMS Experimental Data Set – Mild Steel [77]

Label	Loading Type	Partial Effects	σ_{x_a} [MPa]	σ_{x_m} [MPa]	τ_{xy_a} [MPa]	τ_{xy_m} [MPa]	$\delta_{xy}(^o)$
nMS23	PB	IP	245.3	0.0	0.0	0.0	0.0
nMS24	PB+To	IP	235.6	0.0	48.9	0.0	0.0
nMS25	PB+To	IP	187.3	0.0	93.6	0.0	0.0
nMS26	PB+To	IP	101.3	0.0	122.3	0.0	0.0
nMS27	To	IP	0.0	0.0	142.3	0.0	0.0
nMS28	PB+To	OP	194.2	0.0	97.1	0.0	60.0
nMS29	PB+To	OP	108.9	0.0	131.5	0.0	60.0
nMS30	PB+To	OP	235.6	0.0	48.9	0.0	90.0
nMS31	PB+To	OP	208.1	0.0	104.1	0.0	90.0
nMS32	PB+To	OP	112.6	0.0	136.0	0.0	90.0

Table 4.4: Test Loads for nMS Experimental Data Set – 42CrMo4 [78]

Label	Loading Type	Partial Effects	σ_{x_a} [MPa]	σ_{x_m} [MPa]	τ_{xy_a} [MPa]	τ_{xy_m} [MPa]	$\delta_{xy}(^o)$
nMS33	PB+To	IP	328.0	0.0	157.0	0.0	0.0
nMS34	PB+To	OP	286.0	0.0	137.0	0.0	90.0
nMS35	PB+To	IP	233.0	0.0	224.0	0.0	0.0
nMS36	PB+To	OP	213.0	0.0	205.0	0.0	90.0

Table 4.5: Test Loads for nMS Experimental Data Set – 34Cr4 [78]

Label	Loading Type	Partial Effects	σ_{x_a} [MPa]	σ_{x_m} [MPa]	τ_{xy_a} [MPa]	τ_{xy_m} [MPa]	$\delta_{xy}(^o)$
nMS37	PB+To	IP	314.0	0.0	157.0	0.0	0.0
nMS38	PB+To	OP	315.0	0.0	158.0	0.0	60.0
nMS39	PB+To	OP	316.0	0.0	158.0	0.0	90.0
nMS40	PB+To	OP	315.0	0.0	158.0	0.0	120.0
nMS41	PB+To	OP	224.0	0.0	224.0	0.0	90.0
nMS42	PB+To	OP	380.0	0.0	95.0	0.0	90.0
nMS43	PB+To	OP	129.0	0.0	258.0	0.0	90.0

Table 4.6: Test Loads for nMS Experimental Data Set – 30NCD16 [79], [80]

Label	Loading Type	Partial Effects	σx_a [MPa]	σx_m [MPa]	τxy_a [MPa]	τxy_m [MPa]	δxy(o)
nMS44	PB+To	IP	485.0	0.0	280.0	0.0	0.0
nMS45	PB+To	OP	480.0	0.0	277.0	0.0	90.0
nMS46	RB+To	IP	337.0	0.0	328.0	0.0	0.0
nMS47	RB+To	IP	482.0	0.0	234.0	0.0	0.0
nMS48	PB+To	IP	519.0	0.0	291.0	0.0	0.0
nMS49	PB+To	OP	514.0	0.0	288.0	0.0	90.0
nMS50	PB+To	OP	474.0	0.0	265.0	0.0	90.0
nMS51	PB+To	IP	482.0	0.0	268.0	0.0	0.0

Table 4.7: Test Loads for nMS Experimental Data Set – XC18 [81]

Label	Loading Type	Partial Effects	σ_{x_a} [MPa]	σ_{x_m} [MPa]	τ_{xy_a} [MPa]	τ_{xy_m} [MPa]	$\delta_{xy}(^o)$
nMS52	PB+To	IP	246.0	0.0	138.0	0.0	0.0
nMS53	PB+To	OP	246.0	0.0	138.0	0.0	45.0

nMS54	PB+To	OP	264.0	0.0	148.0	0.0	90.0

Table 4.8: Test Loads for nMS Experimental Data Set – FGS800_2 [82], [83]

Label	Loading Type	Partial Effects	σ_{x_a} [MPa]	σ_{x_m} [MPa]	τ_{xy_a} [MPa]	τ_{xy_m} [MPa]	$\delta_{xy}(^o)$
nMS55	PB+To	IP	228.0	0.0	132.0	0.0	0.0
nMS56	PB+To	OP	245.0	0.0	142.0	0.0	90.0
nMS57	PB+To	IP	199.0	0.0	147.0	0.0	0.0

Table 4.9: Test Loads for nMS Experimental Data Set – S65A [6]

Label	Loading Type	Partial Effects	σ_{x_a} [MPa]	σ_{x_m} [MPa]	τ_{xy_a} [MPa]	τ_{xy_m} [MPa]	$\delta_{xy}(^o)$
nMS58	PB+To	IP	547.5	0.0	156.0	0.0	0.0
nMS59	PB+To	IP	389.2	0.0	259.5	0.0	0.0
nMS60	PB+To	IP	168.3	0.0	335.9	0.0	0.0

Table 4.10: Test Loads for MS Experimental Data Set – 42CrMo4 [78], [45]

Label	Loading Type	Partial Effects	σ_{x_a} [MPa]	σ_{x_m} [MPa]	τ_{xy_a} [MPa]	τ_{xy_m} [MPa]	$\delta_{xy}(^o)$
MS1	PB+To	IP, To_MS	266.0	0.0	128.0	128.0	0.0
MS2	PB+To	OP, To_MS	283.0	0.0	136.0	136.0	90.0
MS3	PB+To	OP, To_MS	333.0	0.0	160.0	160.0	180.0
MS4	PB+To	IP, Ax_MS	280.0	280.0	134.0	0.0	0.0
MS5	PB+To	OP, Ax_MS	271.0	271.0	130.0	0.0	90.0

Table 4.11: Test Loads for MS Experimental Data Set – 34Cr4 [78], [84]

Label	Loading Type	Partial Effects	σ_{x_a} [MPa]	σ_{x_m} [MPa]	τ_{xy_a} [MPa]	τ_{xy_m} [MPa]	$\delta_{xy}(^o)$
MS6	PB+To	IP, To_MS	316.0	0.0	158.0	158.0	0.0
MS7	PB+To	OP, To_MS	314.0	0.0	157.0	157.0	60.0
MS8	PB+To	OP, To_MS	315.0	0.0	158.0	158.0	90.0
MS9	PB+To	IP, Ax_MS	279.0	279.0	140.0	0.0	0.0
MS10	PB+To	OP, Ax_MS	284.0	284.0	142.0	0.0	90.0
MS11	PB+To	IP, To_MS	355.0	0.0	89.0	178.0	0.0
MS12	PB+To	OP, Ax_MS	212.0	212.0	212.0	0.0	90.0

Table 4.12: Test Loads for MS Experimental Data Set – 30NCD16 [79], [80], [85]

Label	Loading Type	Partial Effects	σ_{x_a} [MPa]	σ_{x_m} [MPa]	τ_{xy_a} [MPa]	τ_{xy_m} [MPa]	$\delta_{xy}(^o)$
MS13	PB+To	IP, Ax_MS	480.0	300.0	277.0	0.0	0.0
MS14	PB+To	OP, Ax_MS	480.0	300.0	277.0	0.0	45.0
MS15	PB+To	OP, Ax_MS	470.0	300.0	270.0	0.0	60.0
MS16	PB+To	OP, Ax_MS	473.0	300.0	273.0	0.0	90.0
MS17	PB+To	IP, Ax_MS	590.0	300.0	148.0	0.0	0.0
MS18	PB+To	OP, Ax_MS	565.0	300.0	141.0	0.0	45.0
MS19	PB+To	OP, Ax_MS	540.0	300.0	135.0	0.0	90.0
MS20	PB+To	IP, Ax_MS	211.0	300.0	365.0	0.0	0.0
MS21	PB	IP, Ax_MS	630.0	300.0	0.0	0.0	0.0
MS22	PB+To	IP, Ax_MS	0.0	300.0	370.0	0.0	0.0
MS23	PB+To	OP, Ax_MS	220.0	300.0	385.0	0.0	90.0
MS24	To	IP, Ax_MS	235.0	745.0	0.0	0.0	0.0
MS25	To	IP, Ax_MS	251.0	704.0	0.0	0.0	0.0
MS26	To	IP, Ax_MS	527.0	222.0	0.0	0.0	0.0

MS27	PB	IP, Ax_MS	575.0	375.0	0.0	0.0	0.0
MS28	PB	IP, Ax_MS	558.0	428.0	0.0	0.0	0.0
MS29	PB	IP, Ax_MS	627.0	273.0	0.0	0.0	0.0
MS30	PB	IP, Ax_MS	679.0	156.0	0.0	0.0	0.0
MS31	PB+To	IP, C_MS	451.0	294.0	250.0	191.0	0.0
MS32	PB+To	OP, C_MS	462.0	294.0	258.0	191.0	90.0
MS33	PB+To	OP, Ax_MS	474.0	294.0	265.0	0.0	45.0
MS34	PB+To	OP, Ax_MS	464.0	294.0	259.0	0.0	60.0
MS35	PB+To	OP, Ax_MS	554.0	287.0	135.0	0.0	45.0
MS36	PB+To	OP, Ax_MS	220.0	199.0	368.0	0.0	90.0
MS37	PB+To	OP, Ax_MS	470.0	299.0	261.0	0.0	90.0
MS38	PB+To	OP, Ax_MS	527.0	287.0	129.0	0.0	90.0
MS39	PB+To	OP, Ax_MS	433.0	472.0	240.0	0.0	90.0
MS40	PB+To	OP, Ax_MS	418.0	622.0	234.0	0.0	90.0
MS41	PB+To	IP, Ax_MS	0.0	299.0	396.0	0.0	0.0
MS42	PB+To	IP, Ax_MS	0.0	486.0	411.0	0.0	0.0
MS43	PB+To	IP, Ax_MS	0.0	655.0	364.0	0.0	0.0
MS44	PB+To	IP, Ax_MS	207.0	299.0	350.0	0.0	0.0
MS45	PB+To	IP, Ax_MS	474.0	294.0	265.0	0.0	0.0
MS46	PB+To	IP, Ax_MS	584.0	281.0	142.0	0.0	0.0
MS47	PB+To	IP, Ax_MS	447.0	473.0	252.0	0.0	0.0
MS48	PB+To	IP, Ax_MS	425.0	635.0	223.0	0.0	0.0

Table 4.13: Test Loads for MS Experimental Data Set – S65A [6], [84]

Label	Loading Type	Partial Effects	σ_{x_a} [MPa]	σ_{x_m} [MPa]	τ_{xy_a} [MPa]	τ_{xy_m} [MPa]	$\delta_{xy}(^{o})$
MS49	PB+To	IP, Ax_MS	552.9	266.4	0.0	0.0	0.0
MS50	PB+To	IP, Ax_MS	532.8	532.8	0.0	0.0	0.0
MS51	PB+To	IP, To_MS	549.8	0.0	0.0	169.9	0.0
MS52	PB+To	IP, To_MS	540.6	0.0	0.0	343.6	0.0
MS53	PB+To	IP, C_MS	556.0	266.4	0.0	169.9	0.0
MS54	PB+To	IP, C_MS	556.0	266.4	0.0	343.6	0.0
MS55	PB+To	IP, C_MS	469.5	532.8	0.0	169.9	0.0
MS56	PB+To	IP, C_MS	472.6	532.8	0.0	343.6	0.0
MS57	PB+To	IP, Ax_MS	0.0	266.4	312.0	0.0	0.0
MS58	PB+To	IP, Ax_MS	0.0	532.8	284.2	0.0	0.0
MS59	PB+To	IP, C_MS	0.0	266.4	304.3	169.9	0.0
MS60	PB+To	IP, C_MS	0.0	532.8	281.1	169.9	0.0
MS61	PB+To	IP, C_MS	0.0	266.4	308.9	343.6	0.0
MS62	PB+To	IP, C_MS	0.0	532.8	293.4	343.6	0.0
MS63	PB+To	IP, C_MS	496.5	266.4	141.3	169.9	0.0
MS64	PB+To	IP, C_MS	374.5	266.4	249.4	169.9	0.0
MS65	PB+To	IP, C_MS	161.4	266.4	322.0	169.9	0.0
MS66	PB+To	IP, C_MS	428.6	532.8	121.2	343.6	0.0
MS67	PB+To	IP, C_MS	315.1	532.8	210.0	343.6	0.0
MS68	PB+To	IP, C_MS	126.6	532.8	251.7	343.6	0.0
MS69	PB+To	IP, Ax_MS	386.1	266.4	257.2	0.0	0.0
MS70	PB+To	IP, To_MS	383.8	0.0	255.6	169.9	0.0
MS71	PB	IP, Ax_MS	552.9	266.4	0.0	0.0	0.0
MS72	PB	IP, Ax_MS	532.8	532.8	0.0	0.0	0.0
MS73	To	IP, To_MS	0.0	0.0	339.0	169.9	0.0

MS74	To	IP, To_MS	0.0	0.0	343.6	343.6	0.0

4.4. Assumptions for Endurance Criteria

In practical applications loading history may not be defined with an analytical formulation and it may be a variable amplitude loading defined with discrete data points. Even though the analytical expression of the loading history is available like in this study (harmonic bending/torsion loading), how many data points to be utilized is an optimization problem in terms of the accuracy of the methods i.e. minimum number of data points should be employed which provides the highest possible accuracy of the methods. This optimization procedure may be thought like a mesh convergence study usually carried out for finite element models.

Discretization of loading history may affect the accuracy of all the multiaxial endurance criteria investigated in this study; however, it would have a greater impact in critical plane models. This is due to the complex shear stress calculations which are closely related to the non-proportionality of the loading and which requires a well-defined loading history. Accuracy of the critical plane methods is also affected by another factor; incrementation of Eulerian angles (θ, φ), which is not applicable to equivalent stress or invariant based methods since these methods does not search all material planes. According to Weber et al. [59], usual practice for angle incrementation is to choose both increments as 10^{o}. However, it is questionable whether this incrementation is the optimal value or not as there have not been a study investigating different angle increments found in literature.

Considering the statements above, an optimization study is performed for both the number of data points that define the loading history and for the angle incrementation of the critical plane search. For this study, two critical plane methods namely; Findley and Dang Van are investigated with experimental data including four different type of partial effects specifically nMS, Ax_MS, To_MS and C_MS. Two different critical plane methods are chosen as they reach dissimilar critical planes owing to their damage parameters thus, the optimal

incrementation may differ. The aim of examining loadings with different partial effects is to obtain the optimum number of data points for the load discretization as non-proportional loadings may require much more data points compared to proportional loadings for accurate solutions.

Test data selected for this optimization study is composed of eight experimental data including in phase and out of phase loadings for each set of partial effects. Detailed information involving material, alternating and mean values of normal and torsion loads and phase difference about the evaluated experimental data are shown in Table 4.14.

Table 4.14: Information about the data set chosen for optimization study of load discretization and angle incrementation

Material	Test Label	Loading Type	σ_a [MPa]	σ_m [MPa]	τ_a [MPa]	τ_m [MPa]	δ_{xy} [deg]
Hard Steel	nMS3	PB+To	255.1	0	127.5	0	0
Hard Steel	nMS10	PB+To	308	0	63.9	0	90
42CrMo4	MS4	PB+To	280	280	134	0	0
42CrMo4	MS5	PB+To	271	271	130	0	90
42CrMo4	MS1	PB+To	266	0	128	128	0
42CrMo4	MS2	PB+To	283	0	136	136	90
30NCD16	MS31	PB+To	451	294	250	191	0
30NCD16	MS32	PB+To	462	294	258	191	90

For load discretization, eight different possibilities are investigated and shown in Table 4.15.

Table 4.15: Number of Discrete Points for Harmonic Loading

Tested Discrete Points							
5	10	20	40	60	80	100	200

Estimations are obtained for Findley and Dang Van using as many discrete points as given in Table 4.15 for defining the loading histories and 1^o incrementation is employed for Euler angles as it is assumed to be the lowest incrementation one could employ. Then for each loading fatigue index errors are found and normalized with the calculated fatigue index errors for 1000 discrete points, which is assumed to give the most accurate solution. Finally, these results are presented with respect to number of discrete points and shown through Figure 4.3 to Figure 4.6.

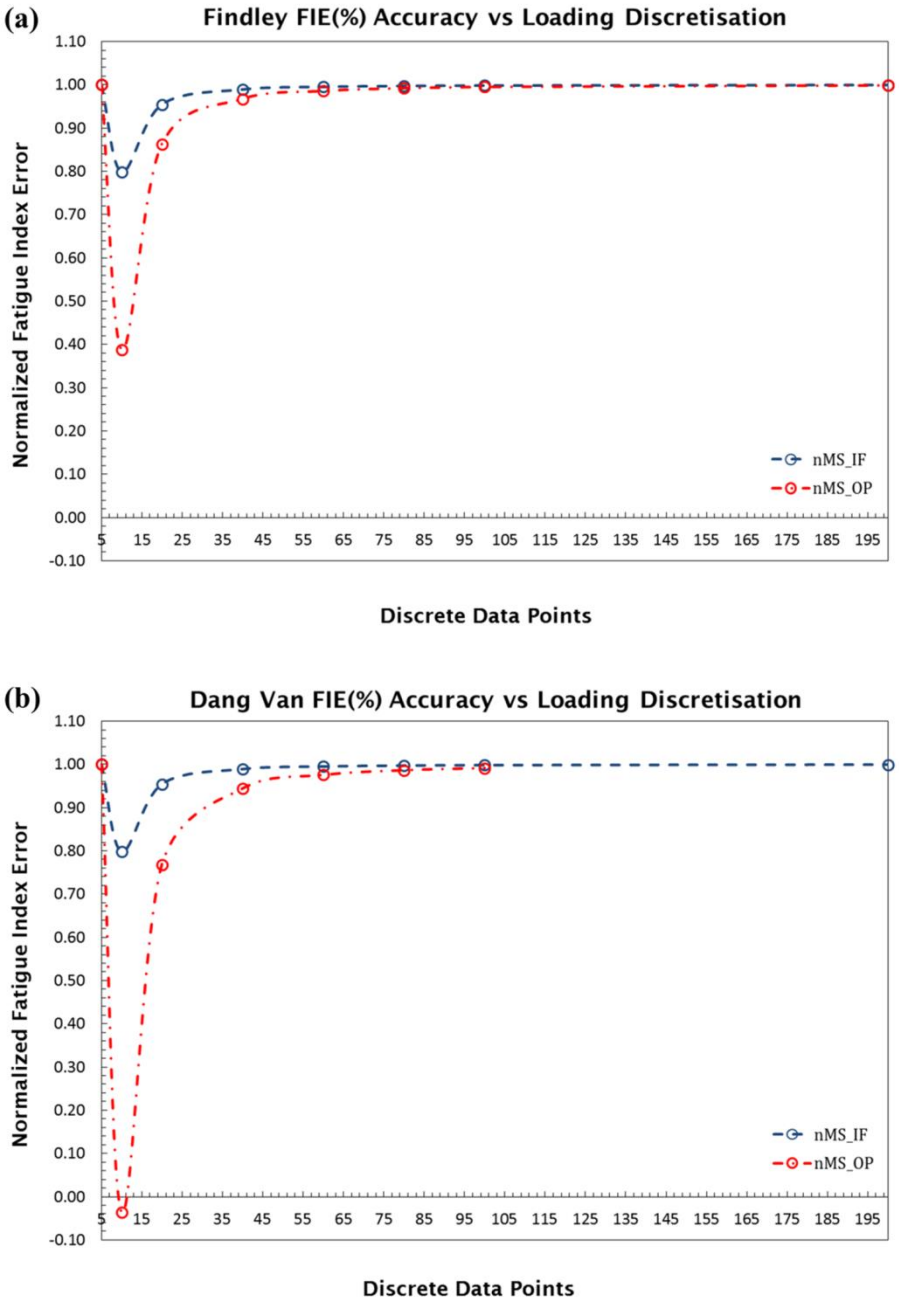

Figure 4.3: Accuracy of a) Findley and b) Dang Van with respect to loading discretizing for loading set nMS

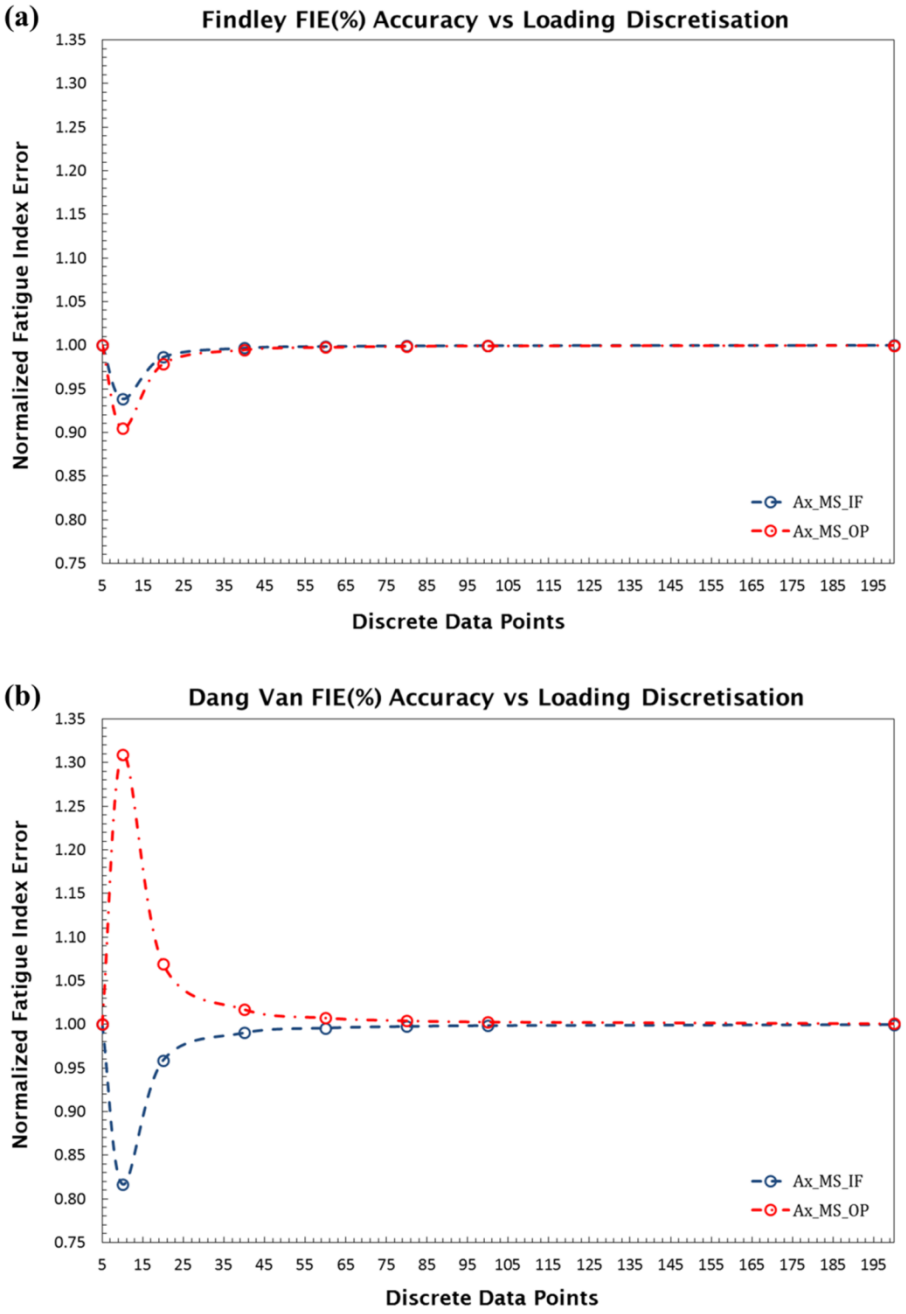

Figure 4.4: Accuracy of a) Findley and b) Dang Van with respect to loading discretizing for loading set Ax_MS

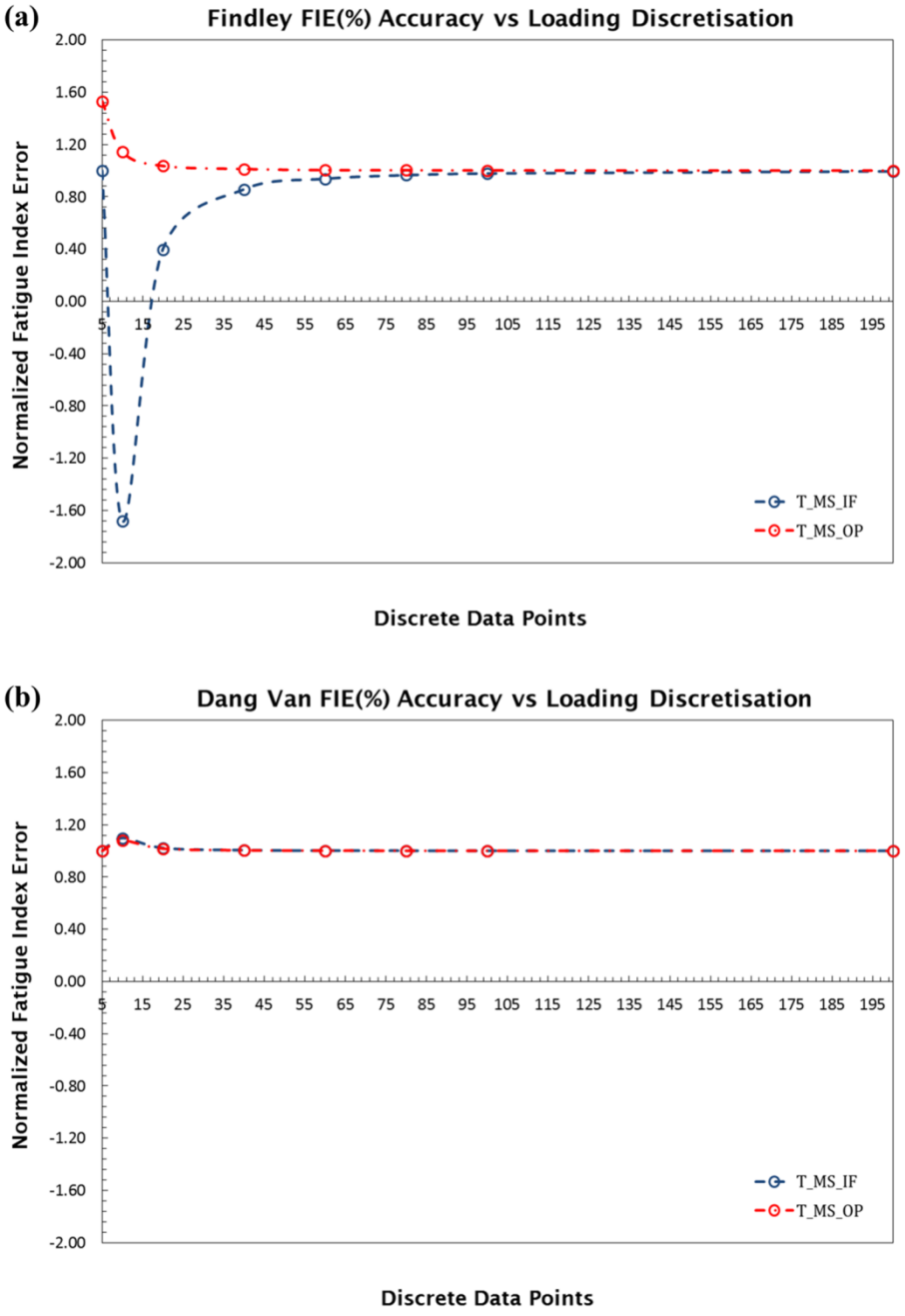

Figure 4.5: Accuracy of a) Findley and b) Dang Van with respect to loading discretizing for loading set To_MS

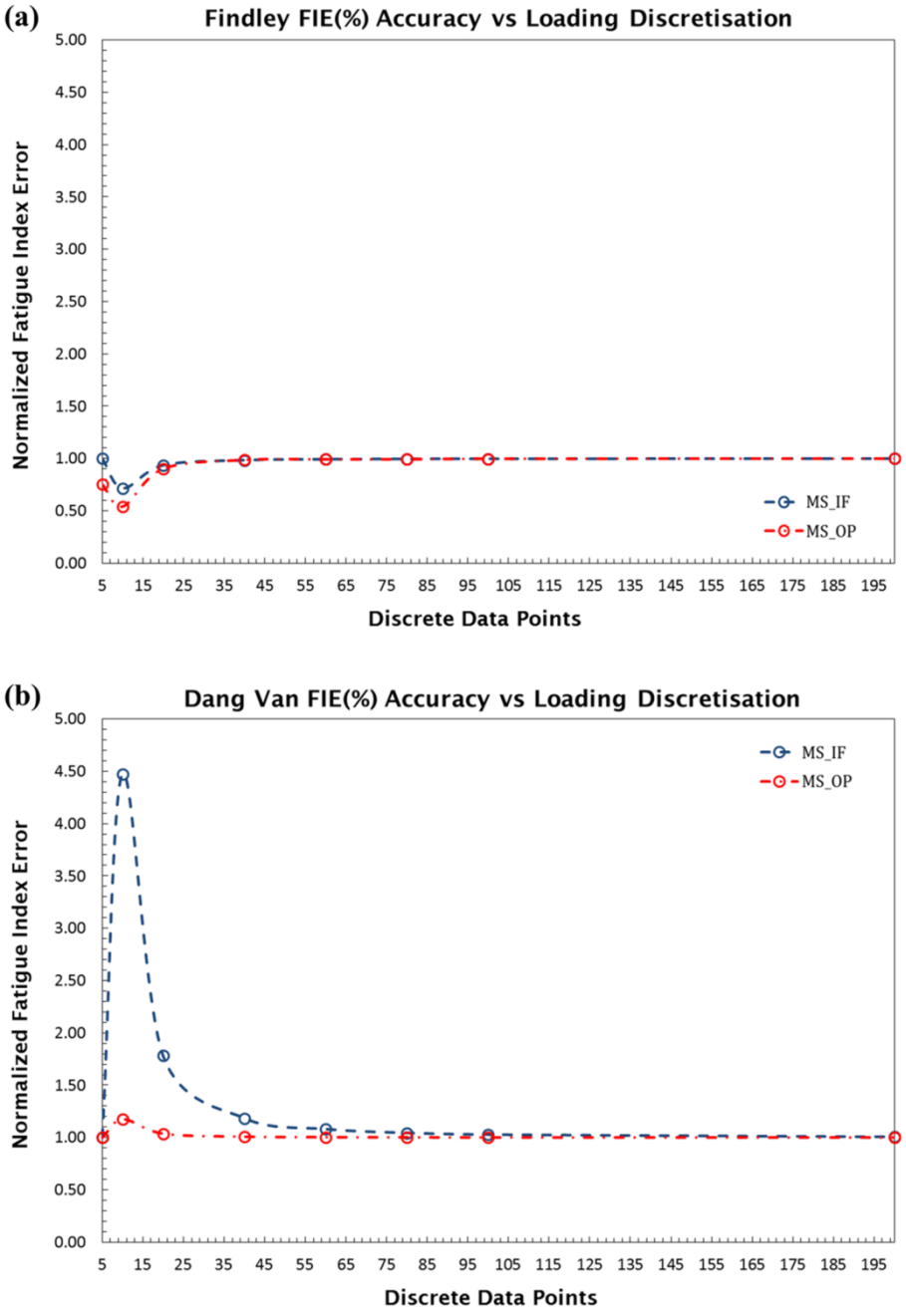

Figure 4.6: Accuracy of a) Findley and b) Dang Van with respect to loading discretizing for loading set C_MS

When Figure 4.3 through Figure 4.6 are evaluated, one may conclude that simulating the loading history with 10 discrete points is not feasible as for most of the cases a sudden drop in accuracy is observed. The main reason of this behavior is that the maximum and minimum peak values of a sine wave will not

be included in the load history if only 10 discrete points are utilized. Another interesting conclusion is related to the results obtained with only 5 discrete points. For this situation, most of the loading cases resulted with the most accurate solution except loading cases of To_MS and C_MS. This result should not be confusing. One could simulate the maximum and minimum peak values of a sine wave by only using 5 points; however, it is clear that for loadings with mean stresses accurate solutions can not be obtained by this amount of (very few) discrete points and in global sense more points should be employed. If all these loading cases are considered, it is clear that the optimum number of discrete points lie between 80-100 points. To be on the safe side, 100 points are chosen for load discretization and utilized for all other calculations presented in this study. For clarifying the differences in discretization, example loading histories with 5 and 100 discrete points are shown in Figure 4.7. From this figure it is seen that discretization with 5 discrete points is a rough estimation which includes sharp turns at peak values while history with 100 discrete points provide a close approximation to the real sinusoidal loading.

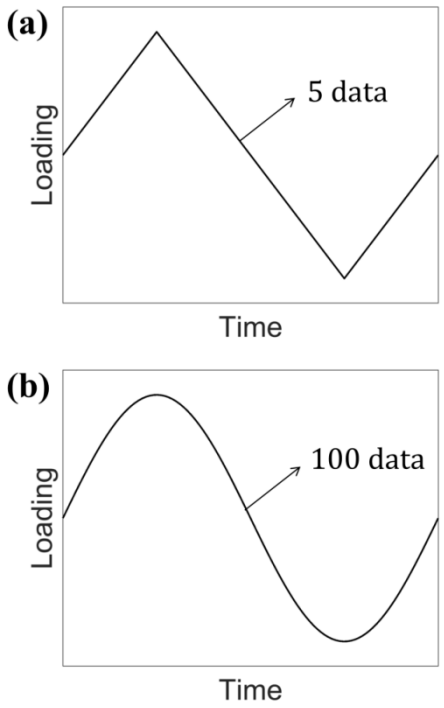

Figure 4.7 Loading history with a) 5 discrete points b) 100 discrete points

For angle incrementation same experimental data set is used but with the chosen loading discretization (100 points) and with eleven different Euler angle incrementations being 1^o is the lowest and these incrementations are given in Table 4.16.

Table 4.16: Euler Angles (θ, φ) Incrementation for Critical Plane Search

Tested Euler Angles (θ, φ) Incrementations										
1	2	4	6	8	10	12	14	16	18	20

Estimations are obtained for Findley and Dang Van using angular increments given in Table 4.16 and results are normalized with the fatigue index errors for 1^o incrementation which is assumed to be the most accurate solution. These results are presented with respect to angle increments and shown through Figure 4.8 to Figure 4.11.

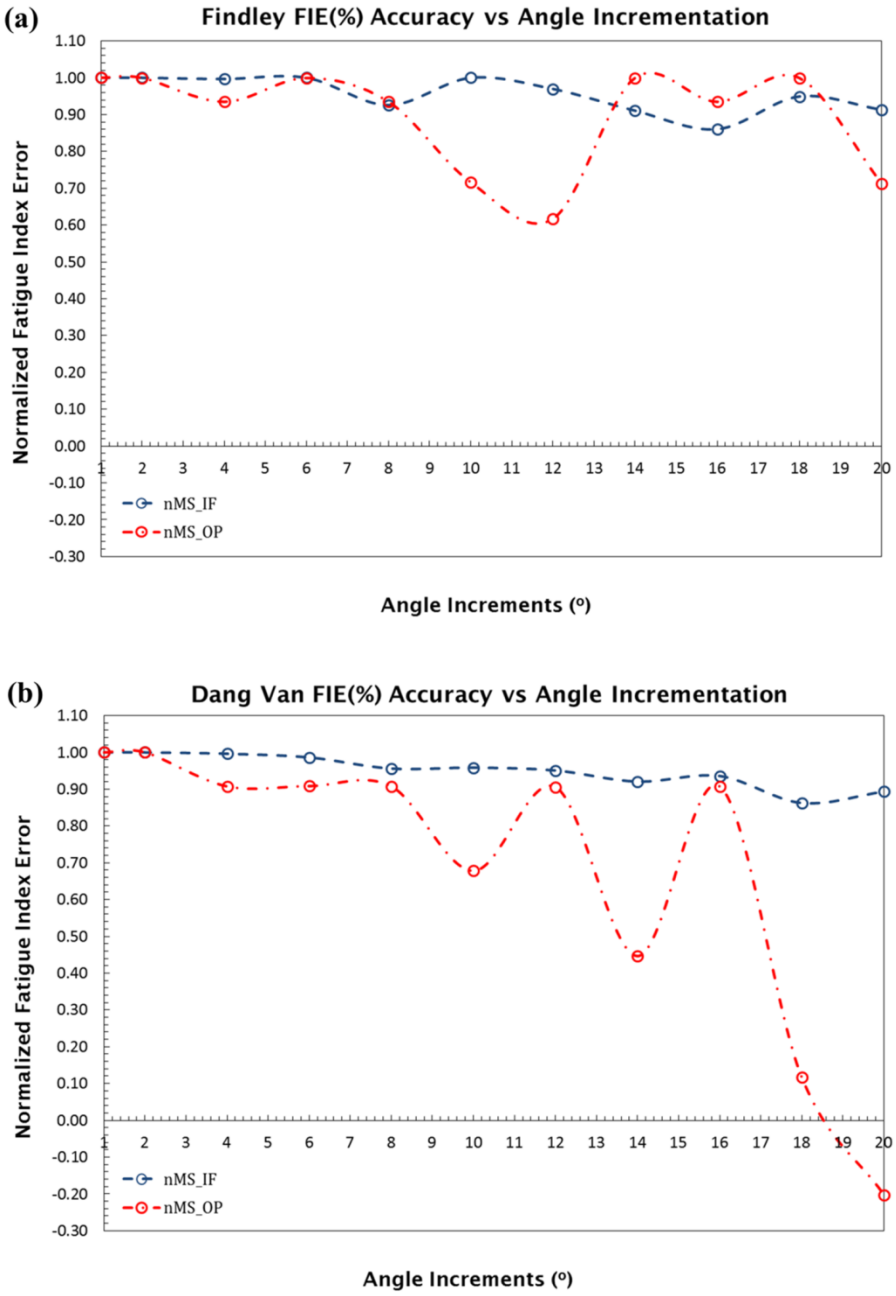

Figure 4.8: Accuracy of a) Findley and b) Dang Van with respect to angular incrementation for loading set Nms

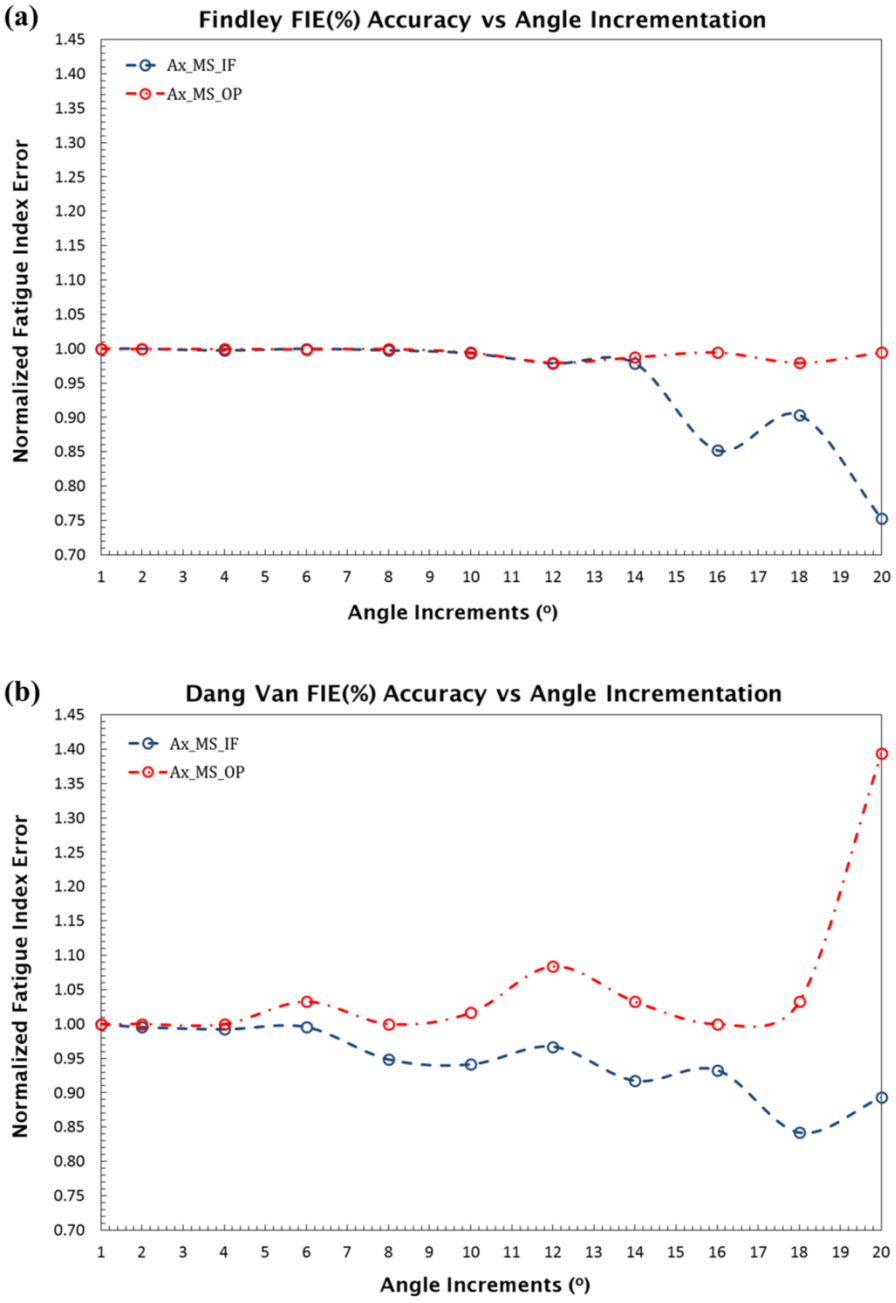

Figure 4.9: Accuracy of a) Findley and b) Dang Van with respect to angular incrementation for loading set Ax_MS

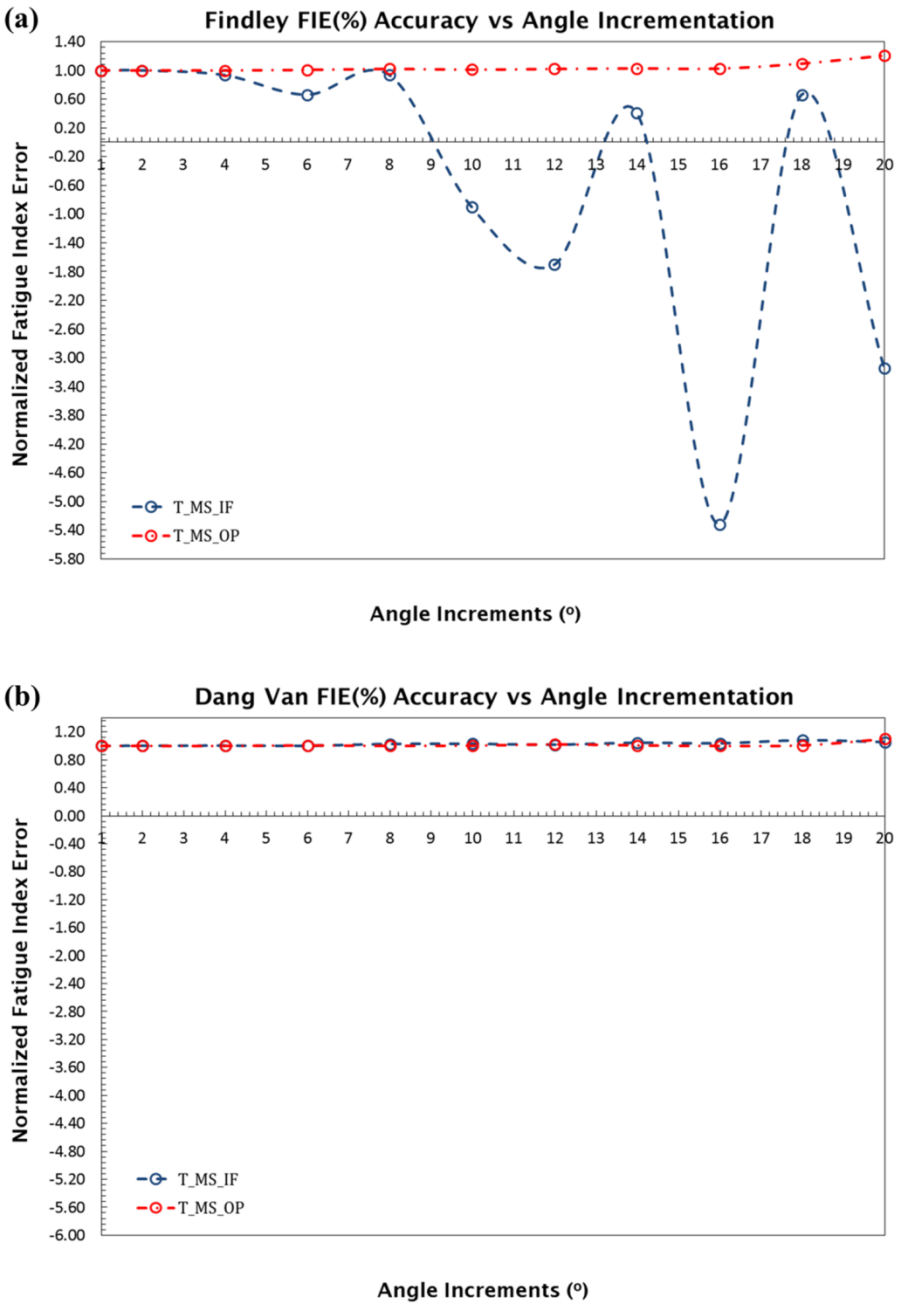

Figure 4.10: Accuracy of a) Findley and b) Dang Van with respect to angular incrementation for loading set To_MS

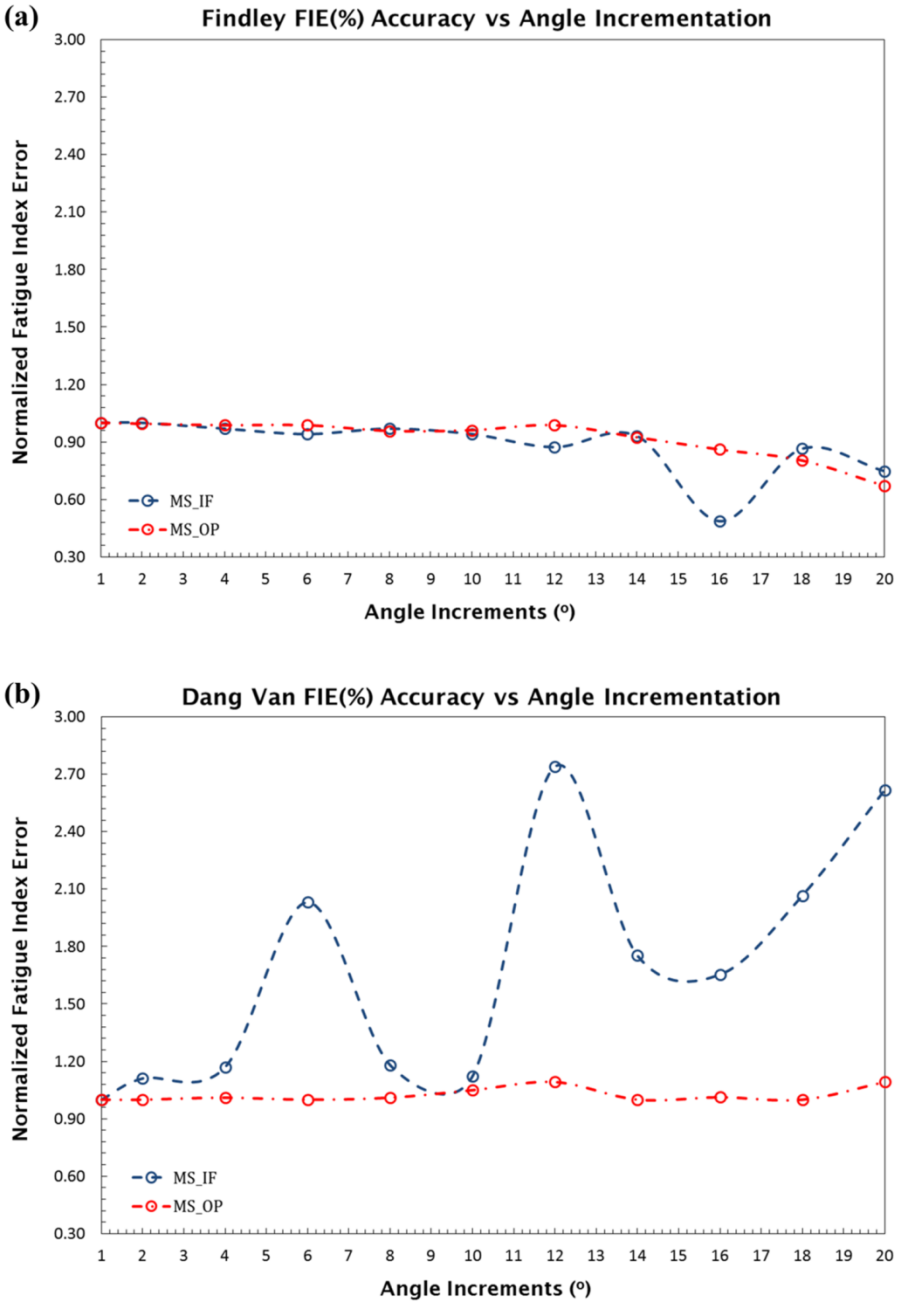

Figure 4.11: Accuracy of a) Findley and b) Dang Van with respect to angular incrementation for loading set C_MS

We conclude from evaluation of Figure 4.8 through Figure 4.11 that higher increments larger than 10^{o} should not be utilized since too many fluctuations are observed. As for incrementation of 10^{o}, which is proposed by Weber et al. [59], critical plane may be missed out as results of nMS and To_MS groups deviate

from the actual solution by at least 30% which is not acceptable. Optimum incrementation seems to be in the range 2^o to 4^o. For the 4^o incrementation, deviation may be as high as 15% as seen from Figure 4.11b (C_MS group) which may be acceptable if calculation time is an issue. However, for this study angle increments of 2^o are employed.

4.5. Pseudocodes

MATLAB codes are written for conducting calculations related to each type of criteria (equivalent stress, invariant based and critical plane). All these MATLAB codes take inputs of experimental data presented in Section 4.2. from an Excel file (input Excel). These inputs are test labels, materials, endurance limits, alternating and mean values of loadings and phase and frequency difference between loading channels. Each code writes damage parameter, fatigue index error and stress values calculated for each test data as outputs to a new Excel file (output Excel). In this section, pseudocodes of each type of criteria are presented. These pseudocodes are useful for comparing the procedures of the different criteria and for a better understanding of their algorithms.

Pseudocode for equivalent stress criteria is as follows:

1. INPUT the name of the Excel that includes experimental data.
2. INPUT the path of the input Excel.
3. INPUT the method name ('AMP' or 'SVM').
4. INPUT the mean stress correction type ('Soderberg', ‘Goodman’, ‘Gerber’ or 'SWT').
5. INPUT the discretization of time (default is 100).
6. OPEN a new Excel for writing outputs.
7. FOR each sheet in input Excel
8. FOR each test data in input Excel
9. FOR the time history from 0 to 2π with user input discretization
10. CALCULATE $\sigma_i(t)$ for which $i = 1,2,3$
11. CALCULATE $\sigma_{eq}(t)$
12. ENDFOR

13. CALCULATE $\sigma_{eq,a}$, $\sigma_{eq,m}$, $\sigma_{eq,max}$ and $\sigma_{eq,min}$
14. IF $\sigma_{eq,m}$ is lower than or equal to 0 THEN
15. SET $\sigma_{eq,m}$ to 0
16. SET damage parameter (DP) to $\sigma_{eq,a}$
17. ELSE
18. CALCULATE $\sigma_{eq,aMSC}$ from the user input mean stress correction
19. SET damage parameter (DP) to $\sigma_{eq,aMSC}$
20. ENDIF
21. CALCULATE FIE(%)
22. STORE FIE,DP and stress variables
23. ENDFOR
24. WRITE FIE,DP and stress variables to a new sheet in output Excel.
25. WRITE endurance limits and material parameters to a new sheet in output Excel.
26. ENDFOR
27. CLOSE the output Excel.

Pseudocode for invariant based criteria is as follows:

1. INPUT the name of the Excel that includes experimental data.
2. INPUT the path of the input Excel.
3. INPUT the method name ('SNS', 'CROSS' or 'GAM').
4. INPUT the type of calibration Bending/Torsion or Axial ('frtr' or 'frf0').
5. INPUT the discretization of time (default is 100).
6. OPEN a new Excel for writing outputs.
7. FOR each sheet in input Excel
8. FOR each test data in input Excel
9. CALCULATE material parameters a and b
10. FOR the time history from 0 to 2π with user input discretization
11. CALCULATE $\sigma_i(t)$ and $S_j(t)$ for which $i = 1,2,3$ and $j = 1,2, \dots 5$

12. ENDFOR
13. IF method is ‘SNS’ or ‘CROSS’ THEN
14. CALCULATE $\sigma_{h,max}, \sigma_{h,min}, \sigma_{h,osci}, \sigma_{h,mean}$
15. CALCULATE $\sqrt{J_{2,a}}$
16. ENDIF
17. IF method is ‘GAM’ THEN
18. CALCULATE $\sigma_{1,max}$
19. CALCULATE $\sqrt{\sum_{j=1}^{5}\left(\frac{1}{2}\left(S_{j,max}-S_{j,min}\right)\right)^2}$
20. ENDIF
21. CALCULATE damage parameter (DP)
22. CALCULATE FIE(%)
23. STORE FIE,DP and stress variables
24. ENDFOR
25. WRITE FIE,DP and stress variables to a new sheet in output Excel.
26. WRITE endurance limits and material parameters to a new sheet in output Excel.
27. ENDFOR
28. CLOSE the output Excel.

Pseudocode for critical plane criteria is as follows:

1. INPUT the name of the Excel that includes experimental data.
2. INPUT the path of the input Excel.
3. INPUT the method name ('FIN', 'DV', 'RB' or 'PCR').
4. INPUT the shear stress calculation method ('MCC' or 'MRH').
5. INPUT the MCC algorithm ('MCC_fminmax' of 'MCC_Randomised').
6. INPUT the type of calibration Bending/Torsion or Axial ('frtr' or 'frf0').
7. INPUT the incrementation of Euler angles θ and φ (default is 1 degree).
8. INPUT the discretization of time (default is 100).
9. OPEN a new Excel for writing outputs.
10. FOR each sheet in input Excel

11. FOR each test data in input Excel
12. IF method is ‘FIN’, ‘DV’ or ‘PCR’ THEN
13. CALCULATE material parameters a and b.
14. ELSEIF method is ‘RB’ THEN
15. CALCULATE material parameters a, b and c.
16. ENDIF
17. IF method is ‘DV’ THEN
18. CALCULATE $\sigma_{h,max}$
19. ENDIF
20. FOR θ from 1^o to 180^o with the user input incrementation
21. FOR φ from 1^o to 180^o with the user input incrementation
22. FOR the time history from 0 to 2π with user input discretization
23. CALCULATE $\boldsymbol{t}, \sigma_n(t), \sigma_{ny}(t), \sigma_{nz}(t)$
24. ENDFOR
25. CALCULATE $\sigma_{n,max}, \sigma_{n,min}, \sigma_{n,osci}, \sigma_{n,mean}$
26. CALCULATE T_a from $\sigma_{ny}(t)$ and $\sigma_{nz}(t)$ for the input shear stress calculation method, algorithm and calibration type
27. CALCULATE Damage Parameter (DP)
28. STORE DP, stress variables, θ and φ in a matrix named CP.
29. ENDFOR
30. ENDFOR
31. SEARCH rows of the matrix CP for the critical plane for which the DP is maximum.
32. CALCULATE FIE (%) for the DP at critical plane
33. WRITE FIE, DP, stress variables, θ and φ to a new sheet in the output Excel
34. WRITE endurance limits, material parameters to another sheet in output Excel.
35. ENDFOR

36. CLOSE the output Excel.

From these psedusocodes we show that the fastest approach is the equivalent stress criteria as these methods require very few calculations and loops and their formulations are very simple which only requires principal stresses. Invariant based criteria involve more computations, particularly the calculation of deviatoric stresses and the hydrostatic stress, compared to equivalent stress criteria; however, their speeds are comparable. The slowest approach is the critical plane criteria as all the material planes are searched with respect to two Euler angles (θ and φ) for the maximum value of a damage parameter and the speed of the process mostly depends on the number of planes to be searched which is related to the square of the angle incrementation.

CHAPTER 5

RESULTS AND COMPARISON OF CRITERIA

Multiaxial endurance criteria introduced in Chapter 2 are tested on high cycle fatigue experimental data which is compiled in Chapter 4. Performance of the criteria are examined for two major effects namely phase effect (PE) and mean stress effect (MSE) and their combinations. Estimations of each method for all experimental data are presented in Appendix. In this chapter, data set is grouped according to investigated effects (PE and MSE). Then, statistical analysis results of these groups and histograms demonstrating general behavior of the criteria are presented. Furthermore, tables showing statistical measures (mean, range and standard deviation) for each group are also included for detailed analysis of the criteria. It is worth to mention that some groups like T_MS group lack enough data (more than 20 data) for a healthy statistical analysis according to Papuga [45].

5.1. Equivalent Stress Criteria

Absolute Maximum Principal (AMP) and Signed von Mises (SVM) criteria are tested for four different mean stress corrections (Soderberg, Goodman, Gerber and SWT) and their histograms are shown below for AMP and SVM in Figure 5.1 and in Figure 5.2 respectively. Also Table 5.1 demonstrates the mean fatigue index errors (mFIE) for each group of data.

When the first criterion AMP is investigated, we conclude that AMP result in highly scattered estimations and include excessively non-conservative estimations up to -70% mFIE. Histogram of SWT shows a better behavior as the most non-conservative estimate shifts to -65%; however, range is still too high being in limits -65% to 30%. Most of the estimations lie in the non-conservative side of

the histogram. When Table 5.1 is examined, one may observe the inefficiency of the criterion for handling the phase effect as mFIE for OP_nMS group decreases up to -20% when compared to IP_nMS groups for which mFIE is -10%. Mean fatigue index errors are 6.32% and -1.73% for Soderberg and Goodman estimations for ALL group and they are in tolerable range; however, these results should not be confusing as it is due to the high conservatism of Soderberg and Goodman curves. As shown in Table 5.1 Gerber yields non-conservative mFIE for all group of data which are out of tolerance. One may observe from Table 5.1 that MS group have conservative estimates such as 24.14% and 9.56% for Soderberg and Goodman while SWT correction leads to -6.29% mFIE which is acceptable compared to Soderberg. Moreover, criterion leads to very high range of FIE (see Table 5.2) which is 275% for Soderberg and takes its' minimum value for SWT with 108% which is still pretty high. Further investigation reveals that criterion has a high standard deviation up to 46.25 for Soderberg (see Table 5.3) for the ALL group and minimum standard deviation is obtained for again SWT correction with 20.37 which is still too much to be accepted.

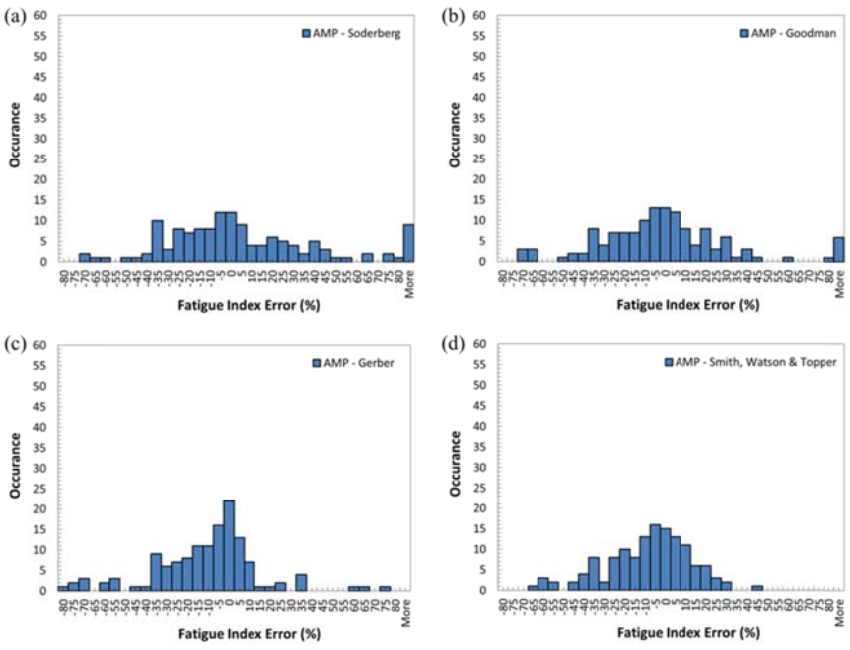

Figure 5.1: Absolute Principal Stress Criterion Histograms for Different Mean Stress Corrections; a) Soderberg, b) Goodman, c) Gerber, d) SWT

Histogram of SVM is much better compared to AMP as the median is shifted to 5%, which is -5% for AMP with SWT correction; however, estimations are again highly scattered and non-conservative estimations up to -70% are obtained. Similar arguments can be made for performance of the criterion with Soderberg and Goodman corrections but much conservative estimations are obtained for SVM (mFIE of 36.53% and 19.74 for Soderberg and Goodman respectively for ALL group). Again best estimations are obtained with SWT correction as the range of histogram is -50% to 40% for which most of the results lie in the range -10% to 20%. Mean fatigue index error for SWT correction is 0.49% for ALL group which is pretty good and other groups are in tolerance except the T_MS group. Like AMP criterion, SVM suffers from phase effect as estimations drop down to non-conservative side for OP groups when mean fatigue index errors of IP_nMS and OP_nMS groups are investigated (3.79% for IP_nMS and -8.24% for OP_nMS). When range of the estimations are investigated (see Table 5.2), very high range values are observed for Soderberg, Goodman and Gerber (%800 for Soderberg decreased to % 417% for Gerber). This behavior can be explained with the highly conservative estimates of mean corrections as the most non-conservative estimation is -70% (obtained for Gerber). Standard deviation is also increased for Soderberg, Goodman and Gerber corrections for SVM (see Table 5.3); however, lower standard deviations is obtained for SWT correction with a value of 18.85.

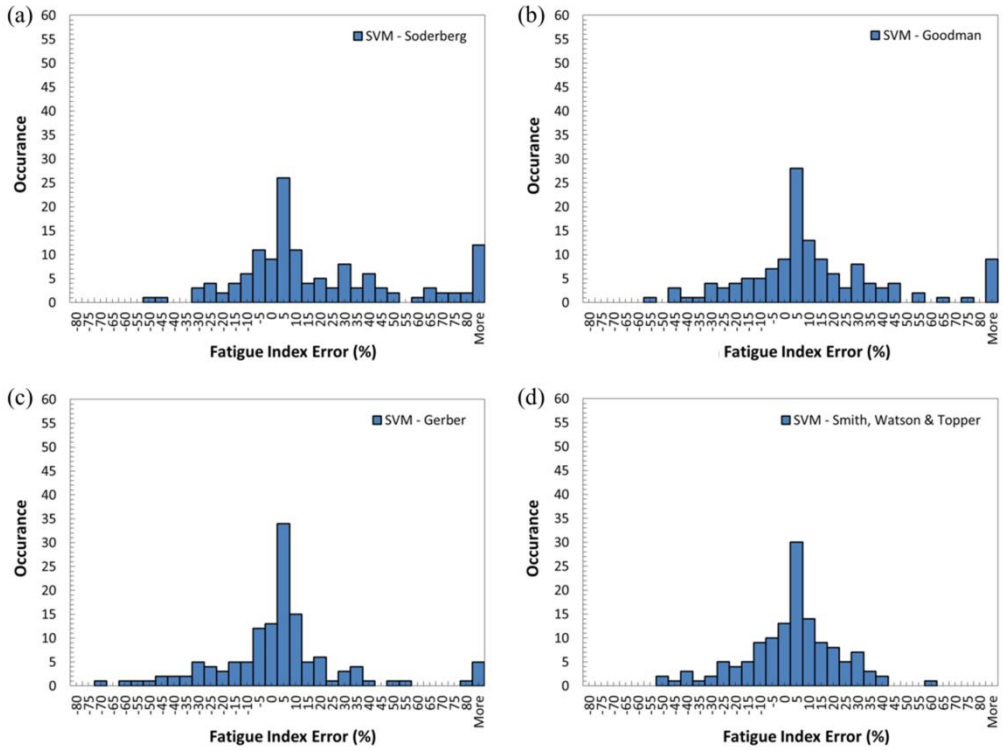

Figure 5.2: Signed von Mises Criterion Histograms for Different Mean Stress Corrections; a) Soderberg, b) Goodman, c) Gerber, d) SWT

Since best results are obtained for SWT correction, histograms of AMP and SVM for this mean stress correction is shown in Figure 5.3.

Discussion about equivalent stress criteria can be concluded with the following statements:

- Equivalent stress criteria yield high range and standard deviation of FIE even when the mFIE is tolerable like in the case of SVM with SWT correction.
- Equivalent stress criteria are unsuitable for out-of-phase loading.
- SVM criterion may be used for in-phase loadings without mean stresses as the mFIE and range are in tolerable limits; however, for loadings with mean stress range is high.

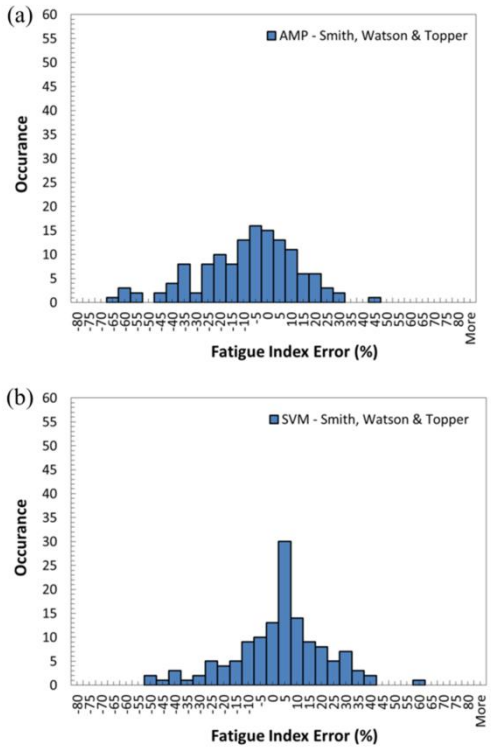

Figure 5.3: Histograms of a) Absolute Maximum Principal Stress and b) Signed von Mises Criterion with SWT Mean Stress Correction

Table 5.1: All partial effects, FIE (%) Mean of Absolute Maximum Principal and Signed von Mises Criteria

FIE (%) Mean	Absolute Maximum Principal				Signed von Mises			
	Soderberg	Goodman	Gerber	SWT	Soderberg	Goodman	Gerber	SWT
ALL (134)	6.32	-1.73	-12.79	-10.48	36.53	19.74	6.94	0.49
IP (79)	16.81	6.08	-9.26	-7.48	60.26	34.61	16.11	3.39
OP (55)	-8.74	-12.95	-17.87	-14.80	2.45	-1.61	-6.24	-3.67
nMS (60)	-15.65	-15.65	-15.65	-15.65	-2.82	-2.82	-2.82	-2.82
IP_nMS (27)	-10.02	-10.02	-10.02	-10.02	3.79	3.79	3.79	3.79
OP_nMS (33)	-20.27	-20.27	-20.27	-20.27	-8.24	-8.24	-8.24	-8.24
MS (74)	24.14	9.56	-10.47	-6.29	68.44	38.04	14.86	3.18
IP_MS (52)	30.74	14.44	-8.86	-6.16	89.58	50.61	22.51	3.18
OP_MS (22)	8.55	-1.98	-14.26	-6.59	18.49	8.33	-3.24	3.18
To_MS (12)	2.26	0.57	-4.80	-0.69	21.95	18.95	12.03	15.71
Ax_MS (62)	28.37	11.30	-11.56	-7.37	77.44	41.74	15.40	0.76
IP_Ax_MS (44)	35.67	16.82	-9.18	-7.30	102.13	56.89	25.86	1.53
OP_Ax_MS (18)	10.53	-2.20	-17.39	-7.54	17.10	4.70	-10.16	-1.12

Table 5.2: All partial effects, FIE (%) Range of Absolute Maximum Principal and Signed von Mises Criteria

FIE (%) Range	Absolute Maximum Principal				Signed von Mises			
	Soderberg	Goodman	Gerber	SWT	Soderberg	Goodman	Gerber	SWT
ALL (134)	275.42	234.60	155.67	108.24	814.34	452.73	417.41	112.77
IP (79)	275.42	234.60	155.67	108.24	814.34	452.73	417.41	112.77
OP (55)	116.12	71.21	64.42	49.38	106.76	70.19	72.22	68.20
nMS (60)	43.94	43.94	43.94	43.94	45.01	45.01	45.01	45.01
IP_nMS (27)	43.77	43.77	43.77	43.77	22.44	22.44	22.44	22.44
OP_nMS (33)	39.80	39.80	39.80	39.80	40.30	40.30	40.30	40.30
MS (74)	275.42	234.60	155.67	108.24	814.34	452.73	417.41	112.77
IP_MS (52)	275.42	234.60	155.67	108.24	814.34	452.73	417.41	112.77
OP_MS (22)	116.12	71.21	64.42	49.38	88.89	63.15	72.22	62.17
To_MS (12)	51.91	51.24	61.18	50.04	91.45	74.34	77.72	66.58
Ax_MS (62)	275.42	234.60	155.67	108.24	814.34	452.73	417.41	112.77
IP_Ax_MS (44)	275.42	234.60	155.67	108.24	814.34	452.73	417.41	112.77
OP_Ax_MS (18)	116.12	71.21	61.17	49.38	88.89	50.03	54.16	46.89

Table 5.3: All partial effects, FIE (%) Standard Deviation of Absolute Maximum Principal and Signed von Mises Criteria

FIE (%) Standard Deviation	Absolute Maximum Principal				Signed von Mises			
	Soderberg	Goodman	Gerber	SWT	Soderberg	Goodman	Gerber	SWT
ALL (134)	46.25	37.17	25.33	20.37	110.31	67.64	52.25	18.85
IP (79)	54.84	44.77	30.47	23.49	137.80	83.98	65.32	21.12
OP (55)	22.50	16.51	13.63	13.64	19.95	15.57	15.15	13.99
nMS (60)	12.44	12.44	12.44	12.44	10.39	10.39	10.39	10.39
IP_nMS (27)	11.55	11.55	11.55	11.55	4.65	4.65	4.65	4.65
OP_nMS (33)	11.17	11.17	11.17	11.17	10.65	10.65	10.65	10.65
MS (74)	55.12	45.73	32.01	24.22	140.25	86.31	68.67	23.23
IP_MS (52)	62.71	52.64	36.62	27.64	162.25	99.77	79.69	25.81
OP_MS (22)	24.08	17.14	16.00	12.89	19.90	16.47	19.70	15.52
To_MS (12)	14.34	13.30	16.57	13.11	24.47	21.80	24.07	20.72
Ax_MS (62)	58.96	49.43	34.09	25.68	151.21	93.35	74.26	22.91
IP_Ax_MS (44)	66.62	56.51	38.93	29.17	173.04	106.75	85.51	26.02
OP_Ax_MS (18)	26.01	18.76	15.79	13.83	20.72	15.02	14.22	12.19

5.2. Invariant Based Criteria

Sines, Crossland and GAM criteria are evaluated in this section with standard calibration (bending-torsion calibration). Evaluations are carried out by comparing the performance of pairs Sines-Crossland and Crossland-GAM criteria. Histograms of the criteria are shown in Figure 5.4 and Figure 5.5. Furthermore, mean, range and standard deviation of FIE are given in Table 5.4 to Table 5.6. When histograms of Sines and Crossland are investigated (see Figure 5.4), one may conclude that the histograms are more compact compared to histograms of equivalent stress criteria. Therefore, it may be stated that inclusion of mean stress into damage parameter instead of using mean stress corrections is an effective way. Median of histograms for Sines and Crossland are -5% and 0% respectively which indicates that Crossland is on conservative side. Improvement of Crossland is also observed by evaluation of ranges of Sines and Crossland. Estimations of Sines are between -35% to 30% while for Crossland, estimations are between -30% to 10% meaning that the range is decreased for Crossland. Mean fatigue index error of Sines for the ALL group is -4.62%; however, it is -7.62% for Crossland (see Table 5.4). Both methods are not adequate for phase effect as sharp drop of FIE is observed for OP groups. This behavior can be verified by comparing IP_nMS and OP_nMS groups. As an example, mFIE is -4.04% for IP_nMS and it drops down to -14.22% for OP_nMS for Sines criterion. Actual improvement in Crossland is observed in the range of FIE as mentioned above. For the ALL group Sines yields a range of 68.10% while the range is 40.48% for Crossland (see Table 5.5) but it is still a high range to be accepted. Another advantage of Crossland is seen in standard deviations (see Table 5.6) as they are reduced for all groups.

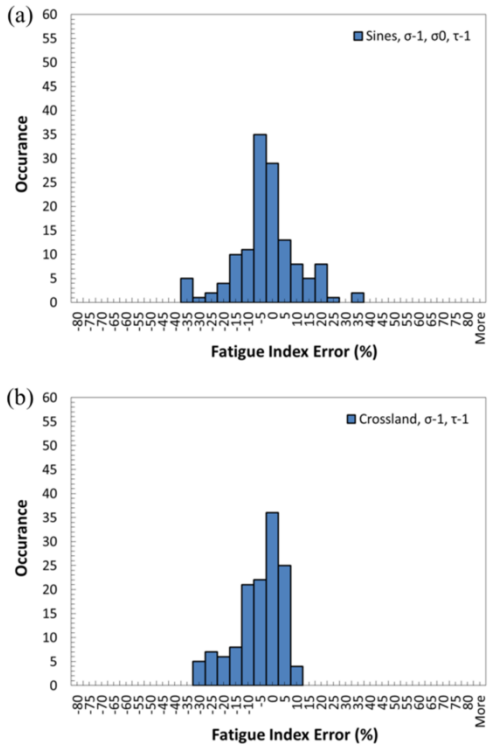

Figure 5.4: Histograms of a) Sines and b) Crossland Criteria

When Figure 5.5 is investigated, one may notice that histogram of GAM criterion is nicer compared to Crossland as the median of the histogram is shifted to 5% and estimations are obtained in a small range (-10% to 20%). Also most of the estimations are in the limits of -5% to 10% which is a desired property of a histogram. If the mean fatigue index errors are evaluated (see Table 5.4), we may conclude that they take values in between -1.40% to 2.30% which is very close to zero and mostly conservative. Moreover, GAM criterion show small difference in estimations of IP and OP groups indicating that phase effect is handled well. Furthermore, MS groups have low mean fatigue indices showing the efficiency of using maximum value of the first principal stress as the normal mean stress inclusion. Range of GAM for ALL group is 31.5% which is slightly high from the optimum value while the criterion result in a standard deviation of 5.8. Also, there is not much change in standard deviations of IP and OP groups showing the outstanding performance of the criterion.

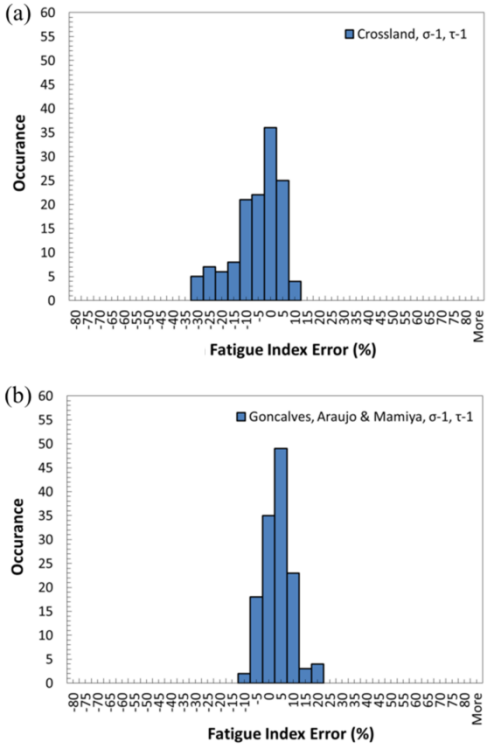

Figure 5.5: Histograms of a) Crossland and b) GAM Criteria

Discussion about invariant based criteria can be concluded with the following statements:

- Combination of the octahedral shear stress and hydrostatic stress seems inadequate for handling the phase and mean stress effects. However, use of maximum value of the hydrostatic stress (Crossland) clearly improves the results as both the range and standard deviation decreases up to reasonable values.

- Combination of alternating value of the deviatoric stress tensor and maximum of the first principal stress (GAM damage parameter) seems promising as all the statistical measures reduce to tolerable values.

- GAM criterion shows exceptional behavior for all groups and the speed of the criterion is a great advantage; however, range and standard deviation are slightly high from the optimum values. Nevertheless, estimations are

mostly on conservative side and the criterion may be used for any loading case.

Table 5.4: All partial effects, FIE (%) Mean of Sines, Crossland and GAM Criteria

FIE (%) Mean	Sines	Crossland	GAM
ALL (134)	-4.62	-7.62	1.31
IP (79)	-0.40	-4.15	1.70
OP (55)	-10.67	-12.60	0.76
nMS (60)	-9.64	-4.81	1.75
IP_nMS (27)	-4.04	1.08	1.35
OP_nMS (33)	-14.22	-9.62	2.07
MS (74)	-0.54	-9.90	0.96
IP_MS (52)	1.49	-6.87	1.88
OP_MS (22)	-5.34	-17.06	-1.20
To_MS (12)	-15.39	-9.35	-0.26
Ax_MS (62)	2.33	-10.01	1.20
IP_Ax_MS (44)	3.95	-6.90	2.26
OP_Ax_MS (18)	-1.62	-17.59	-1.39

Table 5.5: All partial effects, FIE (%) Range of Sines, Crossland and GAM Criteria

FIE (%) Range	Sines	Crossland	GAM
ALL (134)	68.10	40.48	31.50
IP (79)	54.04	32.80	28.94
OP (55)	53.10	39.11	28.83
nMS (60)	42.96	38.60	28.83

IP_nMS (27)	21.73	17.51	17.92
OP_nMS (33)	37.27	34.46	28.83
MS (74)	68.10	39.11	30.26
IP_MS (52)	54.04	29.41	28.89
OP_MS (22)	53.10	39.11	18.08
To_MS (12)	33.36	34.82	14.02
Ax_MS (62)	48.02	37.09	30.26
IP_Ax_MS (44)	43.21	29.41	28.89
OP_Ax_MS (18)	33.02	32.65	18.08

Table 5.6: All partial effects, FIE (%) Standard Deviation of Sines, Crossland and GAM Criteria

FIE (%) Standard Deviation	Sines	Crossland	GAM
ALL (134)	12.50	9.67	5.81
IP (79)	10.70	7.01	5.93
OP (55)	12.42	10.73	5.59
nMS (60)	10.53	9.36	5.11
IP_nMS (27)	5.94	4.12	4.10
OP_nMS (33)	11.24	9.69	5.80
MS (74)	12.49	9.31	6.30
IP_MS (52)	12.05	6.66	6.69
OP_MS (22)	12.21	10.67	4.61
To_MS (12)	9.66	9.20	4.46
Ax_MS (62)	10.83	9.33	6.57
IP_Ax_MS (44)	11.27	7.01	6.95
OP_Ax_MS (18)	8.44	9.93	4.62

5.3. Critical Plane Criteria

Findley, Dang Van, Robert and Papuga PCR criteria are evaluated in this section with standard calibration (bending-torsion calibration) and for shear stress calculation method MCC. First two critical plane criteria include two material parameters and they only differ in mean stress inclusion which also affects the phase effect properties of the criteria. The last two criteria use the same stress measures; however, their combinations are different. Robert uses a linear formulation while Papuga PCR uses a non-linear expression. Evaluations of these criteria are carried out by comparing the performance of pairs Findley-Dang Van, Findley-Robert and Robert-Papuga PCR criteria. Histograms of the criteria are shown in Figure 5.6 to Figure 5.8. Furthermore, mean, range and standard deviation of FIE are given in Table 5.7 to Table 5.9.

One may observe that both Findley and Dang Van criteria have nicely shaped histograms, both having their medians at 5% mFIE. Range of both criteria is close; however, it is lower for Dang Van as the estimations lie in the limits of -25% to 15% while it is -15% to 35% for Findley. From histograms another conclusion can be made that most of the estimations of Findley are on the conservative side compared to Dang Van. If the mean fatigue index errors are investigated from Table 5.7, we conclude that both criterion tends to give estimations in the desired tolerance; however, Findley yields more conservative results with mFIE being 7.24% while Dang Van lead to estimations close to zero with mFIE being -2.05%. This behavior of Dang Van is due to its better performance in IP_MS group as the mFIE is 0.53% while it is 13.37% for Findley. On the other hand, when IP and OP groups are compared, insufficiency of Dang Van for out-of-phase loading is observed (PE) as estimations become non-conservative for OP groups (-5.90% for OP_nMS, -8.87% for OP_MS). Findley performs better for out-of-phase loadings with estimations being on the conservative side and with lower range values compared to Dang Van. When standard deviations are compared, it may be concluded that Dang Van has slightly less standard deviation being 8.83 for ALL group while it is 9.02 for

Findley. However, this is mainly due to the better performance of Dang Van in IP_MS group.

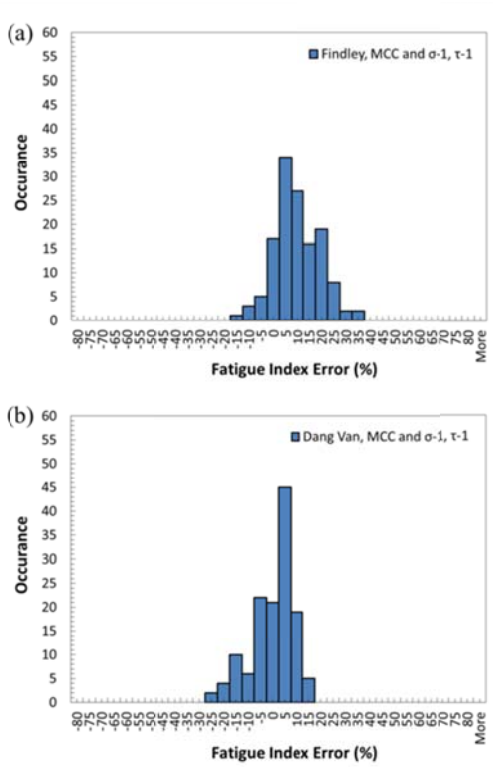

Figure 5.6: Histograms of a) Findley and b) Dang Van Criteria

Histogram of Robert in Figure 5.7 shows that the median remains same for the criterion compared to Findley; however, range is increased as the estimations lie in the limits -15% to 45%. This is due to more conservative estimations obtained by Robert. When mean fatigue index errors for ALL group is examined, a lower mFIE is seen for Robert criterion (6.45% Robert while 7.24% Findley). This is due to better performance of Robert criterion for IP_MS group like in Dang Van as the mFIE decrease down to 7.70% while it is 13.37% for Findley. However, FIE highly increases (more conservatism) for OP_MS group as it is 7.05% for Findley while 15.62% for Robert. When range and standard deviations are examined (see Table 5.8 and Table 5.9), we conclude that Robert criterion is inefficient compared to Findley as both the range and standard deviation are increased for all groups.

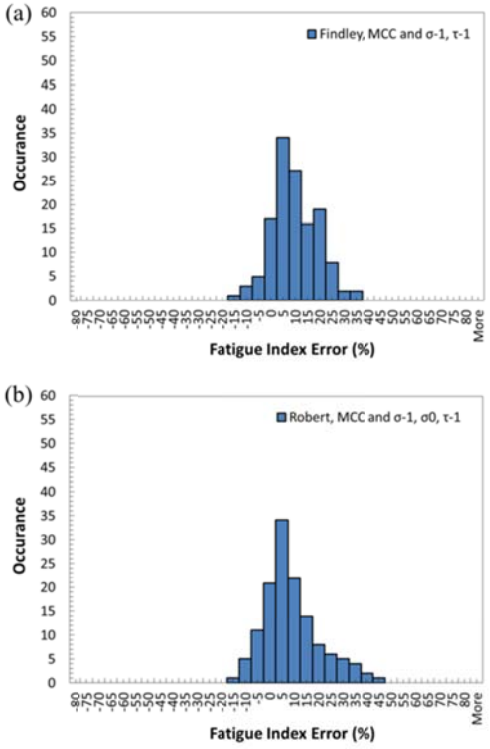

Figure 5.7: Histograms of a) Findley and b) Robert Criteria

Both Robert and Papuga PCR use the same stress values for shear and normal stresses; however, the non-linear relation of Papuga PCR seems to work as seen from Figure 5.8. Papuga PCR yields estimations between -10% to 10% which is the ideal range and the median of the related histogram is at 5% again like in other critical plane criteria. When Table 5.7 is examined, a mean fatigue index error which is very close to zero (0.56%) is seen while for other groups mFIE is between the limits -0.80% to 2.40% which is a superb performance. Moreover, IP and OP estimations do not change much indicating that the phase effect is handled successfully. Same statement can be made for mean stress effect as nMS and MS groups show slight difference in terms of mean fatigue index errors. Criterion also yields tolerable range for all groups which is in limits 15% to 22% (see Table 5.8). Another advantage of the Papuga PCR criterion is that the criterion yields the lowest standard deviations compared to all other criteria investigated in this thesis (see Table 5.9). Standard deviation of Papuga PCR for ALL case is 4.73 and it is in limits of 4.30 to 5.40 for other groups.

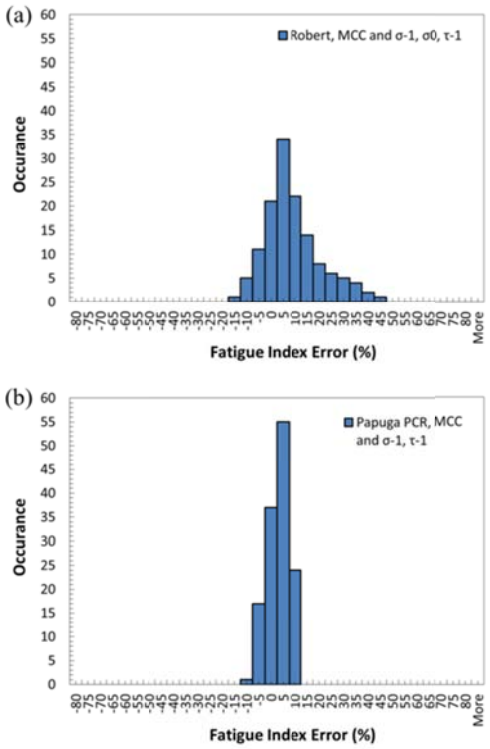

Figure 5.8: Histograms of a) Robert and b) Papuga PCR Criteria

Discussion about critical plane criteria can be concluded with the following statements:

- Findley yields conservative estimations for all groups. Phase effect is well handled. Mean stress inclusion with maximum value of the normal stress is the reason that makes the criterion conservative.

- Dang Van seems better compared to Findley with less mean, range and standard deviation of FIE but the criterion is insufficient for out-of-phase loadings as non-conservative estimations are obtained.

- Separation of alternating and mean values of the normal stress works well when these stress measures are combined in a non-linear formulation with alternating shear stress like in Papuga PCR method.

- Papuga PCR is the best criterion investigated among the critical plane criteria. However, the criterion requires three weighting constants

(σ_{-1}, σ_0 and τ_{-1}) and it is much slower than equivalent stress or invariant based criteria.

Table 5.7: All partial effects, FIE (%) Mean of Findley, Dang Van, Robert and Papuga PCR Criteria

FIE (%) Mean	Findley	Dang Van	Robert	Papuga PCR
ALL (134)	7.24	-2.05	6.45	0.56
IP (79)	9.91	1.45	6.17	0.64
OP (55)	3.42	-7.09	6.85	0.44
nMS (60)	2.00	-1.79	2.00	1.70
IP_nMS (27)	3.23	3.23	3.23	2.35
OP_nMS (33)	1.00	-5.90	1.00	1.17
MS (74)	11.49	-2.26	10.06	-0.37
IP_MS (52)	13.37	0.53	7.70	-0.25
OP_MS (22)	7.05	-8.87	15.62	-0.66
To_MS (12)	6.29	-8.16	6.02	-0.72
Ax_MS (62)	12.50	-1.12	10.84	-0.30
IP_Ax_MS (44)	14.45	1.64	8.26	-0.19
OP_Ax_MS (18)	7.74	-7.89	17.14	-0.57

Table 5.8: All partial effects, FIE (%) Range of Findley, Dang Van, Robert and Papuga PCR Criteria

FIE (%) Range	Findley	Dang Van	Robert	Papuga PCR
ALL (134)	47.80	41.33	56.89	21.33
IP (79)	39.64	25.76	52.14	17.78
OP (55)	37.97	38.17	47.47	21.33
nMS (60)	27.45	38.98	27.45	19.63

FIE (%)	Findley	Dang Van	Robert	Papuga PCR
IP_nMS (27)	18.81	18.81	18.81	15.19
OP_nMS (33)	27.45	35.19	27.45	19.63
MS (74)	42.58	41.33	52.14	21.05
IP_MS (52)	36.16	25.76	52.14	17.78
OP_MS (22)	32.76	38.17	35.96	21.05
To_MS (12)	24.96	37.33	30.17	17.02
Ax_MS (62)	42.58	30.93	52.14	21.05
IP_Ax_MS (44)	34.88	24.47	52.14	17.78
OP_Ax_MS (18)	32.76	27.77	35.96	21.05

Table 5.9: All partial effects, FIE (%) Standard Deviation of Findley, Dang Van, Robert and Papuga PCR Criteria

FIE (%) Standard Deviation	Findley	Dang Van	Robert	Papuga PCR
ALL (134)	9.02	8.83	11.28	4.73
IP (79)	8.65	5.81	11.53	4.39
OP (55)	8.12	9.93	10.90	5.18
nMS (60)	5.84	8.82	5.84	4.31
IP_nMS (27)	3.91	3.91	3.91	3.31
OP_nMS (33)	6.87	9.56	6.87	4.92
MS (74)	8.90	8.84	13.18	4.85
IP_MS (52)	8.40	6.40	13.69	4.61
OP_MS (22)	8.48	10.20	9.88	5.37
To_MS (12)	8.09	9.81	10.04	5.11
Ax_MS (62)	8.70	8.16	13.57	4.80
IP_Ax_MS (44)	8.15	6.02	14.14	4.65
OP_Ax_MS (18)	8.14	8.73	9.46	5.12

5.4. Results of Criteria for Different Calibrations and Shear Stress Calculation Methods

In this section the performance of selected criteria (Crossland, GAM, Findley and Dang Van) are questioned for the axial/bending calibration and a comparison is made with the bending-torsion calibration results. Furthermore, a different shear stress calculation method, MRH is tested for critical plane criteria and performance of MRH is examined.

5.4.1. Crossland Criterion

Figure 5.9 shows histograms of Crossland method for two different calibrations investigated in this study. For axial/bending calibration, estimations become more non-conservative as predictions with -20% and -15% increases while predictions with 5% decreases. If partial effects are investigated from Table 5.10, one may observe that mean fatigue index errors become worse for loadings without mean stress (nMS, IP_nMS, OP_nMS) especially for IP_nMS group (1.08% to -9.65%) and become better for loadings with mean stresses (MS, IP_MS, OP_MS etc.) especially for OP_MS group (-17.06% to -7.45%). Furthermore, range and standard deviations for IP_nMS group are affected most (see Table 5.11 and Table 5.12). If mean fatigue index for all test data (ALL group) is investigated predictions are slight worse (-7.62% to -8.87%). Calibration with axial/bending endurance limits should be used for Crossland method for loading cases with mean stresses.

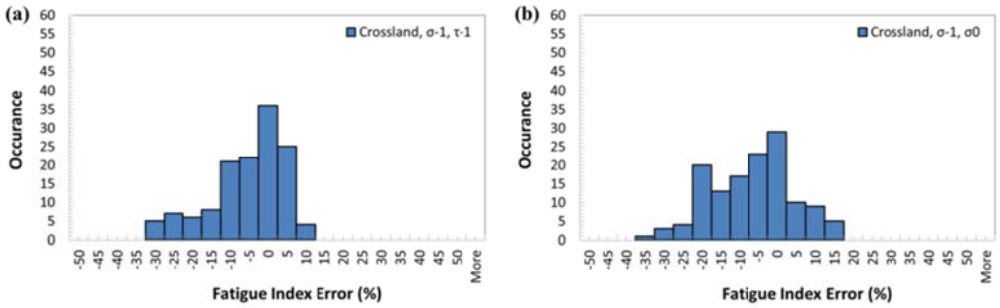

Figure 5.9: Crossland histograms showing results of a) Bending-torsion calibration, b) Axial/bending calibration.

5.4.2. GAM Criterion

Histograms for GAM method are shown in Figure 5.10. When effects of different calibrations are compared, it can be seen that for both calibrations estimation are between -15% and 15% with estimations of -5% to 5% occurrences are in majority leading to mean fatigue indices (for all test data) as 1.31% and -0.37% for calibration with bending-torsion and axial/bending calibration respectively. From histograms in Figure 11, it may be understood that there is a slight shift to the left side (non-conservative) as occurrences with 5%, 10% decreases and -5%, -10% increases. If partial effects are investigated, it may be observed that, like in other methods, estimations become more conservative for loadings with mean stresses and estimations become more non-conservative for loadings without mean stresses. For all partial groups, fatigue index range is not much affected (see Table 5.11) while standard deviation is increased for the axial/bending calibration case (see Table 5.12, max standard deviation is 8.25%). Furthermore, we may conclude that the most affected group is the OP group (for both nMS and MS). To sum up, although for some partial groups estimations worsen, mean fatigue indices of GAM method are still in good bandwidth. Therefore, GAM method may be used with axial/bending calibration.

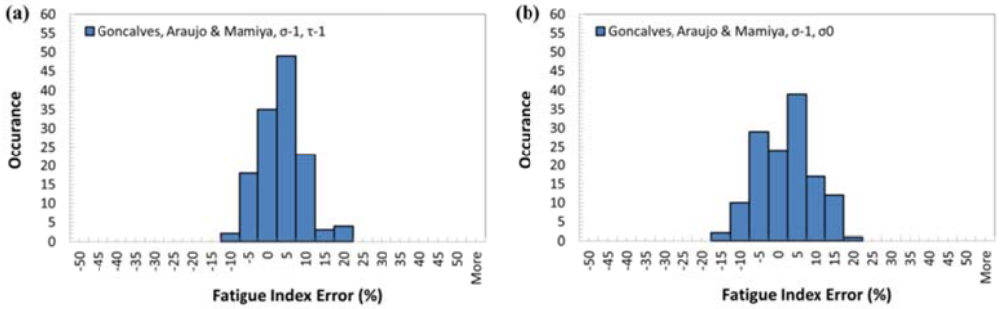

Figure 5.10: GAM histograms showing results of a) Bending-torsion calibration, b) Axial/bending calibration.

5.4.3. Findley Criterion

Figure 5.11 shows histograms of Findley method. From these histograms average effect of different calibrations and shear stress calculation methods may be addressed. If a-c and b-d of Figure 5.11 are compared with each other, we may

conclude that MRH improves the prediction capability of the method by increasing the occurrence of 0%-10% estimations. Furthermore, if a-b and c-d of Figure 5.11 are compared with each other, it is clear that method give better estimations as 0%-5% occurrences are increased. If we investigate the partial effects, from Table 5.10 it may be concluded that for axial/bending calibration mean fatigue index decreases for in phase loadings and loadings with mean stresses. Opposite is observed for out of phase loadings. Moreover, fatigue index range (see Table 5.11) is decreased for loadings with mean stresses. For partial groups standard deviation is increased slightly (see Table 5.12). As a result, we conclude that axial/bending calibration is appropriate for Findley method as range and standard deviation values are not much affected and self-conservatism of the method is reduced.

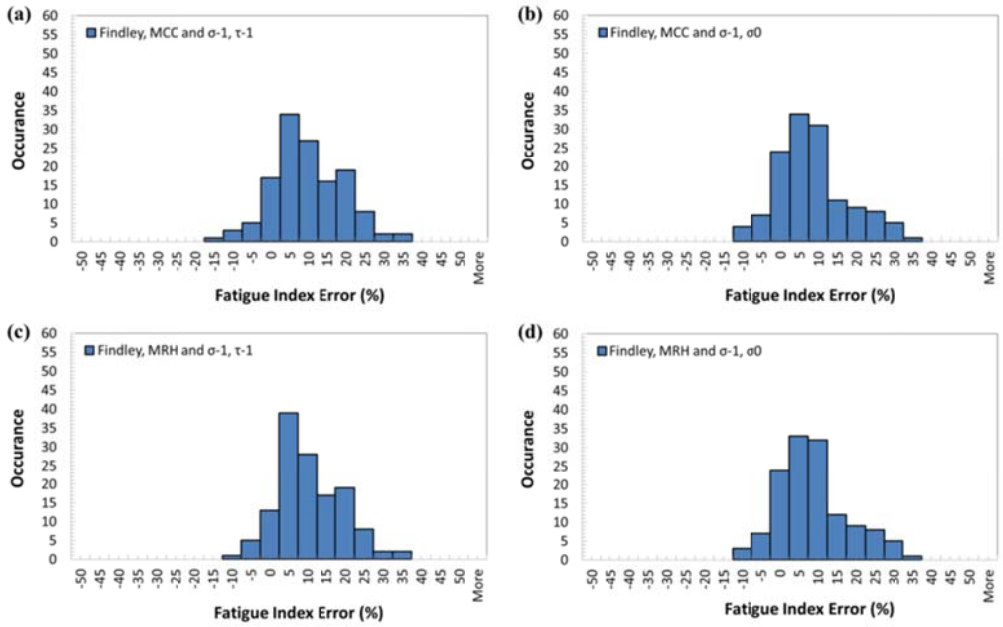

Figure 5.11: Findley histograms showing results of a) MCC and bending-torsion calibration, b) MCC and axial/bending calibration, c) MRH and bending-torsion calibration, d) MRH and axial/bending calibration combinations

5.4.4. Dang Van Criterion

Figure 5.12 shows histograms of Dang Van method. MRH method like in Findley improves the predictions and increases the occurrences of fatigue index errors in

range -5% to 5%. However, axial/bending calibration seems not improving the estimations as seen from Figure 5.12b and Figure 5.12d. Moreover, from Table 5.11 and Table 5.12 it can be interpreted that all partial groups except MS group worsen with increased range and standard deviations. For the combination MRH with the axial/bending calibration, mean fatigue index errors are within -8.90% to 2.18% (for partial groups); however, the best combination is obtained with MRH and bending-torsion calibration with mean fatigue index errors within -3.45% to 3.23%.

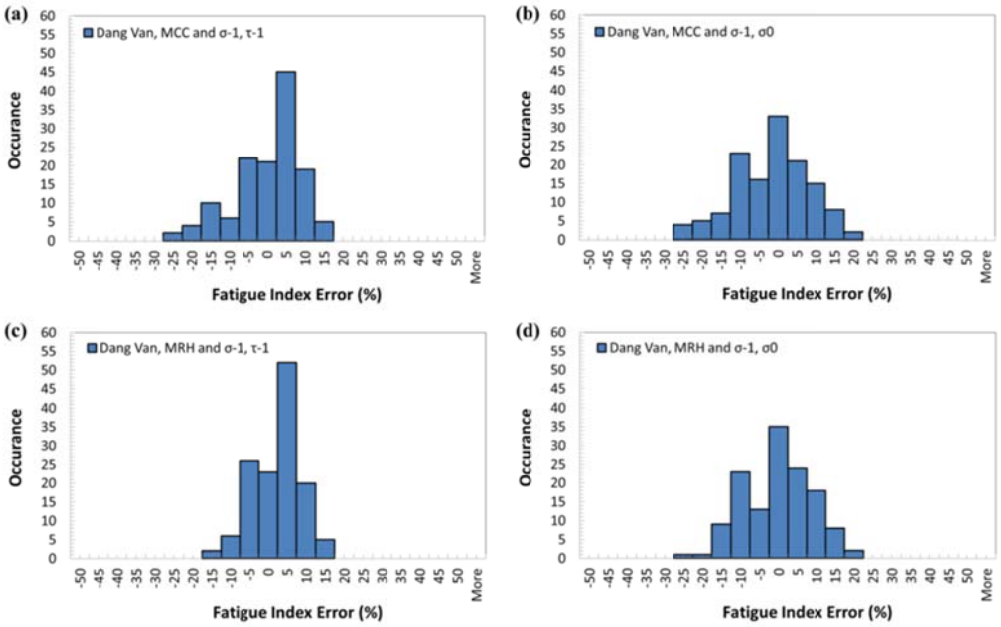

Figure 5.12: Dang Van histograms showing results of a) MCC and bending-torsion calibration, b) MCC and axial/bending calibration, c) MRH and bending-torsion calibration, d) MRH and axial/bending calibration combinations

Table 5.10: All partial effects, FIE (%) Mean of Crossland, Findley, Dang Van and GAM Criteria for Bending-Torsion (σ_{-1}, τ_{-1}) and Axial/Bending (σ_{-1}, σ_0) Calibrations and Shear Stress Calculation Methods (MCC and MRH)

FIE (%) Mean	Crossland		Findley				Dang Van				GAM	
			MCC		MRH		MCC		MRH			
Cases	σ_{-1}, τ_{-1}	σ_{-1}, σ_0	σ_{-1}, τ_{-1}	σ_{-1}, σ_0	σ_{-1}, τ_{-1}	σ_{-1}, σ_0	σ_{-1}, τ_{-1}	σ_{-1}, σ_0	σ_{-1}, τ_{-1}	σ_{-1}, σ_0	σ_{-1}, τ_{-1}	σ_{-1}, σ_0
ALL (134)	-7.62	-8.87	7.24	6.06	7.82	6.28	-2.05	-4.23	0.06	-2.68	1.31	-0.37
IP (79)	-4.15	-5.78	9.91	6.27	9.91	6.27	1.45	-0.82	1.45	-0.82	1.70	0.30
OP (55)	-12.60	-13.30	3.42	5.76	4.83	6.30	-7.09	-9.13	-1.93	-5.35	0.76	-1.32
nMS (60)	-4.81	-13.81	2.00	0.61	3.10	1.03	-1.79	-8.91	0.95	-6.91	1.75	-3.18
IP_nMS (27)	1.08	-9.65	3.23	1.02	3.23	1.02	3.23	-4.49	3.23	-4.49	1.35	-1.38
OP_nMS (33)	-9.62	-17.21	1.00	0.28	2.99	1.04	-5.90	-12.53	-0.91	-8.90	2.07	-4.66
MS (74)	-9.90	-4.86	11.49	10.48	11.66	10.54	-2.26	-0.43	-0.66	0.75	0.96	1.91
IP_MS (52)	-6.87	-3.77	13.37	8.99	13.37	8.99	0.53	1.09	0.53	1.09	1.88	1.16
OP_MS (22)	-17.06	-7.45	7.05	13.99	7.61	14.19	-8.87	-4.02	-3.45	-0.04	-1.20	3.69
To_MS (12)	-9.35	-11.82	6.29	8.14	6.43	8.14	-8.16	-7.40	-5.63	-5.51	-0.26	0.30
Ax_MS (62)	-10.01	-3.52	12.50	10.93	12.67	11.00	-1.12	0.92	0.31	1.97	1.20	2.23
IP_Ax_MS (44)	-6.90	-2.83	14.45	9.11	14.45	9.11	1.64	1.88	1.64	1.88	2.26	1.23
OP_Ax_MS (18)	-17.59	-5.20	7.74	15.38	8.32	15.62	-7.89	-1.44	-2.96	2.18	-1.39	4.67

Table 5.11: All partial effects, FIE (%) Range of Crossland, Findley, Dang Van and GAM Criteria for Bending-Torsion (σ_{-1}, τ_{-1}) and Axial/Bending (σ_{-1}, σ_0) Calibrations and Shear Stress Calculation Methods (MCC and MRH)

FIE (%) Range	Crossland		Findley				Dang Van				GAM	
			MCC		MRH		MCC		MRH			
Cases	σ_{-1}, τ_{-1}	σ_{-1}, σ_0	σ_{-1}, τ_{-1}	σ_{-1}, σ_0	σ_{-1}, τ_{-1}	σ_{-1}, σ_0	σ_{-1}, τ_{-1}	σ_{-1}, σ_0	σ_{-1}, τ_{-1}	σ_{-1}, σ_0	σ_{-1}, τ_{-1}	σ_{-1}, σ_0
ALL (134)	40.48	52.95	47.80	45.13	43.32	42.93	41.33	45.11	28.77	45.11	31.50	30.63
IP (79)	32.80	52.95	39.64	42.93	39.64	42.93	25.76	45.11	25.76	45.11	28.94	28.72
OP (55)	39.11	38.24	37.97	42.45	33.50	39.74	38.17	38.07	25.60	28.45	28.83	28.14
nMS (60)	38.60	42.87	27.45	25.42	22.98	23.49	38.98	39.21	26.36	39.21	28.83	21.01
IP_nMS (27)	17.51	42.87	18.81	23.22	18.81	23.22	18.81	39.21	18.81	39.21	17.92	19.10
OP_nMS (33)	34.46	31.39	27.45	24.96	22.98	22.98	35.19	28.22	22.89	21.34	28.83	20.68
MS (74)	39.11	43.18	42.58	36.77	39.60	36.77	41.33	44.83	28.77	35.21	30.26	28.20
IP_MS (52)	29.41	38.57	36.16	36.77	36.16	36.77	25.76	33.91	25.76	33.91	28.89	28.20
OP_MS (22)	39.11	35.83	32.76	31.64	29.78	31.13	38.17	38.07	25.60	28.45	18.08	24.74
To_MS (12)	34.82	27.32	24.96	23.07	24.73	23.07	37.33	35.34	24.77	25.73	14.02	19.66
Ax_MS (62)	37.09	38.57	42.58	36.77	39.60	36.77	30.93	31.43	24.47	31.43	30.26	28.20
IP_Ax_MS (44)	29.41	38.57	34.88	36.77	34.88	36.77	24.47	31.43	24.47	31.43	28.89	28.20
OP_Ax_MS (18)	32.65	27.67	32.76	31.64	29.78	29.57	27.77	21.54	21.15	21.54	18.08	24.74

Table 5.12: All partial effects, FIE (%) Standard Deviation of Crossland, Findley, Dang Van and GAM Criteria for Bending-Torsion (σ_{-1}, τ_{-1}) and Axial/Bending (σ_{-1}, σ_0) Calibrations and Shear Stress Calculation Methods (MCC and MRH)

FIE (%) Standard Deviation	Crossland		Findley				Dang Van				GAM	
			MCC		MRH		MCC		MRH			
Cases	σ_{-1}, τ_{-1}	σ_{-1}, σ_0	σ_{-1}, τ_{-1}	σ_{-1}, σ_0	σ_{-1}, τ_{-1}	σ_{-1}, σ_0	σ_{-1}, τ_{-1}	σ_{-1}, σ_0	σ_{-1}, τ_{-1}	σ_{-1}, σ_0	σ_{-1}, τ_{-1}	σ_{-1}, σ_0
ALL (134)	9.67	10.91	9.02	9.17	8.42	9.01	8.83	9.91	6.13	8.96	5.81	7.27
IP (79)	7.01	10.68	8.65	8.93	8.65	8.93	5.81	9.15	5.81	9.15	5.93	7.35
OP (55)	10.73	9.63	8.12	9.49	7.07	9.13	9.93	8.85	6.03	7.93	5.59	7.04
nMS (60)	9.36	10.31	5.84	5.53	4.99	5.44	8.82	9.13	5.40	8.17	5.11	5.88
IP_nMS (27)	4.12	11.27	3.91	6.10	3.91	6.10	3.91	9.67	3.91	9.67	4.10	5.81
OP_nMS (33)	9.69	7.98	6.87	4.98	5.73	4.82	9.56	6.77	5.72	6.00	5.80	5.50
MS (74)	9.31	9.67	8.90	9.15	8.68	9.09	8.84	8.84	6.58	8.06	6.30	7.49
IP_MS (52)	6.66	9.78	8.40	8.95	8.40	8.95	6.40	8.26	6.40	8.26	6.69	7.90
OP_MS (22)	10.67	8.89	8.48	8.66	7.94	8.36	10.20	9.14	6.16	7.50	4.61	6.06
To_MS (12)	9.20	8.26	8.09	7.18	7.97	7.18	9.81	11.08	6.42	8.50	4.46	5.45
Ax_MS (62)	9.33	9.34	8.70	9.42	8.44	9.35	8.16	7.64	6.17	7.38	6.57	7.78
IP_Ax_MS (44)	7.01	10.13	8.15	9.26	8.15	9.26	6.02	8.08	6.02	8.08	6.95	8.25
OP_Ax_MS (18)	9.93	6.75	8.14	8.26	7.49	7.83	8.73	5.80	5.22	5.28	4.62	5.81

CHAPTER 6

CONCLUSIONS AND RECOMMENDATIONS

FOR FUTURE WORK

Understanding the multiaxial fatigue problem is an essential part of the reliability assesment of engineering components, which experience high cycles of complex loadings, and design against the multiaxial high cycle fatigue. Multiaxial fatigue is a sophisticated problem as it involves at least two loading channels. Multiaxial loading may cause principal axes to rotate while magnitudes of principal stresses vary non-proportionally which makes it difficult to estimate critical locations and life of the components. Furthermore, assesment of fatigue critical parts with testing is expensive and time-consuming and it is not possible and feasible to test all loading scenarios. Therefore, a methodology involving analytical and/or numerical methods that would replace test campaigns is required. Objectives of this thesis are to evaluate the state-of-art multiaxial endurance criteria in terms of their predictive capabilities, to validate the criteria with experimental test results and to develop a multiaxial life estimation code in which the multiaxial endurance criteria are implemented.

In this thesis, several multiaxial endurance criteria (a total of nine criteria) belong to three different types (equivalent stress, invariant based and critical plane criteria) are explained in Chapter 2. These criteria include weighting constants for adjusting the effects of shear and normal stresses on damage parameter, which is the failure indicator. Calibration of weighting constants usually made by using fully reversed bending and torsion endurance limits; however, as torsional endurance limit may not always be available, calibration of several invariant

based (Crossland and GAM) and critical plane (Findley and Dang Van) criteria based on only axial/bending endurance limits with different R ratios (R=-1 and R=0) are derieved. In addition, there are several shear stress calculation methods in literature which is used in critical plane criteria. Two of those most popular and accepted shear stress calculation methods namely minimum circumscribed circle (MCC) and maximum rectangular hull (MRH) are also investigated in this thesis. A MATLAB code is written for evaluating the criteria with regards to their estimations of the experimental data presented in Chapter 4. Code is written in such a way that it may easily be adapted to finite element programs as a post processor that utilize finite element analysis results in order to find the fatigue critical locations and the fatigue lives of engineering components. Pseudocodes of the MATLAB code are presented in Chapter 4 for clarification of the processes involved in the criteria. Evaluation of the criteria is carried out by comparing the mean, range and standard deviation of the fatigue index errors of each criterion, which show the deviation of fatigue lives from the real situation, and their general behavior is demonstrated by related histograms. Performance of each criterion for phase effect, mean stress effect and their combined effects are investigated. In addition, effect of different calibrations is examined for Crossland, GAM, Findley and Dang Van criteria and effect of different shear stress calculation methods (MCC and MRH) is investigated for critical plane criteria.

When the criteria with the usual calibration of weighting constants (fully reversed bending and torsion endurance limits) and the shear stress calculation method MCC for critical plane criteria are examined following conclusions are made:

- Equivalent stress criteria (Absolute Maximum Principal and Signed von Mises) found out to be highly scattered and non-conservative especially for out-of-phase loading.

- Highly conservative estimations are obtained with well-known mean stress corrections like Soderberg or Goodman while SWT mean stress correction yields the best results for the equivalent stress criteria.

- Equivalent stress criteria may be used for an initial solution as they are simple and fast; however, for accurate results more advanced methods (invariant based and critical plane) should be preferred.

- Invariant based criteria seems more successful compared to equivalent stress criteria with lower range and mean fatigue index errors However, Sines and Crossland criteria are inadequate for both phase and mean stress effects as estimations are non-conservative.

- Among the invariant criteria, GAM draws attention since both effects are successfully handled which is indicated by small mean, range and standard deviation of fatigue index errors. GAM owes this outstanding performance to the use of alternating deviatoric stress tensor and maximum of the first principal stress in it's formulation unlike Sines and Crossland which use alternating octahedral stress and hydrostatic stress.

- Critical plane criteria search all material planes in order to find the maximum of a proposed damage parameter. Main idea of this search is based on the fact that principal stress directions change in time for non-proportional loading and relying on a stress state at a specified plane is assumed to be improper like done in equivalent stress and invariant based criteria. This assumption seems to work as the best estimations are obtained by the critical plane criteria.

- Findley is the oldest critical plane criteria and estimations are conservative for the data set investigated. Phase effect is well handled with this method and the conservatism is due to the use of maximum normal stress as mean stress inclusion.

- Dang Van has lower mean, range and standard deviation compared to Findley; however, this method gives non-conservative estimations for non-proportional loadings.

- Among the critical plane criteria, Papuga PCR is the best criterion with tolerable mean, range and standard deviation of fatigue index errors. However, method requires three endurance limits (fully reversed bending, fully reversed torsion and pulsating bending).

When the criteria with the new calibration of weighting constants (axial/bending endurance limits) and the shear stress calculation method MRH for critical plane criteria are examined following conclusions are made:

- Calibration with axial/bending endurance limits (axial/bending calibration) give more conservative estimations for loadings with mean stresses especially with normal mean stresses.

- Estimations become more non-consevative for loadings without mean stresses from which we conclude that the use of torsion endurance limit is necessary for handling the phase effect.

- Axial/bending calibration decrease the self-conservatism of Findley criterion and still estimations are in tolerable range. Therefore, this calibration is appropriate for Findley criterion.

- Axial/bending calibration is not appropriate for Crossland and Dang Van as estimations become non-conservative in general while range and standard deviation of fatigue index errors are increased.

- Shear stress calculation method MRH shows excellent behavior for all critical plane criteria compared to MCC as estimations are improved for loadings with phase differences. Moreover, this method is much faster than MCC even for the randomized algorithm which is another advantage of MRH. Therefore, this method should be utilized in critical plane methods instead of MCC.

Following recommendations are made for future work:

- In this thesis only phase and mean stress effects are investigated. Performance of the criteria may be evaluated for the frequency effects.

- Critical plane obtained by the critical plane criteria do not always show the fracture plane (direction of the crack in macro scale) and most of the data in literature do not share the fracture plnae orientation. Therefore, deviation of critical plane and fracture plane may be investigated for enhancing the applicability of the criteria and for estimating the direction of cracks.

- In this thesis, constant amplitude loadings are investigated. However, real service loadings would possibly be variable amplitude loadings. Therefore, cycle counting methodologies may be developed for multiaxial loadings applicable to multiaxial endurance criteria.

- Critical plane criteria are the slowest approach compared to invariant based and equivalent stress criteria. This is due to the search of critical plane in material planes with a user specified angle incrementation. The angle incrementation proposed in this thesis, which preserve the accuracy of the criteria, is between 2 to 4 degrees that results in 8100 to 2025 planes to be searched. In literature several researchers proposed ways to decrease the amount of computation without missing the critical plane. One of these proposals is to use genetic algorithms. Another suggestion is to use greater increments at the start of analysis (10 degrees for example) than decreasing the incrementation for angle intervals for which the critical plane is suspected. This procedure continues until the incrementation is decreased up to a user specified lower value. Algorithms like these may be searched for increasing the speed of critical plane criteria as they give the most accurate solutions in literature.

- GAM method draws attention with its' remarkable prediction capability and speed. However, formulation presented in this thesis is

applicable only to elliptical loading paths. As explained in Chapter 2, a proposal is made by Mamiya and Araujo [47] that is to be used for general loadings. This proposal may be investigated and the criteria may be validated for general loadings.

- Criteria evaluated in this thesis are all stress based and applicable to multiaxial high cycle fatigue. However, there are stress and strain based criteria which are applicable to both low cycle and high cycle fatigue regime. Performance of these criteria may be investigated.

- In this thesis, experiment results of smooth specimens are investigated. However, most critical regions of components are usually the notched areas or locations with stress concentrations. Therefore, adaptation of the multiaxaial endurance criteria for notched areas may be examined.

REFERENCES

[1] Lanza, G., 1886, Strength of shafting subjected to both twisting and bending, Transactions of ASME, 8, pp. 121-196.

[2] Mason, W., 1917, Alternating stress experiments, Institution of Mechanical Engineers.

[3] Haigh, B. P., 1923, The thermodynamic theory of mechanical fatigue and hysteresis in metals, Report of British Association for the Advancement of Science, pp. 358-368.

[4] Nishihara, T., and Kawamoto, M., 1941, The strength of metals under combined alternating bending and torsion memoirs, College of Engineering, 10, Kyoto Imperial University, Japan.

[5] Gough H. J., and Pollard H. V., 1935, The strength of metals under combined alternating stresses, Proceedings of the Institute of Mechanical Engineers, 131, pp. 3-103.

[6] Gough H. J., 1950, Engineering steels under combined cyclic and static stresses, Journal of Applied Mechanics, 50, pp. 113-125.

[7] Socie D. F., and Marquis G. B., 2000, Multiaxial fatigue, Warrandale, Society of Automotive Engineers.

[8] Park, J., and Nelson, D., 2000, Evaluation of an energy-based approach and a critical plane approach for predicting constant amplitude multiaxial fatigue life, International Journal of Fatigue, 22, pp. 23-39.

[9] Reis, L., Li, B., Freitas, M., 2004, Biaxial fatigue for proportional and non-proportional loading paths, Fatigue and Fracture of Engineering Materials and Structures, 27, pp. 775-784.

[10] Ion, D., Lorand, K., Mircea, D., Karoly, M., 2011, The equivalent stress concept in multiaxial fatigue, Journal of Engineering Studies and Research, 17 (2), pp. 53-62.

[11] Li, B. C., Jiang, C., Han, X., Li, Y., 2015, A new approach of fatigue life prediction for metallic materials under multiaxial loading, International Journal of Fatigue, 78, pp. 1-10.

[12] Pederson, M. M., 2016, Multiaxial fatigue assesment of welded joints using the notch stress approach, International Journal of Fatigue, 83 (2), pp. 269-279.

[13] Papuga, J., Vargas, M., Hronek, M., 2012, Evaluation of uniaxial fatigue criteria applied to multiaxially loaded unnotched samples, Engineering Mechanics, 19, p. 99-111.

[14] Papuga, J., and Fojtik, F., 2017, Multiaxial fatigue strength of common steel and the response of some estimation methods, International Journal of Fatigue, 104, pp. 27-42.

[15] Sines, G., 1955, Failure of materials under combined repeated stresses with superimposed static stresses, Tech Note 3495, National Advisory Committee for Aeronautics, Washington, DC, p. 69.

[16] Crossland, B., 1956, Effect of large hydrostatic pressures on the torsional fatigue strength of an alloy steel. In: Proceedings, International Conference on Fatigue of Metals. Institution of Mechanical Engineers, London, pp. 138–149.

[17] Claudio, R. A., Reis, L., Freitas, M., 2014, Biaxial high-cycle fatigue assesment of ductile aluminum cruciform specimens, Theoretical and Applied Fracture Mechanics, 73, pp. 82-90.

[18] Papadopoulos, I. V., Davoli, P., Gorla, C., Filippini, M., Bernasconi, A., 1997, A comparative study of multiaxial high-cycle fatigue criteria for metals, International Journal of Fatigue, 19 (3), pp. 219-235.

[19] Papuga, J., 2011, A survey on evaluating the fatigue limit under multiaxial loading, International Journal of Fatigue, 33, pp. 153-165.

[20] Stanfield, G., 1935, Discussion on the strength of metals under combined alternating stresses, in: H. Gough, H. Pollard (Eds.), Proc. Institution of Mechanical Engineers, vol. 131.

[21] Findley, W. N., 1959, A theory for the effect of mean stress on fatigue of metals under combined torsion and axial load or bending, Journal of Engineering Industry, 81, pp. 301–306.

[22] McDiarmid D. L., 1991, A general criterion for high cycle multiaxial fatigue failure, Fatigue and Fracture of Engineering Materials and Structure, 14(4), pp. 429-453.

[23] McDiarmid D. L., 1994, A shear stress based critical-plane criterion of multiaxial fatigue failure for design and life prediction, Fatigue and Fracture of Engineering Materials and Structures, 17(2), pp. 1475-1485.

[24] Dang Van, K., Griveau, B., Message, O., 1989, On a new multiaxial fatigue limit criterion: theory and applications, Brown MW, Miller KJ (editors), Biaxial and multiaxial fatigue, EGF 3 London, Mechanical Engineering Publications, pp. 479–496.

[25] Budynas, R. G., and Nisbett, J. K., 2011, Shigley's Mechanical Engineering Design, New York, NY: McGraw-Hill.

[26] Kluger, K., and Lagoda, T., 2016, Fatigue life estimation for selected materials in multiaxial stress states with mean stress, Journal of Theoretical and Applied Mechanics, 54, pp. 385-396.

[27] Susmel, L., 2010, A simple and efficient numerical algorithm to determine the orientation of the critical plane in multiaxial fatigue problems, International Journal of Fatigue, 32, pp. 1875-1883.

[28] Araújo, J. A., Dantas, A. P., Castro, F. C., Mamiya, E. N., Ferreira, J. L. A., 2011, On the characterization of the critical plane with simple and fast alternative measure of the shear stress amplitude in multiaxial fatigue, International Journal of Fatigue, 33, pp. 1092-1100.

[29] Dantas, A. P., Araújo, J. A., Castro, F. C., Junior, T. D., 2011, The use of genetic algorithms and the maximum rectangular hull for a strong reduction in computational cost for critical plane approaches in multiaxial fatigue, 21st Brazilian Congress of Mechanical Engineering, Natal, Brasil

[30] Lönnqvist, C., Kaas, J., Rabb, R., 2007, Comprehensive multiaxial fatigue analysis with ABAQUS, 2007 ABAQUS Users' Conference.

[31] Bishop, N. W. M., and Sherrat, F., 2000 Finite element based fatigue calculations, Netherlands, NAFEMS Ltd.

[32] Sines, G., 1959, Behavior of metals under complex static and alternating stresses, Metal fatigue, McGraw-Hill, New York, pp. 145–169.

[33] Soderberg, C. R., 1939, Factor safety and working stress, Transaction of ASME, 52, pp. 13-28.

[34] Goodman, J., 1899, Mechanics applied to engineering, Longmans, Green and Co., London, pp. 631-636.

[35] Gerber, W., 1874, Relation between the superior and inferior stresses of a cycle of limiting stress (in German), Z. Bayer. Arch. Ing. Ver., 6, pp. 101-110.

[36] Dowling, N. E., 2004, Mean Stress Effects in Stress-Life and Strain-Life Fatigue, SAE Paper No. 2004-01-2227, Fatigue 2004: Second SAE Brasil International Conference on Fatigue, São Paulo, Brasil, 14 pages.

[37] Dowling, N. E., 2009, Mean stress effects in strain-life fatigue, Fatigue and Fracture of Engineering Materials and Structures, 32, pp. 1004-1019.

[38] Dowling, N. E., 2012, Mechanical behavior of materials, England: Essex, Pearson.

[39] Mamiya, E. N., and Araujo, J. A., 2002, Fatigue limit under multiaxial loadings: on the definition of the equivalent shear stress. Mechanics Research Communications, 29, pp. 141-151.

[40] Gonçalves, C. A., Araujo, J. A., Mamiya, E. N., 2005, Multiaxial fatigue: a stress based criterion for hard metals, International Journal of Fatigue, 27, pp. 177-187.

[41] Balthazar, J. C., and Malcher, L., 2007, A review on the main approaches for determination of the multiaxial high cycle fatigue strength, Brazilian Society of Mechanical Sciences and Engineering, ISBN 97B-85-85769-30-7.

[42] Bernasconi, A., 2002, Efficient algorithms for calculation of shear stress amplitude and amplitude of the second invariant of the stress deviator in fatigue criteria applications, International Journal of Fatigue, 24, pp. 649-657.

[43] Freitas, M., Li, B., Santos, J., 2000, A numerical approach for high-cycle fatigue life prediction with multiaxial loading, Kaluri, S., Bonacuse, P.J. (Eds.), Multiaxial Fatigue and Deformation: Testing and Prediction, ASTM STP 1387, ASTM, West Conshohocken, pp. 139–156.

[44] Ilyushin, A. A., 1963, Plasticity foundations of general mathematical theory, Akad. Nauk, Moscow, p. 16.

[45] Papuga J., 2005, Mapping of fatigue damages – Program shell of FE – calculation (Doctoral dissertation, Czech Technical University, Prague), Retrieved from http://www.pragtic.com/docu/Papuga_Thesis.zip

[46] Deperrois A., 1991, Sur le calcul des limites d'e´ndurance des aciers.The`se de Doctorat. Ecole Polytechnique, Paris.

[47] Mamiya, E. N., Araujo, J. A., Castro, F. C., 2009, Prismatic hull: A new measure of shear stress amplitude in multiaxial high cycle fatigue, International Journal of Fatigue, 31, pp. 1144-1153.

[48] Smith, J. O., 1939, The effect of range of stress on the torsional fatigue strength of steels, Bulletin Series, 316, Engineering Experiment Station, University of Illinois.

[49] Smith, J. O., 1942, The effect of range of stress on the torsional fatigue strength of metals, Bulletin Series, 334, Engineering Experiment Station, University of Illinois.

[50] Liu, Y. and Mahadevan, S., 2005, Multiaxial high-cycle fatigue criterion and life prediction for metals, International Journal of Fatigue, 27, pp. 790-800.

[51] Krgo A., Kallmeyer A. R., Kurath P., 2000, Evaluation of HCF multiaxial fatigue life prediction methodologies for Ti-6Al-4V, Proceedings of the 5th National Turbine Engine High Cycle Fatigue Conference, Arizona

[52] Kallmeyer, A. R., Krgo, A., Kurath, P., 2002, Evaluation of Multiaxial Fatigue Life Prediction Methodologies for Ti-6Al-4V, Journal of Engineering Materials and Technology, 124, pp. 229-237.

[53] Kluger K. and Łagoda T., 2013, Fatigue life of metallic material estimated according to selected models and load conditions, Journal of Theoretical and Applied Mechanics, 51 (3), pp. 581-592.

[54] Kluger K. and Łagoda T., 2014, New energy model for fatigue life determination under multiaxial loading with different mean values, International Journal of Fatigue, 66, pp. 229-245

[55] Kluger K., 2015, Fatigue life estimation for 2017A-T4 and 6082-T6 aluminum alloys subjected to bending-torsion with mean stress, International Journal of Fatigue, 80, pp. 22-29:

[56] Niesłony A., Łagoda T., Walat K., 2014, Multiaxial fatigue behavior of AA6068 and AA2017A aluminum alloys under in-phase bending with torsion loading condition, *Mat.-wiss. u. Werkstofftech*, 45 (10), pp. 947-952

[57] Bernasconi, A. and Papadopoulos, I.V., 2005, Efficiency of algorithms for shear stress amplitude calculation in critical plane class fatigue criteria, Computational Materials Science, 34, pp. 355-368.

[58] Dang Van, K., Le Douaron, A., Lieurade, H. P., 1984, Multiaxial fatigue limit: A new approach, Advances in Fracture Research, Sixth International Conference on Fracture, New Dehli, pp. 1879-1885.

[59] Weber, B., Kenmeugne, B., Clement, J. C., Robert, J. L., 1999, Improvements of multiaxial fatigue criteria computation for a strong reduction of calculation duration, Computational Materials Science, 15, pp. 381-399.

[60] Ballard, P., Dang Van, K., Deperrois, A., Papadopoulos, I., V., 1995, High cycle fatigue and a finite element analysis, Fatigue and Fracture of Engineering Materials and Structures, 18 (3), pp. 397-441.

[61] Papadopoulos, I.V., 1998, Critical plane approaches in high-cycle fatigue: The definition of the amplitude and mean value of the shear stress acting on the critical plane, Fatigue and Fracture of Engineering Materials and Structures, 21, pp. 269-285.

[62] Berg, M., Cheong, O., Kreveld, M., Overmars, M., 2000, Computational Geometry Algorithms and Applications, Berlin, Springer, pp. 86-89.

[63] Castro, F. C., Araújo, J. A., Mamiya, E. N., Pinheiro, P. A., 2014, Combined resolved stresses as an alternative to enclosing geometrical objects as a measure of shear stress amplitude in critical plane approaches, International Journal of Fatigue, 66, pp. 161-167.

[64] Matake, T., 1977, An explanation on fatigue limit under combined stress, Bulletin of JSME, 20, pp. 257–63.

[65] Susmel, L., 2008, Multiaxial fatigue limits and material sensitivity to non-zero mean stresses normal to the critical planes, Fatigue and Fracture of Engineering Materials and Structures, 31, pp. 295–309.

[66] Papuga, J. and Ruzicka, M., 2008, Two new multiaxial criteria for high cycle fatigue computation, International Journal of Fatigue, 30, pp. 58-66.

[67] Carpinteri, A. and Spagnoli, A., 2001, Multiaxial high-cycle fatigue criterion for hard metals, International Journal of Fatigue, 23, pp. 135-145.

[68] Macha, E., 1989, Simulation investigations of the position of fatigue fracture plane in materials with biaxial loads, Mat-wiss u Werkstofftech; 20, pp. 132–136 (see also pp. 153–163).

[69] Stulen, F. B. and Cummings, H. N., 1954, A failure criterion for multiaxial fatigue stresses, Proc. ASTM 54, pp. 822–835.

[70] Karolczuk, A. and Kluger, K., 2014, Analysis of the coefficient of normal stress effect in chosen multiaxial fatigue criteria, Theoretical and Applied Fracture Mechanics, 73, pp. 39-47.

[71] Karolczuk, A., Kluger, K., Lagoda, T., 2016, A correction in the algorithm of fatigue life calculation based on the critical plane approach, International Journal of Fatigue, 83, pp. 174-183.

[72] Karolczuk, A. and Macha, E., 2008, Selection of the critical plane orientation in two-parameter multiaxial fatigue failure criterion under combined bending and torsion, Engineering Fracture Mechanics, 75, pp. 389-403.

[73] Fojtik, F., Fuxa, J., Poruba, Z., 2010, Application of selected multi-axial fatigue criteria on the results of non-proportional fatigue experiments, Applied and Computational Mechanics, 4, pp. 149-156.

[74] Robert, J. L., 1994, Fatigue life prediction under periodical or random multiaxial stress states, Automation in fatigue and fracture: testing and analysis, ASTM STP 1231; pp. 369–387.

[75] Vidal, E., Kenmeugne, B., Robert, J. L., Bahuaud, J., 1996, Fatigue life prediction of components using multiaxial criteria, Multiaxial Fatigue and Design, ESIS 21 (Edited by Pineau, A., Cailletaud, G. and Lindley, T., C.), Mechanical Engineering Publications, London, pp. 365- 378.

[76] Kallmeyer, A. R. and Kurath, P., 2006, Development of multiaxial fatigue damage assessment methods considering high cycle fatigue (HCF)/low cycle fatigue (LCF) interactions, Materials and Manufacturing Directorate, Department of Mechanical Engineering and Applied Mechanics, 1301 12th Avenue N Fargo, ND 58105-3400.

[77] Nishihara, T. and Kawamoto, M., 1945, The strength of metals under combined alternating bending and torsion with phase difference, Memorial College of Engineering and Technology, Kyoto Imperial University, 11, pp. 85-112.

[78] Zenner, H., Heidenreich, R., Richter, I. Z., 1985, Fatigue strength under nonsynchronous multiaxial stresses, Mat. Wiss und Werkstofftech 16, pp. 101-112.

[79] Froustey, C. and Lasserre, S., 1989, Multiaxial fatigue endurance of 30NCD16 steel, International Journal of Fatigue, 11 (3), pp.169-175.

[80] Froustey, C., Lasserre, S., Dubar, L., 1989, Validité des critéres de fatigue multiaxiale a l'endurance en flexion-torsion, In: Fatigue des structures industrielles, 40 promenade Marx-Dormoy, F-93460 Gournay-sur-Marne, France, IITT International, pp. 126-138.

[81] Galtier, A., 1993, Contribution a l'étude de l'endommagement des aciers sous solicitations uni ou multiaxials. [PhD thesis]. ENSAM CER de Bordeaux, p. 193.

[82] Bennebach, M., 1993, Fatigue d'une fonte GS. Influence de l'entaille et d'un traitement de surface. [PhD thesis]. ENSAM CER Bordeaux, p. 157.

[83] Palin-Luc, T., 1996, Fatigue multiaxiale d'une fonte GS sous solicitations combinées d'amplitude variable. [PhD thesis]. ENSAM CER de Bordeaux, p. 261.

[84] Davoli, P., Bernasconi, A., Filippini, M., Foletti, S., Papadopoulos, I., V., 2003, Independence of the torsional fatigue limit upon mean shear stress, International Journal of Fatigue, 25, pp. 471-480.

[85] Banvillet, A., Palin-Luc, T., Lasserre, S., 2003, A volumetric energy based high cycle multiaxial fatigue criterion, International Journal of Fatigue, 25, pp. 755-769.

[86] McGinty, B., 2012, Principal Stresses and Invariants, Retrieved from http://www.continuummechanics.org/principalstress.html

APPENDICES

A. FIE (%) RESULTS OF MULTIAXIAL ENDURANCE CRITERIA FOR ALL EXPERIMENTAL DATA

In the following tables estimations of multiaxial endurance criteria are presented in terms of FIE (%) for each experimental data and materials presented in section 4.3.

Table A. 1: FIE (%) of Multiaxial Endurance Criteria for Bending-Torsion Calibration and nMS Experimental Data Set – Hard Steel

Label	AMP	SVM	SNS	CROSS	FIN	DV	RB	GAM	PCR
nMS1	4.17	4.17	-3.77	4.17	4.17	4.17	4.17	4.17	3.25
nMS2	2.18	4.26	-3.69	3.79	4.60	4.60	4.60	3.89	3.53
nMS3	-1.91	7.49	-0.71	5.49	8.17	8.16	8.17	5.79	6.33
nMS4	-18.33	4.77	-3.22	0.23	3.54	3.54	3.54	0.60	2.62
nMS5	-35.94	10.96	2.50	2.50	2.49	2.49	2.49	2.50	2.37
nMS6	-4.65	3.91	-4.02	2.18	6.89	5.00	6.89	5.30	5.29
nMS7	-20.96	2.65	-5.18	-1.73	3.36	1.96	3.36	0.10	2.44
nMS8	-12.09	-6.44	-13.58	-7.38	2.55	-4.15	2.55	3.96	2.07
nMS9	-25.90	1.28	-6.44	-2.87	6.76	2.06	6.76	2.40	5.29
nMS10	-1.88	-1.88	-9.37	-1.88	-0.21	-1.88	-0.21	3.15	-0.01
nMS11	-15.61	-15.61	-22.05	-15.61	-0.90	-15.61	-0.90	6.70	0.59
nMS12	-35.54	1.64	-6.12	-2.41	10.34	3.60	10.33	3.95	8.25
nMS13	-20.40	2.16	-5.63	-2.28	0.95	0.95	0.95	-1.91	0.36
nMS14	-21.67	1.81	-5.96	-2.55	2.50	1.11	2.50	-0.74	1.69
nMS15	-26.51	0.52	-7.15	-3.61	5.92	1.27	5.92	1.59	4.58

nMS16	-36.43	0.26	-7.39	-3.74	8.81	2.18	8.81	2.51	6.97
nMS17	-5.67	3.38	-4.51	1.45	4.03	4.02	4.03	1.74	2.95
nMS18	-6.66	1.73	-6.04	0.03	4.64	2.80	4.64	3.09	3.47
nMS19	-13.01	-7.42	-14.48	-8.35	1.49	-5.15	1.49	2.87	1.24
nMS20	-17.81	-17.81	-24.08	-17.81	-3.46	-17.81	-3.46	3.94	-1.27
nMS21	-0.68	1.39	-6.35	0.92	1.73	1.72	1.73	1.02	1.25
nMS22	-2.99	-2.99	-10.40	-2.99	-1.30	-3.00	-1.30	2.09	-0.85

Table A. 2: FIE (%) of Multiaxial Endurance Criteria for Bending-Torsion Calibration and nMS Experimental Data Set – Mild Steel

Label	AMP	SVM	SNS	CROSS	FIN	DV	RB	GAM	PCR
nMS23	4.21	4.21	3.15	4.21	4.20	4.20	4.20	4.21	3.56
nMS24	4.23	6.36	5.28	6.29	7.18	7.17	7.18	6.30	6.08
nMS25	-3.97	5.23	4.17	4.97	7.78	7.77	7.78	5.01	6.65
nMS26	-22.25	-0.25	-1.26	-0.83	2.55	2.55	2.55	-0.78	2.10
nMS27	-39.55	4.70	3.64	3.64	3.63	3.64	3.63	3.64	3.55
nMS28	-10.75	-5.01	-5.98	-5.14	3.50	-1.62	3.50	8.66	3.03
nMS29	-26.86	0.00	-1.02	-0.55	8.53	4.66	8.53	6.43	7.40
nMS30	0.08	0.08	-0.93	0.08	1.28	0.08	1.28	6.21	1.16
nMS31	-11.60	-11.60	-12.49	-11.60	0.00	-11.56	0.00	16.28	0.96
nMS32	-36.53	0.07	-0.95	-0.46	11.32	5.88	11.32	9.77	9.81

Table A. 3: FIE (%) of Multiaxial Endurance Criteria for Bending-Torsion Calibration and nMS Experimental Data Set – 42CrMo4

Label	AMP	SVM	SNS	CROSS	FIN	DV	RB	GAM	PCR
nMS33	-1.75	7.05	-5.39	4.19	6.65	6.65	6.65	4.63	4.72
nMS34	-28.14	-28.14	-36.49	-28.14	-16.13	-28.14	-16.13	-12.54	-9.82
nMS35	-7.29	13.71	0.50	7.30	10.84	10.83	10.84	7.94	8.29
nMS36	-39.72	-10.79	-21.15	-14.93	0.16	-8.60	0.16	-8.00	-0.39

Table A. 4: FIE (%) of Multiaxial Endurance Criteria for Bending-Torsion Calibration and nMS Experimental Data Set – 34Cr4

Label	AMP	SVM	SNS	CROSS	FIN	DV	RB	GAM	PCR
nMS37	-7.55	1.31	-6.32	-0.55	1.98	1.97	1.98	-0.27	1.27
nMS38	-16.83	-11.44	-18.11	-12.32	-2.89	-9.24	-2.89	-1.54	-2.16
nMS39	-22.93	-22.93	-28.73	-22.93	-9.52	-22.93	-9.52	-2.48	-5.70
nMS40	-16.83	-11.44	-18.11	-12.32	-2.91	-9.25	-2.91	-1.54	-2.15
nMS41	-36.91	-5.37	-12.50	-8.38	6.51	-1.62	6.51	1.04	4.99
nMS42	-7.32	-7.32	-14.30	-7.32	-5.03	-7.32	-5.03	-0.48	-3.64
nMS43	-35.01	8.99	0.78	3.15	10.15	7.05	10.15	4.81	8.72

Table A. 5: FIE (%) of Multiaxial Endurance Criteria for Bending-Torsion Calibration and nMS Experimental Data Set – 30NCD16

Label	AMP	SVM	SNS	CROSS	FIN	DV	RB	GAM	PCR
nMS44	-11.17	-0.60	-7.48	-2.61	0.16	0.16	0.16	-2.33	-0.24
nMS45	-30.43	-30.43	-35.25	-30.43	-10.20	-21.79	-10.20	-6.36	-6.98
nMS46	-22.14	-4.27	-10.90	-7.51	-4.38	-4.39	-4.38	-7.20	-4.23
nMS47	-16.39	-8.73	-15.05	-10.21	-7.97	-7.97	-7.97	-9.99	-6.90
nMS48	-5.88	4.85	-2.41	2.80	5.68	5.68	5.68	3.09	4.36
nMS49	-25.51	-25.51	-30.66	-25.51	-5.80	-18.27	-5.80	-1.00	-3.53
nMS50	-31.30	-31.30	-36.06	-31.30	-13.26	-24.76	-13.26	-8.79	-9.14
nMS51	-12.84	-3.02	-9.73	-4.90	-2.25	-2.25	-2.25	-4.63	-2.24

Table A. 6: FIE (%) of Multiaxial Endurance Criteria for Bending-Torsion Calibration and nMS Experimental Data Set – XC18

Label	AMP	SVM	SNS	CROSS	FIN	DV	RB	GAM	PCR
nMS52	-7.27	3.31	6.47	4.21	7.34	7.35	7.34	4.08	6.61
nMS53	-13.44	-4.54	-1.63	-3.89	2.38	-0.09	2.38	4.52	2.09
nMS54	-20.48	-20.48	-18.05	-20.48	-3.91	-11.88	-3.91	13.10	-2.82

Table A. 7: FIE (%) of Multiaxial Endurance Criteria for Bending-Torsion Calibration and nMS Experimental Data Set – FGS800_2

Label	AMP	SVM	SNS	CROSS	FIN	DV	RB	GAM	PCR
nMS55	-1.90	9.83	-15.26	2.45	5.00	5.00	5.00	3.49	2.43
nMS56	-16.67	-16.34	-35.45	-16.42	11.32	-7.81	11.32	-0.70	6.91
nMS57	-5.78	9.92	-15.19	0.27	3.14	3.14	3.14	1.43	1.08

Table A. 8: FIE (%) of Multiaxial Endurance Criteria for Bending-Torsion Calibration and nMS Experimental Data Set – S65A

Label	AMP	SVM	SNS	CROSS	FIN	DV	RB	GAM	PCR
nMS58	0.86	4.58	-4.91	3.60	4.92	4.91	4.91	3.78	3.64
nMS59	-11.11	1.83	-7.41	-1.36	1.64	1.64	1.64	-0.95	0.86
nMS60	-26.27	3.75	-5.67	-3.05	-0.47	-0.47	-0.47	-2.70	-0.87

Table A. 9: FIE (%) of Multiaxial Endurance Criteria for Bending-Torsion (σ_{-1}, τ_{-1}) and Axial/Bending (σ_{-1}, σ_0) Calibrations and Shear Stress Calculation Methods (MCC and MRH) for nMS Experimental Data Set – Hard Steel

Label	CROSS		FIN				DV				GAM	
			MCC		MRH		MCC		MRH			
Cases	σ_{-1}, τ_{-1}	σ_{-1}, σ_0	σ_{-1}, τ_{-1}	σ_{-1}, σ_0	σ_{-1}, τ_{-1}	σ_{-1}, σ_0	σ_{-1}, τ_{-1}	σ_{-1}, σ_0	σ_{-1}, τ_{-1}	σ_{-1}, σ_0	σ_{-1}, τ_{-1}	σ_{-1}, σ_0
nMS1	4.17	4.17	4.17	4.17	4.17	4.17	4.17	4.17	4.17	4.17	4.17	4.17
nMS2	3.79	1.72	4.60	4.01	4.60	4.01	4.60	2.86	4.60	2.86	3.89	3.40
nMS3	5.49	-3.37	8.17	5.69	8.17	5.69	8.16	0.96	8.16	0.96	5.79	3.60
nMS4	0.23	-19.90	3.54	-1.82	3.54	-1.82	3.54	-12.08	3.54	-12.08	0.60	-4.80
nMS5	2.50	-35.00	2.49	-6.91	2.49	-6.91	2.49	-24.95	2.49	-24.95	2.50	-8.46
nMS6	2.18	-5.47	6.89	5.10	6.89	5.10	5.00	-1.35	5.01	-1.35	5.30	2.46
nMS7	-1.73	-21.13	3.36	-1.85	3.36	-1.85	1.96	-13.23	1.96	-13.23	0.10	-5.91
nMS8	-7.38	-11.53	2.55	2.84	2.85	2.85	-4.15	-8.05	-1.47	-6.09	3.96	-0.62
nMS9	-2.87	-21.25	6.76	1.77	6.76	1.78	2.06	-12.71	2.06	-12.71	2.40	-5.67
nMS10	-1.88	-1.88	-0.21	0.42	2.34	2.34	-1.88	-1.89	1.49	0.59	3.15	1.72
nMS11	-15.61	-15.61	-0.90	2.93	5.47	5.47	-15.61	-15.61	1.25	-3.27	6.70	0.34
nMS12	-2.41	-20.34	10.34	5.56	10.34	5.56	3.60	-11.13	3.60	-11.13	3.95	-7.31

nMS13	-2.28	-21.93	0.95	-4.28	0.95	-4.28	0.95	-14.30	0.95	-14.30	-1.91	-7.19
nMS14	-2.55	-21.83	2.50	-2.68	2.50	-2.68	1.11	-13.99	1.11	-13.99	-0.74	-6.71
nMS15	-3.61	-21.89	5.92	0.94	5.92	0.96	1.27	-13.41	1.27	-13.41	1.59	-6.42
nMS16	-3.74	-21.45	8.81	4.09	8.81	4.09	2.18	-12.37	2.18	-12.37	2.51	-8.59
nMS17	1.45	-7.07	4.03	1.65	4.03	1.65	4.02	-2.91	4.02	-2.91	1.74	-0.37
nMS18	0.03	-7.46	4.64	2.89	4.64	2.89	2.80	-3.43	2.80	-3.43	3.09	0.31
nMS19	-8.35	-12.46	1.49	1.77	1.78	1.78	-5.15	-9.02	-2.50	-7.08	2.87	-1.66
nMS20	-17.81	-17.81	-3.46	0.27	2.74	2.74	-17.81	-17.81	-1.38	-5.78	3.94	-2.26
nMS21	0.92	-1.14	1.73	1.13	1.73	1.13	1.72	-0.01	1.72	-0.01	1.02	0.53
nMS22	-2.99	-2.99	-1.30	-0.66	1.27	1.27	-3.00	-3.00	0.42	-0.50	2.09	0.64

Table A. 10: FIE (%) of Multiaxial Endurance Criteria for Bending-Torsion (σ_{-1}, τ_{-1}) and Axial/Bending (σ_{-1}, σ_0) Calibrations and Shear Stress Calculation Methods (MCC and MRH) for nMS Experimental Data Set – Mild Steel

Label	CROSS		FIN				DV				GAM	
			MCC		MRH		MCC		MRH			
Cases	σ_{-1}, τ_{-1}	σ_{-1}, σ_0	σ_{-1}, τ_{-1}	σ_{-1}, σ_0	σ_{-1}, τ_{-1}	σ_{-1}, σ_0	σ_{-1}, τ_{-1}	σ_{-1}, σ_0	σ_{-1}, τ_{-1}	σ_{-1}, σ_0	σ_{-1}, τ_{-1}	σ_{-1}, σ_0
nMS23	4.21	4.21	4.20	4.20	4.20	4.20	4.20	4.20	4.20	4.20	4.21	4.21
nMS24	6.29	3.76	7.18	6.09	7.18	6.09	7.17	4.93	7.17	4.93	6.30	5.47
nMS25	4.97	-5.40	7.78	3.47	7.78	3.47	7.77	-1.16	7.77	-1.16	5.01	1.42
nMS26	-0.83	-23.74	2.55	-6.53	2.55	-6.53	2.55	-16.30	2.55	-16.30	-0.78	-9.36
nMS27	3.64	-38.67	3.63	-12.16	3.63	-12.16	3.64	-29.18	3.64	-29.18	3.64	-13.63
nMS28	-5.14	-10.19	3.50	4.42	4.42	4.42	-1.62	-6.65	1.29	-4.66	8.66	0.90
nMS29	-0.55	-22.26	8.53	0.46	8.53	0.47	4.66	-13.83	4.66	-13.83	6.43	-6.88
nMS30	0.08	0.08	1.28	2.44	4.39	4.39	0.08	0.08	3.78	2.60	6.21	3.76
nMS31	-11.60	-11.60	0.00	7.88	10.52	10.52	-11.56	-11.58	7.36	1.36	16.28	5.14
nMS32	-0.46	-21.57	11.32	3.93	11.32	3.93	5.88	-12.50	5.88	-12.50	9.77	-8.74

Table A. 11: FIE (%) of Multiaxial Endurance Criteria for Bending-Torsion (σ_{-1}, τ_{-1}) and Axial/Bending (σ_{-1}, σ_0) Calibrations and Shear Stress Calculation Methods (MCC and MRH) for nMS Experimental Data Set – 42CrMo4

Label	CROSS		FIN				DV				GAM	
			MCC		MRH		MCC		MRH			
Cases	σ_{-1}, τ_{-1}	σ_{-1}, σ_0	σ_{-1}, τ_{-1}	σ_{-1}, σ_0	σ_{-1}, τ_{-1}	σ_{-1}, σ_0	σ_{-1}, τ_{-1}	σ_{-1}, σ_0	σ_{-1}, τ_{-1}	σ_{-1}, σ_0	σ_{-1}, τ_{-1}	σ_{-1}, σ_0
nMS33	4.19	-3.15	6.65	5.42	6.65	5.42	6.65	0.96	6.65	0.96	4.63	3.41
nMS34	-28.14	-28.14	-16.13	-14.36	-11.66	-11.66	-28.14	-28.14	-15.53	-18.49	-12.54	-15.54
nMS35	7.30	-9.14	10.84	8.18	10.84	8.18	10.83	-1.44	10.83	-1.44	7.94	5.01
nMS36	-14.93	-25.57	0.16	-1.39	0.16	-1.39	-8.60	-17.49	-8.54	-17.45	-8.00	-14.09

Table A. 12: FIE (%) of Multiaxial Endurance Criteria for Bending-Torsion (σ_{-1}, τ_{-1}) and Axial/Bending (σ_{-1}, σ_0) Calibrations and Shear Stress Calculation Methods (MCC and MRH) for nMS Experimental Data Set – 34Cr4

Label	CROSS		FIN				DV				GAM	
			MCC		MRH		MCC		MRH			
Cases	σ_{-1}, τ_{-1}	σ_{-1}, σ_0	σ_{-1}, τ_{-1}	σ_{-1}, σ_0	σ_{-1}, τ_{-1}	σ_{-1}, σ_0	σ_{-1}, τ_{-1}	σ_{-1}, σ_0	σ_{-1}, τ_{-1}	σ_{-1}, σ_0	σ_{-1}, τ_{-1}	σ_{-1}, σ_0
nMS37	-0.55	-8.93	1.98	-0.38	1.98	-0.38	1.97	-4.85	1.97	-4.85	-0.27	-2.36
nMS38	-12.32	-16.30	-2.89	-2.62	-2.62	-2.62	-9.24	-12.98	-6.72	-11.14	-1.54	-5.93
nMS39	-22.93	-22.93	-9.52	-5.97	-3.66	-3.66	-22.93	-22.93	-7.50	-11.64	-2.48	-8.35
nMS40	-12.32	-16.30	-2.91	-2.64	-2.62	-2.63	-9.25	-12.99	-6.72	-11.14	-1.54	-5.93
nMS41	-8.38	-21.94	6.51	3.43	6.51	3.43	-1.62	-13.37	-1.62	-13.36	1.04	-9.86

nMS42	-7.32	-7.32	-5.03	-4.12	-1.54	-1.53	-7.32	-7.32	-2.68	-3.93	-0.48	-2.45
nMS43	3.15	-23.12	10.15	1.92	10.15	1.92	7.05	-13.25	7.05	-13.25	4.81	-6.63

Table A. 13: FIE (%) of Multiaxial Endurance Criteria for Bending-Torsion (σ_{-1}, τ_{-1}) and Axial/Bending (σ_{-1}, σ_0) Calibrations and Shear Stress Calculation Methods (MCC and MRH) for nMS Experimental Data Set – 30NCD16

Label	CROSS		FIN				DV				GAM	
			MCC		MRH		MCC		MRH			
Cases	σ_{-1}, τ_{-1}	σ_{-1}, σ_0	σ_{-1}, τ_{-1}	σ_{-1}, σ_0	σ_{-1}, τ_{-1}	σ_{-1}, σ_0	σ_{-1}, τ_{-1}	σ_{-1}, σ_0	σ_{-1}, τ_{-1}	σ_{-1}, σ_0	σ_{-1}, τ_{-1}	σ_{-1}, σ_0
nMS44	-2.61	-12.66	0.16	-2.79	0.16	-2.79	0.16	-8.00	0.16	-8.00	-2.33	-4.98
nMS45	-30.43	-30.43	-10.20	-7.91	-7.27	-7.27	-21.79	-24.16	-11.76	-16.87	-6.36	-13.57
nMS46	-7.51	-23.69	-4.38	-9.00	-4.38	-9.00	-4.39	-17.17	-4.39	-17.17	-7.20	-11.67
nMS47	-10.21	-17.60	-7.97	-10.16	-7.97	-10.16	-7.97	-14.04	-7.97	-14.04	-9.99	-11.90
nMS48	2.80	-7.42	5.68	2.67	5.68	2.67	5.68	-2.65	5.68	-2.65	3.09	0.40
nMS49	-25.51	-25.51	-5.80	-3.07	-2.13	-2.12	-18.27	-20.25	-6.66	-11.81	-1.00	-8.34
nMS50	-31.30	-31.30	-13.26	-10.73	-9.84	-9.84	-24.76	-26.55	-14.00	-18.73	-8.79	-15.53
nMS51	-4.90	-14.25	-2.25	-5.00	-2.25	-5.00	-2.25	-9.87	-2.25	-9.87	-4.63	-7.09

Table A. 14: FIE (%) of Multiaxial Endurance Criteria for Bending-Torsion (σ_{-1}, τ_{-1}) and Axial/Bending (σ_{-1}, σ_0) Calibrations and Shear Stress Calculation Methods (MCC and MRH) for nMS Experimental Data Set – XC18

Label	CROSS		FIN				DV				GAM	
			MCC		MRH		MCC		MRH			
Cases	σ_{-1}, τ_{-1}	σ_{-1}, σ_0	σ_{-1}, τ_{-1}	σ_{-1}, σ_0	σ_{-1}, τ_{-1}	σ_{-1}, σ_0	σ_{-1}, τ_{-1}	σ_{-1}, σ_0	σ_{-1}, τ_{-1}	σ_{-1}, σ_0	σ_{-1}, τ_{-1}	σ_{-1}, σ_0
nMS52	4.21	-8.79	7.34	1.16	7.34	1.16	7.35	-4.08	7.35	-4.08	4.08	-1.07
nMS53	-3.89	-13.39	2.38	-0.01	2.38	-0.01	-0.09	-8.97	-0.09	-8.96	4.52	-3.63
nMS54	-20.48	-20.48	-3.91	3.50	4.51	4.50	-11.88	-14.84	1.82	-5.85	13.10	-2.14

Table A. 15: FIE (%) of Multiaxial Endurance Criteria for Bending-Torsion (σ_{-1}, τ_{-1}) and Axial/Bending (σ_{-1}, σ_0) Calibrations and Shear Stress Calculation Methods (MCC and MRH) for nMS Experimental Data Set – FGS800_2

Label	CROSS		FIN				DV				GAM	
			MCC		MRH		MCC		MRH			
Cases	σ_{-1}, τ_{-1}	σ_{-1}, σ_0	σ_{-1}, τ_{-1}	σ_{-1}, σ_0	σ_{-1}, τ_{-1}	σ_{-1}, σ_0	σ_{-1}, τ_{-1}	σ_{-1}, σ_0	σ_{-1}, τ_{-1}	σ_{-1}, σ_0	σ_{-1}, τ_{-1}	σ_{-1}, σ_0
nMS55	2.45	-3.54	5.00	7.40	5.00	7.40	5.00	1.61	5.00	1.61	3.49	4.97
nMS56	-16.42	-16.48	11.32	10.59	11.32	11.32	-7.81	-8.90	2.03	-0.27	-0.70	3.69
nMS57	0.27	-7.58	3.14	6.24	3.14	6.24	3.14	-1.23	3.14	-1.23	1.43	3.41

Table A. 16: FIE (%) of Multiaxial Endurance Criteria for Bending-Torsion (σ_{-1}, τ_{-1}) and Axial/Bending (σ_{-1}, σ_0) Calibrations and Shear Stress Calculation Methods (MCC and MRH) for nMS Experimental Data Set – S65A

Label	CROSS		FIN				DV				GAM	
			MCC		MRH		MCC		MRH			
Cases	σ_{-1}, τ_{-1}	σ_{-1}, σ_0	σ_{-1}, τ_{-1}	σ_{-1}, σ_0	σ_{-1}, τ_{-1}	σ_{-1}, σ_0	σ_{-1}, τ_{-1}	σ_{-1}, σ_0	σ_{-1}, τ_{-1}	σ_{-1}, σ_0	σ_{-1}, τ_{-1}	σ_{-1}, σ_0
nMS58	3.60	3.55	4.92	6.73	4.92	6.73	4.91	6.57	4.91	6.57	3.78	4.22
nMS59	-1.36	-1.53	1.64	7.35	1.64	7.35	1.64	6.83	1.64	6.83	-0.95	0.60
nMS60	-3.05	-3.42	-0.47	11.06	-0.47	11.06	-0.47	10.03	-0.47	10.03	-2.70	0.88

Table A. 17: FIE (%) of Multiaxial Endurance Criteria for Bending-Torsion Calibration and MS Experimental Data Set – 42CrMo4

Label	AMP				SVM				SNS	CROSS	FIN	DV	RB	GAM	PCR
	SG	GN	GR	SWT	SG	GN	GR	SWT							
MS1	-5.67	-7.13	-13.01	-4.36	13.91	10.91	0.24	13.05	-23.11	-15.34	0.49	-13.33	3.49	-7.80	-4.96
MS2	-9.39	-9.39	-9.39	-9.39	18.37	18.37	18.37	18.37	-37.16	-28.89	-6.18	-28.90	-3.09	-8.01	-7.49
MS3	-2.24	-0.62	9.28	-4.91	5.16	7.84	26.74	1.47	-3.80	5.93	18.78	8.44	21.31	1.93	9.53
MS4	-5.48	-14.93	-32.16	-7.77	-6.40	-16.96	-34.37	-9.56	18.08	-2.89	22.40	7.54	29.19	7.04	4.78
MS5	-3.52	-9.96	-25.47	-3.72	-3.54	-9.97	-25.48	-3.73	-3.71	-24.00	11.49	-15.94	18.33	1.63	0.06

Table A. 18: FIE (%) of Multiaxial Endurance Criteria for Bending-Torsion Calibration and MS Experimental Data Set – 34Cr4

Label	AMP				SVM				SNS	CROSS	FIN	DV	RB	GAM	PCR
	SG	GN	GR	SWT	SG	GN	GR	SWT							
MS6	22.67	15.02	4.17	12.17	62.21	44.29	26.01	33.49	-5.72	0.08	16.15	2.62	22.84	6.01	6.68
MS7	10.06	6.14	-0.57	5.22	41.91	38.88	33.13	36.90	-18.46	-12.69	3.85	-9.64	10.87	3.33	-2.68
MS8	-0.04	-0.04	-0.04	-0.04	33.49	33.49	33.49	33.49	-28.96	-23.17	-0.54	-22.98	6.10	1.45	-3.58
MS9	64.08	1.86	-1.43	-10.93	84.93	3.29	7.55	-12.26	16.68	-6.38	16.26	4.30	28.70	-0.21	2.08
MS10	43.23	7.75	-5.56	-2.06	43.23	7.74	-5.56	-2.07	-2.04	-25.51	8.92	-16.93	22.22	-0.01	-1.25
MS11	19.91	15.47	7.94	13.81	43.94	34.93	22.17	29.70	-12.72	-6.19	11.78	-5.20	19.99	-0.77	2.25
MS12	-15.88	-29.52	-39.29	-26.90	-7.26	-23.57	-34.19	-22.48	8.13	-9.40	21.41	3.41	31.34	3.41	7.81

Table A. 19: FIE (%) of Multiaxial Endurance Criteria for Bending-Torsion Calibration and MS Experimental Data Set – 30NCD16

Label	AMP				SVM				SNS	CROSS	FIN	DV	RB	GAM	PCR
	SG	GN	GR	SWT	SG	GN	GR	SWT							
MS13	27.31	18.77	1.33	11.60	37.35	30.05	13.30	22.52	17.61	3.91	20.44	12.44	29.25	7.63	8.62
MS14	20.23	11.97	-4.69	5.96	28.61	22.11	6.86	16.16	10.33	-3.36	17.84	5.80	26.67	6.77	6.74

MS15	13.06	5.09	-10.76	0.27	20.32	14.68	1.02	10.23	2.89	-10.91	13.39	-1.29	22.27	3.94	3.61
MS16	5.87	-2.65	-18.29	-6.55	9.79	3.88	-9.61	0.49	-11.36	-25.12	10.30	-10.56	19.51	3.97	1.93
MS17	36.19	25.24	5.11	15.25	38.90	28.31	8.20	18.16	12.62	0.11	12.84	6.80	20.76	4.32	3.81
MS18	28.03	17.42	-1.71	8.91	29.59	19.26	0.18	10.68	5.56	-7.22	6.04	-0.89	13.76	-0.13	-0.83
MS19	19.58	9.09	-9.12	2.05	19.58	9.09	-9.12	2.05	-1.92	-14.97	-4.10	-9.32	2.72	-4.47	-6.93
MS20	-33.79	-45.77	-56.29	-41.58	-5.24	-26.25	-39.94	-29.79	15.89	-0.68	16.63	7.77	25.84	1.86	5.20
MS21	39.51	27.27	6.03	15.98	39.51	27.27	6.03	15.98	10.75	-1.34	6.94	4.32	13.25	3.05	0.89
MS22	-65.86	-70.78	-76.40	-60.36	-34.26	-46.78	-57.04	-42.46	12.28	-6.55	7.73	-0.89	16.83	-5.22	-2.28
MS23	-39.15	-45.44	-55.14	-40.48	-12.32	-24.26	-38.72	-25.27	15.94	-0.53	21.84	9.27	31.05	3.73	9.53
MS24	94.47	10.68	8.99	-14.30	94.47	10.68	8.99	-14.30	19.34	-25.50	25.36	-12.04	1.49	18.95	4.57
MS25	73.09	8.44	-0.58	-12.57	73.09	8.44	-0.58	-12.57	16.68	-24.43	22.98	-11.71	0.58	17.57	4.07
MS26	22.80	15.47	-0.46	12.19	22.80	15.47	-0.46	12.19	-2.79	3.80	16.03	7.81	9.92	17.05	5.58
MS27	37.68	21.21	-1.29	7.11	37.68	21.21	-1.29	7.11	3.84	-12.90	-2.85	-6.13	5.04	-7.77	-7.06
MS28	47.18	25.70	1.46	7.50	47.18	25.70	1.46	7.50	5.26	-14.84	-3.22	-7.11	5.96	-8.97	-7.93
MS29	27.51	17.63	-0.95	8.87	27.51	17.63	-0.95	8.87	3.71	-6.39	0.75	-1.46	6.28	-2.65	-3.14
MS30	17.74	13.11	1.13	9.13	17.74	13.11	1.13	9.13	2.52	-0.03	3.95	2.78	6.98	2.11	0.88
MS31	37.62	20.42	-2.18	6.00	69.25	43.48	15.69	18.56	4.94	-8.19	4.85	-0.40	12.75	-1.68	-2.18

MS32	13.84	7.25	-7.27	2.40	28.90	25.45	15.43	21.63	-17.08	-30.09	3.25	-18.47	14.12	-2.57	-3.51
MS33	11.96	4.39	-11.02	-0.76	19.55	13.49	-0.72	8.29	2.84	-10.06	9.48	-1.58	17.86	-0.61	0.93
MS34	5.44	-1.89	-16.57	-5.95	12.10	6.82	-5.95	2.95	-3.98	-16.98	5.36	-8.16	13.80	-3.12	-1.81
MS35	17.69	8.45	-8.79	1.56	19.11	10.09	-7.11	3.11	-1.62	-13.29	-1.32	-7.52	5.82	-6.90	-5.77
MS36	-40.66	-43.36	-49.97	-40.25	-13.43	-18.00	-28.52	-18.46	-0.08	-9.82	7.01	-2.24	12.94	-6.17	0.19
MS37	0.29	-7.87	-22.76	-11.45	4.00	-1.81	-14.84	-4.99	-15.65	-28.88	2.41	-17.41	11.32	-2.72	-3.16
MS38	9.44	0.39	-15.95	-5.08	9.44	0.39	-15.95	-5.08	-8.80	-20.74	-10.91	-15.56	-4.63	-11.31	-11.52
MS39	24.72	3.44	-16.68	-9.28	24.72	3.44	-16.68	-9.28	-8.52	-32.51	5.29	-18.49	19.36	-5.77	-4.05
MS40	75.46	25.77	6.03	-4.44	75.46	25.77	6.03	-4.44	-0.03	-33.18	11.52	-16.10	30.06	-4.75	-2.27
MS41	-63.34	-68.84	-74.87	-59.42	-27.47	-42.25	-53.24	-40.59	13.47	-4.48	9.09	0.92	17.90	-3.28	-0.62
MS42	-53.45	-65.84	-71.53	-57.88	-6.24	-37.85	-45.15	-41.66	30.08	0.90	22.99	9.68	37.32	3.37	6.29
MS43	-47.82	-69.61	-70.60	-62.70	4.17	-47.13	-42.86	-50.74	30.94	-8.38	21.41	3.45	40.76	-4.20	0.50
MS44	-39.97	-50.50	-60.12	-45.70	-15.69	-33.62	-46.11	-35.18	7.36	-8.51	7.89	-0.51	16.80	-6.11	-1.67
MS45	18.39	10.59	-5.52	4.41	27.52	20.77	5.27	14.19	9.60	-3.29	12.03	4.64	20.39	0.15	2.58
MS46	25.18	15.87	-2.07	7.82	27.64	18.60	0.67	10.36	5.17	-5.84	5.46	0.17	12.61	-2.13	-1.08
MS47	52.28	8.78	-8.13	-13.73	71.79	13.79	0.47	-14.23	17.42	-6.49	16.54	4.55	30.08	-0.92	2.23
MS48	133.92	38.89	32.41	-6.49	180.00	44.34	53.97	-8.86	21.96	-11.90	17.71	1.76	35.89	-4.17	0.18

Table A. 20: FIE (%) of Multiaxial Endurance Criteria for Bending-Torsion Calibration and MS Experimental Data Set – S65A

Label	AMP				SVM				SNS	CROSS	FIN	DV	RB	GAM	PCR
	SG	GN	GR	SWT	SG	GN	GR	SWT							
MS49	31.78	29.06	2.85	15.29	31.78	29.06	2.85	15.29	-5.38	-1.15	7.58	4.40	-1.02	4.51	-0.13
MS50	108.69	95.19	33.55	29.07	108.69	95.19	33.55	29.07	0.00	-0.45	18.13	10.67	-0.02	10.87	1.47
MS51	2.45	2.45	2.45	2.45	6.82	6.82	6.82	6.82	-14.37	-5.82	6.15	-5.83	-1.75	-4.05	-0.92
MS52	21.18	21.18	21.18	21.18	37.72	37.72	37.72	37.72	-15.81	-7.41	16.91	-7.41	0.87	-1.27	1.46
MS53	41.24	38.65	12.30	23.99	45.57	43.10	17.09	28.39	-4.90	-0.62	19.66	4.93	3.39	6.28	3.56
MS54	62.23	59.71	32.25	42.66	76.57	74.42	48.81	58.04	-4.90	-0.62	31.67	4.93	7.71	9.62	6.89
MS55	103.24	84.64	23.03	11.73	119.98	94.34	28.61	6.75	-9.87	-11.29	18.42	-0.18	-6.86	1.05	-2.46
MS56	193.36	145.24	64.35	9.60	625.99	315.93	275.63	-1.14	-9.39	-10.77	30.43	0.35	-2.25	4.46	1.20
MS57	-71.07	-72.03	-79.19	-62.21	-46.83	-49.14	-63.55	-45.50	-7.34	-11.70	3.23	-6.15	-9.33	-9.94	-8.58
MS58	-71.68	-74.04	-82.60	-65.58	-50.88	-55.60	-70.48	-54.73	-6.33	-15.06	14.88	-3.94	-10.28	-9.67	-8.74
MS59	-41.83	-44.49	-60.45	-42.57	26.71	17.38	-20.63	-13.05	-9.42	-13.78	4.90	-8.23	-10.21	-6.10	-9.15
MS60	-26.88	-34.98	-56.95	-45.38	61.08	35.22	-9.54	-24.34	-7.16	-15.89	17.47	-4.78	-9.96	-5.45	-8.14

MS61	4.01	-2.78	-33.54	-21.30	213.36	168.35	78.32	23.00	-8.17	-12.53	11.41	-6.98	-7.54	1.36	-6.67
MS62	70.29	41.78	-4.82	-23.26	763.47	397.13	346.93	11.01	-3.83	-12.56	25.68	-1.44	-5.24	3.56	-4.14
MS63	43.27	39.44	7.08	19.14	58.72	53.89	15.95	26.60	-5.28	-1.92	15.38	4.83	1.87	6.60	2.01
MS64	35.42	31.30	-1.05	11.46	68.59	62.30	18.81	27.49	-2.45	-0.99	13.29	7.46	2.80	8.10	2.10
MS65	-3.36	-8.04	-34.98	-20.12	64.91	52.82	3.37	4.40	-1.07	-2.92	15.89	5.12	2.27	5.70	1.46
MS66	203.73	160.57	73.07	21.04	475.70	320.56	207.40	25.42	-8.66	-10.72	24.58	1.42	-4.11	6.47	-0.52
MS67	177.26	140.38	59.30	17.55	427.03	308.55	185.87	34.43	-8.04	-11.86	16.30	1.69	-7.24	5.98	-4.04
MS68	107.10	77.20	17.78	-6.94	446.83	295.70	191.39	18.94	-12.27	-19.03	17.36	-5.97	-11.39	-1.77	-7.87
MS69	17.09	15.33	-4.07	7.68	29.68	28.23	10.49	20.42	0.31	1.95	19.59	10.49	7.22	6.57	5.53
MS70	5.08	4.20	-7.46	1.24	36.67	34.61	11.89	23.06	-8.75	-2.78	10.29	0.18	3.58	3.04	2.57
MS71	31.78	29.06	2.85	15.29	31.78	29.06	2.85	15.29	-5.38	-1.15	7.58	4.40	-1.02	4.51	-0.13
MS72	108.69	95.19	33.55	29.07	108.69	95.19	33.55	29.07	0.00	-0.45	18.13	10.67	-0.02	10.87	1.47
MS73	-29.24	-30.06	-40.00	-28.85	-29.24	-30.06	-40.00	-28.85	-8.55	-8.55	-4.49	-8.57	-7.33	-2.30	-6.95
MS74	-7.62	-10.36	-32.21	-16.76	-7.62	-10.36	-32.21	-16.76	-7.30	-7.30	2.31	-7.32	-4.65	5.34	-4.52

Table A. 21: FIE (%) of Multiaxial Endurance Criteria for Bending-Torsion (σ_{-1}, τ_{-1}) and Axial/Bending (σ_{-1}, σ_0) Calibrations and Shear Stress Calculation Methods (MCC and MRH) for MS Experimental Data Set – 42CrMo4

Label	CROSS		FIN				DV				GAM	
			MCC		MRH		MCC		MRH			
	σ_{-1}, τ_{-1}	σ_{-1}, σ_0	σ_{-1}, τ_{-1}	σ_{-1}, σ_0	σ_{-1}, τ_{-1}	σ_{-1}, σ_0	σ_{-1}, τ_{-1}	σ_{-1}, σ_0	σ_{-1}, τ_{-1}	σ_{-1}, σ_0	σ_{-1}, τ_{-1}	σ_{-1}, σ_0
MS1	-15.34	-21.35	0.49	2.24	0.49	2.24	-13.33	-17.99	-13.33	-17.99	-7.80	-5.17
MS2	-28.89	-28.89	-6.18	-3.06	-5.96	-3.05	-28.90	-28.90	-16.33	-19.28	-8.01	-8.27
MS3	5.93	-1.58	18.78	18.27	18.78	18.27	8.44	2.62	8.44	2.62	1.93	-1.58
MS4	-2.89	11.81	22.40	27.12	22.40	27.12	7.54	15.32	7.54	15.32	7.04	14.97
MS5	-24.00	-3.71	11.49	18.45	11.88	18.45	-15.94	-3.71	-3.95	5.47	1.63	8.27

Table A. 22: FIE (%) of Multiaxial Endurance Criteria for Bending-Torsion (σ_{-1}, τ_{-1}) and Axial/Bending (σ_{-1}, σ_0) Calibrations and Shear Stress Calculation Methods (MCC and MRH) for MS Experimental Data Set – 34Cr4

Label	CROSS		FIN				DV				GAM	
			MCC		MRH		MCC		MRH			
	σ_{-1}, τ_{-1}	σ_{-1}, σ_0	σ_{-1}, τ_{-1}	σ_{-1}, σ_0	σ_{-1}, τ_{-1}	σ_{-1}, σ_0	σ_{-1}, τ_{-1}	σ_{-1}, σ_0	σ_{-1}, τ_{-1}	σ_{-1}, σ_0	σ_{-1}, τ_{-1}	σ_{-1}, σ_0
MS6	0.08	-8.35	16.15	20.02	16.15	20.02	2.62	-4.24	2.62	-4.24	6.01	11.38
MS7	-12.69	-16.62	3.85	9.30	3.85	9.31	-9.64	-13.34	-7.12	-11.50	3.33	6.00
MS8	-23.17	-23.17	-0.54	6.41	0.93	6.42	-22.98	-23.03	-7.70	-11.85	1.45	1.02
MS9	-6.38	9.19	16.26	24.71	16.26	24.71	4.30	12.84	4.30	12.84	-0.21	12.54
MS10	-25.51	-2.04	8.92	22.39	9.99	22.39	-16.93	-2.04	-3.07	8.10	-0.01	11.06
MS11	-6.19	-8.84	11.78	17.73	11.78	17.73	-5.20	-7.41	-5.20	-7.41	-0.77	5.62
MS12	-9.40	-4.70	21.41	26.17	21.41	26.17	3.41	3.41	3.41	3.41	3.41	3.41

Table A. 23: FIE (%) of Multiaxial Endurance Criteria for Bending-Torsion (σ_{-1}, τ_{-1}) and Axial/Bending (σ_{-1}, σ_0) Calibrations and Shear Stress Calculation Methods (MCC and MRH) for MS Experimental Data Set – 30NCD16

Label	CROSS		FIN				DV				GAM	
			MCC		MRH		MCC		MRH			
	σ_{-1}, τ_{-1}	σ_{-1}, σ_0	σ_{-1}, τ_{-1}	σ_{-1}, σ_0	σ_{-1}, τ_{-1}	σ_{-1}, σ_0	σ_{-1}, τ_{-1}	σ_{-1}, σ_0	σ_{-1}, τ_{-1}	σ_{-1}, σ_0	σ_{-1}, τ_{-1}	σ_{-1}, σ_0
MS13	3.91	9.19	20.44	24.86	20.44	24.86	12.44	14.00	12.44	14.00	7.63	14.73
MS14	-3.36	4.60	17.84	23.75	17.84	23.75	5.80	9.17	5.81	9.17	6.77	12.60
MS15	-10.91	-0.71	13.39	20.53	13.39	20.53	-1.29	3.60	0.38	4.81	3.94	9.09
MS16	-25.12	-9.51	10.30	19.74	11.05	19.74	-10.56	-3.03	-0.25	4.48	3.97	7.87
MS17	0.11	12.95	12.84	19.28	12.84	19.28	6.80	14.43	6.80	14.43	4.32	14.45
MS18	-7.22	6.93	6.04	13.28	6.04	13.28	-0.89	7.80	-0.69	7.95	-0.13	9.66
MS19	-14.97	0.65	-4.10	3.90	-0.79	6.19	-9.32	0.64	-5.20	3.64	-4.47	4.95
MS20	-0.68	-8.78	16.63	17.18	16.63	17.18	7.77	-0.49	7.77	-0.49	1.86	3.15
MS21	-1.34	14.28	6.94	13.45	6.94	13.45	4.32	14.28	4.32	14.28	3.05	14.28
MS22	-6.55	-24.29	7.73	5.51	7.73	5.51	-0.89	-15.50	-0.89	-15.50	-5.22	-8.65
MS23	-0.53	-8.18	21.84	21.62	21.84	21.62	9.27	0.97	9.27	0.97	3.73	-0.21
MS24	-25.50	-2.93	25.36	3.42	25.36	3.42	-12.04	-2.93	-12.04	-2.93	18.95	-2.93

MS25	-24.43	-3.11	22.98	2.17	22.98	2.17	-11.71	-3.11	-11.71	-3.11	17.57	-3.11
MS26	3.80	10.53	16.03	9.71	16.03	9.71	7.81	10.52	7.81	10.52	17.05	10.53
MS27	-12.90	5.84	-2.85	5.20	-2.85	5.20	-6.13	5.84	-6.13	5.84	-7.77	5.84
MS28	-14.84	6.56	-3.22	6.08	-3.22	6.08	-7.11	6.56	-7.11	6.56	-8.97	6.56
MS29	-6.39	7.26	0.75	6.47	0.75	6.47	-1.46	7.25	-1.46	7.25	-2.65	7.26
MS30	-0.03	7.77	3.95	7.13	3.95	7.13	2.78	7.76	2.78	7.76	2.11	7.77
MS31	-8.19	-2.20	4.85	10.78	4.85	10.78	-0.40	1.88	-0.40	1.88	-1.68	10.09
MS32	-30.09	-15.39	3.25	14.05	3.93	14.05	-18.47	-10.81	-7.95	-3.17	-2.57	3.97
MS33	-10.06	-2.14	9.48	15.24	9.48	15.24	-1.58	1.94	-1.58	1.94	-0.61	5.14
MS34	-16.98	-7.03	5.36	12.31	5.36	12.31	-8.16	-3.24	-6.41	-1.96	-3.12	1.99
MS35	-13.29	-0.25	-1.32	5.39	-1.32	5.39	-7.52	0.51	-7.32	0.66	-6.90	2.20
MS36	-9.82	-20.73	7.01	5.01	7.01	5.01	-2.24	-12.37	-2.24	-12.37	-6.17	-12.13
MS37	-28.88	-13.93	2.41	11.87	3.52	11.87	-17.41	-9.52	-6.55	-1.63	-2.72	1.53
MS38	-20.74	-6.39	-10.91	-3.56	-7.93	-1.48	-15.56	-6.40	-11.87	-3.72	-11.31	-2.54
MS39	-32.51	-8.91	5.29	18.55	5.53	18.55	-18.49	-4.92	-8.44	2.38	-5.77	5.29
MS40	-33.18	-2.08	11.52	28.08	11.52	28.08	-16.10	2.16	-6.64	9.04	-4.75	11.86
MS41	-4.48	-23.82	9.09	6.32	9.09	6.32	0.92	-14.82	0.92	-14.82	-3.28	-7.39

MS42	0.90	-10.39	22.99	23.91	22.99	23.91	9.68	-1.04	9.68	-1.04	3.37	3.69
MS43	-8.38	-7.16	21.41	27.13	21.41	27.13	3.45	1.12	3.45	1.12	-4.20	2.58
MS44	-8.51	-15.24	7.89	8.70	7.89	8.70	-0.51	-7.66	-0.51	-7.66	-6.11	-4.50
MS45	-3.29	2.12	12.03	16.35	12.03	16.35	4.64	6.46	4.64	6.46	0.15	7.08
MS46	-5.84	5.72	5.46	11.29	5.46	11.29	0.17	7.05	0.17	7.05	-2.13	7.09
MS47	-6.49	8.27	16.54	25.28	16.54	25.28	4.55	12.41	4.55	12.41	-0.92	12.14
MS48	-11.90	12.39	17.71	30.77	17.71	30.77	1.76	15.93	1.76	15.93	-4.17	15.09

Table A. 24: FIE (%) of Multiaxial Endurance Criteria for Bending-Torsion (σ_{-1}, τ_{-1}) and Axial/Bending (σ_{-1}, σ_0) Calibrations and Shear Stress Calculation Methods (MCC and MRH) for MS Experimental Data Set – S65A

Label	CROSS		FIN				DV				GAM	
			MCC		MRH		MCC		MRH			
	σ_{-1}, τ_{-1}	σ_{-1}, σ_0	σ_{-1}, τ_{-1}	σ_{-1}, σ_0	σ_{-1}, τ_{-1}	σ_{-1}, σ_0	σ_{-1}, τ_{-1}	σ_{-1}, σ_0	σ_{-1}, τ_{-1}	σ_{-1}, σ_0	σ_{-1}, τ_{-1}	σ_{-1}, σ_0
MS49	-1.15	-0.93	7.58	-1.02	7.58	-1.02	4.40	-0.93	4.40	-0.93	4.51	-0.93
MS50	-0.45	0.00	18.13	-0.01	18.13	-0.01	10.67	-0.01	10.67	-0.01	10.87	0.00
MS51	-5.82	-5.82	6.15	-0.96	6.15	-0.96	-5.83	-5.83	-5.83	-5.83	-4.05	-5.03
MS52	-7.41	-7.41	16.91	2.44	16.91	2.44	-7.41	-7.41	-7.41	-7.41	-1.27	-4.67

MS53	-0.62	-0.40	19.66	4.18	19.66	4.18	4.93	-0.50	4.93	-0.50	6.28	0.15
MS54	-0.62	-0.40	31.67	9.31	31.67	9.31	4.93	-0.41	4.93	-0.41	9.62	1.64
MS55	-11.29	-10.85	18.42	-6.00	18.42	-6.00	-0.18	-10.85	-0.18	-10.85	1.05	-10.39
MS56	-10.77	-10.32	30.43	-0.55	30.43	-0.55	0.35	-10.33	0.35	-10.33	4.46	-8.58
MS57	-11.70	-11.93	3.23	5.53	3.23	5.53	-6.15	1.02	-6.15	1.02	-9.94	-8.56
MS58	-15.06	-15.03	14.88	4.47	14.88	4.47	-3.94	-3.23	-3.94	-3.23	-9.67	-13.01
MS59	-13.78	-14.00	4.90	3.67	4.90	3.67	-8.23	-1.38	-8.23	-1.38	-6.10	-8.12
MS60	-15.89	-15.85	17.47	4.05	17.47	4.05	-4.78	-4.19	-4.78	-4.19	-5.45	-11.64
MS61	-12.53	-12.76	11.41	5.92	11.41	5.92	-6.98	0.06	-6.98	0.06	1.36	-4.03
MS62	-12.56	-12.54	25.68	8.71	25.68	8.71	-1.44	-0.36	-1.44	-0.36	3.56	-5.59
MS63	-1.92	-1.75	15.38	3.64	15.38	3.64	4.83	1.00	4.83	1.00	6.60	0.07
MS64	-0.99	-0.93	13.29	7.99	13.29	7.99	7.46	7.11	7.46	7.11	8.10	2.46
MS65	-2.92	-3.05	15.89	13.50	15.89	13.50	5.12	9.85	5.12	9.85	5.70	2.23
MS66	-10.72	-10.32	24.58	-2.29	24.58	-2.29	1.42	-7.98	1.42	-7.98	6.47	-7.24
MS67	-11.86	-11.56	16.30	-3.15	16.30	-3.15	1.69	-4.78	1.69	-4.78	5.98	-7.08
MS68	-19.03	-18.86	17.36	-2.31	17.36	-2.31	-5.97	-8.78	-5.97	-8.78	-1.77	-13.12
MS69	1.95	2.00	19.59	13.57	19.59	13.57	10.49	10.30	10.49	10.30	6.57	3.46

MS70	-2.78	-2.95	10.29	9.16	10.29	9.16	0.18	5.29	0.18	5.29	3.04	1.55
MS71	-1.15	-0.93	7.58	-1.02	7.58	-1.02	4.40	-0.93	4.40	-0.93	4.51	-0.93
MS72	-0.45	0.00	18.13	-0.01	18.13	-0.01	10.67	-0.01	10.67	-0.01	10.87	0.00
MS73	-8.55	-9.04	-4.49	6.91	-4.49	6.91	-8.57	5.01	-8.57	5.01	-2.30	-0.71
MS74	-7.30	-7.80	2.31	9.15	2.31	9.15	-7.32	6.45	-7.32	6.45	5.34	3.46